Dissertation

Complementary omics strategies to dissect p53 signaling networks under nutrient stress

submitted by

Mag.rer.nat. Markus Galhuber

for the academic degree of

Doctor of Philosophy (PhD)

at the

Medical University of Graz

Lehrstuhl of Cell Biology, Histology, and Embryology

under the supervision of

Assoc.-Prof. Dr. Andreas Prokesch

2022

Declaration

I hereby declare that this thesis is my own original work and that I have fully acknowledged by name all of those individuals and organizations that have contributed to the research for this thesis. Due acknowledgement has been made in the text to all other material used. Throughout this thesis and in all related publications I followed the “Standards of Good Scientific Practice and Ombuds Committee at the Medical University of Graz.

Graz, June 2022

Disclosures

Parts of this thesis have been published in:

Complementary omics strategies to dissect p53 signaling networks under nutrient stress. Galhuber, M. et al. (2022), Cellular and Molecular Life Sciences, 79:326. DOI:10.1007/s00018-022-04345-8.

Establishing a BioID system to study the p53 interactome under starvation. Michenthaler, H (2020). (Master thesis).

Actively contributing co-authors of this thesis:

Helene Michenthaler[1]

Christoph Nössing[2]

Elisabeth Moyschewitz[1]

Martina Auer[1]

Ellen Heitzer[3]

Ruth Birner-Grünberger[4,5]

Laura Liesinger[4,5]

Riccardo Zenezini Chiozzi[7,8,9]

Emil Spreitzer[6]

Tobias Madl[6,10]

[1] Gottfried Schatz Research Center for Cell Signaling, Metabolism & Aging, Division of Cell Biology, Histology and Embryology, Medical University of Graz, 8010 Graz, Austria

[2] Cancer Research UK Beatson Institute, Garscube Estate, Glasgow, UK

[3] Diagnostic and Research Institute of Human Genetics, Medical University of Graz, 8010 Graz, Austria

[4] Diagnostic and Research Institute of Pathology, Medical University of Graz, 8010 Graz, Austria

[5] Institute of Chemical Technologies and Analytics, Technische Universität Wien, 1060 Vienna, Austria

[6] Gottfried Schatz Research Center for Cell Signaling, Metabolism & Aging, Division of Molecular Biology and Biochemistry, Medical University of Graz, 8010 Graz, Austria

[7] Biomolecular Mass Spectrometry and Proteomics, Bijvoet Center for Biomolecular Research and Utrecht Institute of Pharmaceutical Sciences, Utrecht University, 3584CH Utrecht, The Netherlands

[8] Netherlands Proteomics Center, 3584CH Utrecht, The Netherlands

[9] Mass-Spectrometry STP facility, Structural & Molecular Biology, University College London, Gower Street, London, WC1E 6BT, United Kingdom

[10] BioTechMed-Graz, 8010 Graz, Austria

Acknowledgements

PhD student Markus Galhuber received funding from the Medical University of Graz through the PhD program Molecular Medicine, from the Austrian Science Fund FWF (grants P29328, I3165, P34109) and by a MEFOgraz grant from the Medical University of Graz. This work has also been supported by EPIC-XS project (EPIC-XS-0000206) funded by the Horizon 2020 program of the European Union, the Franz-Lanyar-Stiftung, Medical University of Graz (grant: 414) and the European Molecular Biology Organization (EMBO, Short term fellowship, grant: 8858). Co-supervisors Sen.Scientist Priv.-Doz. Mag.rer.nat. Dr.scient.med. Alexander Deutsch and Assoz. Univ.-Prof. Mag. Dr.rer.nat. Günter Hämmerle.

Contents

Abbreviations

AA	Amino acid
a-KG	Alpha-Ketoglutarate
AMP	Adenosine monophosphate
ANOVA	Analysis of variance
ATP	Adenosine triphosphate
BCA	Bicinchoninic acid assay
BioID	Proximity biotin labeling
BirA	Biotin ligase
cDNA	Complementary DNA
ChIP	Chromatin immuno precipitation
CHX	Cycloheximide
CSP	Chemical shift perturbation
DBD	DNA binding domain
DNA	Deoxyribonucleic acid
ECM	Extracellular matrix
EGF	Epidermal growth factor
EGFP	Enhanced Green Fluorescent Protein
ETC	Electron transport chain
FADH2	Dihydro-flavin adenine dinucleotide
FBS	Fetal bovine serum
FDR	False discovery rate
GM	Growth medium
GO	Gene ontology
HA	Human influenza hemagglutinin
HRP	Horseradish peroxidase
KEGG	Kyoto Encyclopedia of Genes and Genomes
KO	Knock-out
LC-MS	Liquid chromatography–mass spectrometry
mRNA	messenger RNA
MS	Mass spectrometry
mT	miniTurbo
NAD	Nicotinamide adenine dinucleotide
NADH	Nicotinamide adenine dinucleotide
NADP	Nicotinamide adenine dinucleotide phosphate
NADPH	Nicotinamide adenine dinucleotide phosphate reduced form
NES	Nuclear export signal
NMR	Nuclear magnetic resonance
OXPHOS	Oxidative phosphorylation
p53RE	p53 recogniton element
PBS	Phosphate buffered saline

PCA	Principal component analysis
PCR	Polymerase chain reaction
PhD	Doctor of Philosophy
PIC	Protease inhibitor cocktail
PPI	Protein protein interaction
PPP	Pentose phosphate pathway
PTM	Post-translational modification
qPCR	Real time quantitative PCR
RF	Refeeding medium
RIME	Rapid immunoprecipitation mass spectrometry of endogenous protein
RIPA	Radioimmunoprecipitation assay buffer
RNA	Ribonucleic acid
ROS	Reactive oxygen species
SAINT	Significance analysis of interactome
SM	Starvation medium
SP	SAINT probability
TAD	Transactivation domain
TCA	Tricarboxylic acid cycle
UDP	Uridine-5′-diphosphate
UTP	Uridine-5′-triphosphate
wt	Wild type
XL-AP-MS	Cross-linking affinity purification mass spectrometry

German abstract

Die zelluläre Signaltransduktion durch Tumorsuppressorprotein TP53 (p53) ist ein wichtiger Stressreaktionsmechanismus, welcher Zellen vor ungewollten Veränderungen, wie zum Beispiel DNA-Schäden, DNA Replikationsstress, Telomer-Erosion, ribosomalem Stress, Hypoxie, Produktion von reaktivem Sauerstoff (ROS) oder epigenetischen Veränderungen schützt. Darüber hinaus wird p53 damit in Verbindung gebracht, die Zelle an Schwankungen der Nährstoffverfügbarkeit (z.B. Kohlehydrate, Fette) anzupassen. Die zellulären Reaktionen auf Nährstoffentzug sind reversible Prozesse wie Zellzyklusstillstand, DNA-Reparatur oder Autophagie, die über den p53 Stoffwechselweg vermittelt werden. Die Funktionen von p53 werden dabei durch direkte Protein-Protein Interaktion („Interaktom“) mit Signalproteinen vermittelt, was letztlich zu einer Aktivierung von p53 als Transkriptionsfaktor führt, wodurch zellprotektive Programme gestartet werden.

In dieser Studie zeigen wir in einer humanen Hepatoma-Zelllinie (HepG2), dass der Entzug von Nährstoffen zu einer robusten Stabilisierung von p53 im Zellkern führt. Mithilfe von Proteomik-Methoden (BioID) bestimmen wir das zytoplasmatische p53-Interaktionsnetzwerk während der unmittelbar nach Nahrungsentzug stattfindenden Hungerreaktion und zeigen, dass p53 sowohl von mehreren Stoffwechselenzymen als auch von Proteinkinase PAK2, deren direkte Bindung an die DNA-Bindungsdomäne von p53 mittels Nukleärer Magnetresonanz (NMR)-Studien bestätigt wurde, dissoziiert. Nach Translokation von p53 in den Zellkern analysierten wir das das nukleäre Interaktom mit einer weiteren Proteomik-Methode („Chromatin-Immunopräzipitation“), welche die Proteininteraktion von p53 mit anderen DNA-bindenden Proteinen ermöglicht. Mit dieser Methode war es uns möglich, die neue p53-Interaktoren SORBS1 (Insulinrezeptor-Signalisierung) und UGP2 (Glykogensynthese) zu bestätigen. Schließlich konnten wir auch zeigen, dass die DNA-Bindung von p53 nach verlängertem Nährstoffentzug hungerspezifische Transkriptionsprogramme startet, welche bisher nicht bekannt waren.

Zusammengenommen beschreiben unsere komplementären Ansätze mehrere Knotenpunkte der p53-Signalkaskade bei Nährstoffentzug und werfen ein neues Licht auf die Mechanismen von p53 als Sensor für Nährstoffstress. In Anbetracht der zentralen Rolle von p53 in der Krebsbiologie und der positiven Auswirkungen des Fastens in der Krebsbehandlung, könnten die in dieser Studie identifizierten Interaktionspartner und Netzwerke neue pharmakologische Ziele zur Feinabstimmung der p53-Aktivität aufzeigen.

Abstract

Cellular signal transduction by tumor suppressor protein TP53 (p53) is an important stress response mechanism that protects cells from detrimental changes such as DNA damage, replication stress, telomere erosion, ribosomal stress, hypoxia, reactive oxygen species (ROS) production or epigenetic changes. In addition, p53 is involved in adapting the cell to fluctuations in nutrient availability (e.g., carbohydrates, lipids). The cellular responses to nutrient deprivation are reversible processes such as cell cycle arrest, alternate substrate utilization and distribution or autophagy, which have been associated with the p53 pathway. The functions of p53 are mediated by direct protein-protein interaction ("interactome") with signaling proteins, which mainly leads to activation of p53 as a transcription factor, thereby initiating protective cellular programs.

In this study, we show in a p53-proficient human hepatoma cell line (HepG2) that nutrient deprivation leads to robust stabilization of p53 in the nucleus. Using the proximity proteomics method BioID, we determine the cytoplasmic p53 interaction network during the starvation response that occurs immediately after nutrient deprivation and show that p53 dissociates from several metabolic enzymes as well as the protein kinase PAK2. Direct binding of PAK2 to the DNA-binding domain of p53 has been confirmed using nuclear magnetic resonance (NMR) interaction studies. After translocation of p53 into the nucleus, we analyzed the nuclear interactome using a chromatin immunoprecipitation-based proteomics method, which interrogates protein interaction of p53 with other DNA-binding proteins. From these analyses, we were able to confirm new p53 interactors SORBS1 (insulin receptor signaling) and UGP2 (glycogen synthesis) with co-immunoprecipitation experiments. Finally, we demonstrated that binding of p53 to DNA after prolonged nutrient deprivation coordinates starvation-specific transcriptional programs, which included nutrient-dependent p53 target genes that were previously unknown.

In summary, we have established the role of p53 in protein interaction networks, as well as in its function as a transcription factor in sensing cellular nutrient availability. Considering the diverse roles of p53 in cellular metabolism and its important role in the suppression of carcinogenesis, we have attempted to identify cellular targets that may be exploited in the future for either cancer prevention or pharmacological cancer intervention.

Graphical abstract

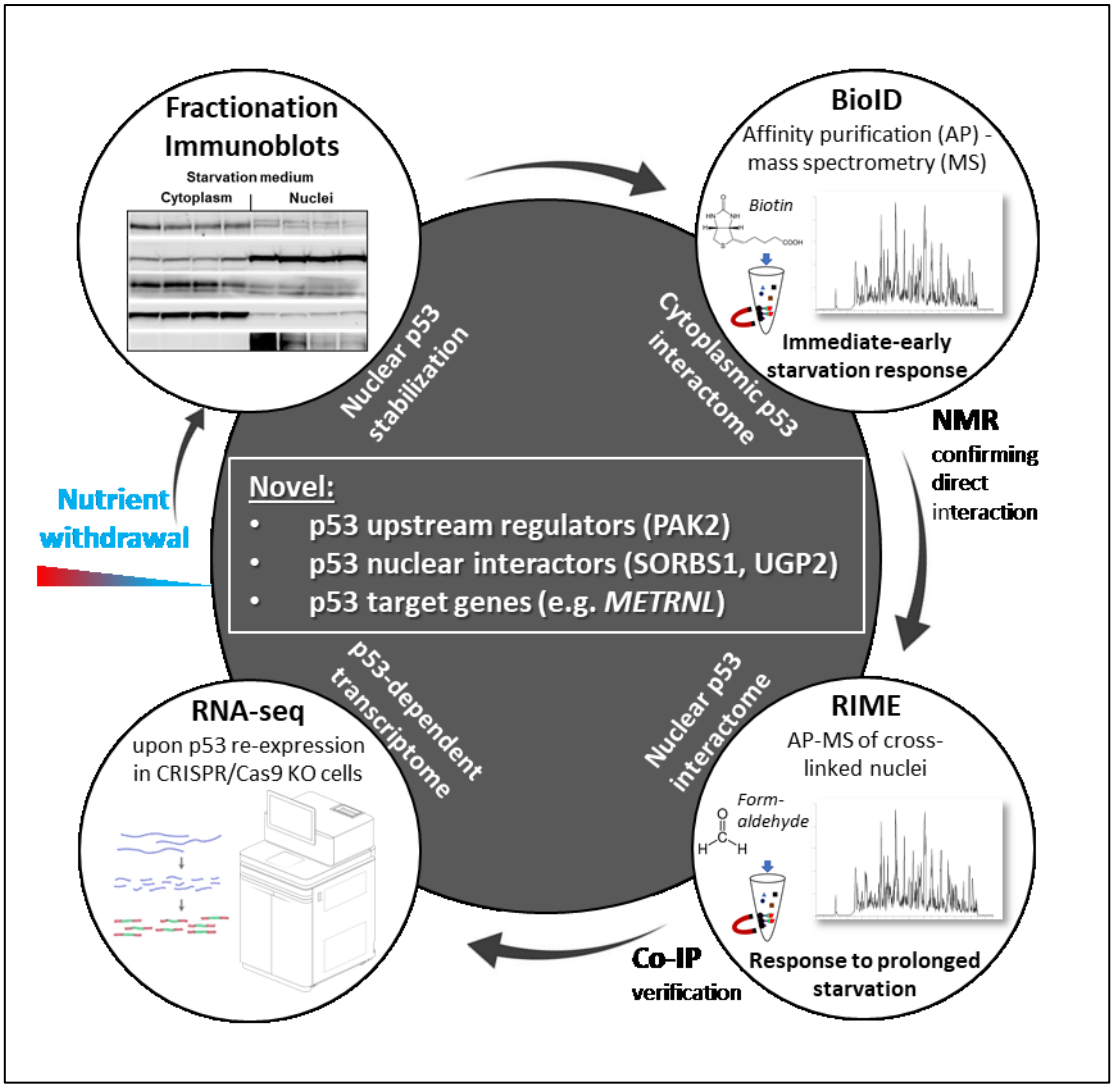

Highlights

- p53 is sustainably stabilized in nuclei upon nutrient withdrawal
- Early remodeling of the p53 interactome under starvation includes dissociation from PAK2
- Nuclear p53 associates with metabolic regulators (SORBS1, UGP2) under prolonged starvation
- Prolonged starvation specifically reprograms the p53-dependent transcriptome

Chapter 1: Introduction

Tumor suppressor protein TP53 is a linchpin in understanding tumor development and progression (Levine, 2020). Since its discovery over 40 years ago, a growing body of evidence describes how p53 regulates cellular growth and stress response and, that aberrations in p53 signaling lead to detrimental outcomes e.g., tumor development. Various intrinsic and extrinsic stress signals are integrated in the Mouse double minute 2 homolog (MDM2)-p53 hub which emanates responses that result in two broad, adaptive mechanisms: either cellular repair and homeostasis or terminal cell death (Kruiswijk, Labuschagne and Vousden, 2015; Krstic *et al.*, 2018). Consequently, functional alterations in the MDM2-p53 hub led to detrimental outcomes in cellular growth control. Over time, efforts in understanding p53 functions have fostered an increasingly complex picture of p53's role in metazoan cells (Vousden and Prives, 2009; Kastenhuber and Lowe, 2017; Hafner *et al.*, 2019; Levine, 2020).

In an attempt to explain p53 functions, stress signals leading to p53 activation are often subsumed under terms like genomic instability (i.e., DNA damage, replication stress, telomere erosion) ribosomal stress, hypoxia, reactive oxygen species (ROS) production, epigenetic changes, and metabolic challenges. Emanating cellular programs in response to those stresses include cell cycle arrest, DNA repair, apoptosis, ferroptosis, senescence, or autophagy and are partly mediated via p53 protein-protein interaction (Maiuri *et al.*, 2010; Comel *et al.*, 2014; Ho, Tan and Lane, 2020) or p53 acting as transcription factor (Riley *et al.*, 2008; Sullivan *et al.*, 2018; Hafner *et al.*, 2019). Beyond that, new downstream effects of p53 are continuously reported, e.g. limited nutrient availability, which represents a disadvantageous stress condition for cellular growth and is sensed and integrated in the MDM2-p53 hub (Maddocks and Vousden, 2011; Flöter, Kaymak and Schulze, 2017; Simabuco *et al.*, 2018).

p53 regulation

The MDM2-p53 hub has evolved as cellular surveillance system that readily reacts to previously mentioned stressors and produces adequate outcomes to protect cellular integrity and organismal health. p53 regulation generally relies on protein stability and protein turn over, regulated by feedback loops with its own negative regulators. In normal, unstressed cells, p53's half-life is rather short (between 6 and 40min) (Maltzman and Czyzyk, 1984; Maki and Howley, 1997) and association with the ubiquitin ligase MDM2 in combination with its homolog Mouse Double Minute 4 MDM4 (also called MDMX), as well as other ubiquitin ligases, leads to p53 ubiquitination and proteasomal degradation (Oliner *et al.*, 1993; Wade, Wang and Wahl, 2010; Hock and Vousden, 2014; Pant and Lozano, 2014; Sane and Rezvani, 2017). Cellular

signals that lead to MDM2 inactivation or degradation extend p53's half-life by a large margin, resulting in sustained p53 activation. Signal transducing and regulatory events on the MDM2-p53 hub are founded on multiple layers (e.g., protein or mRNA abundances, presence or absence of up- or downregulators), and are mediated mostly via protein-protein interactions and posttranslational modifications (PTMs). PTMs (e.g. phosphorylation, acetylation, methylation, ubiquitination, farnesylation, glycosylation (Gonzalez-Rellan *et al.*, 2021), hydroxylation, ADP ribosylation, prolyl isomerization) in turn affect p53 stability, conformation, localization, and binding partners (Liu, Tavana and Gu, 2019). Especially p53's subcellular localization plays a major role in p53 activity. Constant proteasomal degradation during unstressed conditions takes place in the cytoplasm and is dependent on p53 ubiquitination, whereas stabilized p53 protein accumulates in nuclei and associates with p53 recognition elements (p53RE) within specific promotors/enhancers and consequently affects transcriptional regulation on a wide array of target genes (Fischer, 2017). The high diversity in p53-mediated differential transcriptional responses depends on the type of stress activation (Porter, Fisher and Batchelor, 2016) and is mediated by co-activators/co-repressors across diverse chromatin environments and cell types (Sammons *et al.*, 2015; Sullivan *et al.*, 2018; Hafner *et al.*, 2020). Furthermore, heterogeneous patterns in p53REs add another layer of complexity to its selective, context-specific transactivation (Donner *et al.*, 2007; Hafner *et al.*, 2019; Senitzki *et al.*, 2021). In contrast to immediate upstream p53-protein interactions (integration of the stress input signal), transmission of p53-dependent activation to different transcriptional responses (p53-dependent output signal) is in general slower. However, if transcriptional responses are rapid, delayed, or oscillatory is often dependent on assembly of transcription complexes and core promotor structures (Morachis, Murawsky and Emerson, 2010; Harton *et al.*, 2019).

Importantly, transcription-independent, cytoplasmic p53 functions, like interaction with apoptotic effectors or with proteins involved in biological processes such as autophagy, metabolism, or oxidative stress, are described in more recent works, indicating functional importance of cytoplasmic p53 protein (Comel *et al.*, 2014; Ho, Tan and Lane, 2020).

Cancer metabolism

Cellular homeostasis is achieved through constantly balancing macromolecular synthesis and degradation. Thereby, cellular growth and proliferation are tightly controlled and aberrations in this regulation can have dramatic, detrimental effects on organismal integrity which potentially leads to tumorigenic transformation. In healthy cells, proliferative events are heavily dependent on favorable conditions like sufficient exogenous nutrient supply or growth factor signaling.

Often those growth factor signaling pathways are affected or altered in cancer development (Breuhahn, Longerich and Schirmacher, 2006). Given the importance of exogenous nutrient supply on cellular proliferation in normal and tumorigenic tissue, metabolic pathways have long been a field of experimental interest. Metabolic (re-)wiring in proliferating or cancer cells (that is equal to uncontrolled cell division) differs in many characteristics from cells in normally dividing (controlled cell division) tissues or non-proliferating cells (Heiden, Cantley and Thompson, 2009; Pavlova and Thompson, 2016; Zhang, Pavlova and Thompson, 2017). The key for understanding those differences is in understanding metabolite distribution and utilization across different tumor areas as well as within different subcellular compartments.

In comparison to non-dividing cells, which cover their energetic demands mostly via ATP production through oxidative phosphorylation (OXPHOS), proliferating cells are dependent on cellular mass expansion to divide and maintain a minimum cell mass. Therefore, cell division not only requires energy in form of ATP and reducing equivalents (NADH, $FADH_2$) to drive mitochondrial ATP production but also biosynthetic building blocks to provide macromolecules, e.g. amino acids, lipids, ribonucleic acids, and structural components (Heiden, Cantley and Thompson, 2009), for cell division. This demand is mainly covered with principal, exogenous metabolic substrates like carbohydrates (e.g. glucose) or amino acids (e.g. glutamine, serine, glycine) which are utilized in biosynthetic pathways branching from glycolysis (Wise and Thompson, 2010; Hensley, Wasti and DeBerardinis, 2013; Choi and Park, 2017; Geeraerts *et al.*, 2021). In cancer cells, these metabolic pathways can be initiated undesirably, either as a result of higher-order input signals (e.g., altered growth factor signaling) or as a direct cause when metabolic enzymes mutate themselves and thereby trigger tumorigenic transformation (e.g., Isocitrate dehydrogenase [NADP] cytoplasmic IDH1, Isocitrate dehydrogenase [NADP], mitochondrial IDH2). In an interesting tumor metabolism review, Pavlova and Thompson elegantly reduced the understanding of cancer-associated metabolic changes into six hallmarks (Pavlova and Thompson, 2016) layered into 3 categories, that are potentially reprogrammed or affected in tumorigenic cells. First, altered oncogene-directed nutrient uptake of low-molecular weight nutrients like glucose or amino acids via transporters or complex nutrient sources like proteins via macropinocytosis or entosis and subsequent lysosomal degradation. Second, reprogramming of intracellular metabolism, including change in the pools of intermediates (e.g. acetyl-CoA) (Pietrocola *et al.*, 2015), one-carbon-metabolism metabolites (Ducker and Rabinowitz, 2017), nitrogen-containing molecules (e.g. nucleotides or specific amino acids), and glycolytic and tricarboxylic acid (TCA) cycle intermediates. And third, metabolite-directed changes in cell behavior/function, i.e. gene regulation or chromatin modifications (Schvartzman, Thompson and Finley, 2018) as well as altered interaction with

the tumor microenvironment. These described hallmarks determine a core set of metabolic dependencies that might prove to be excellent therapeutic targets across diverse cancer types. Currently, cancer metabolism is investigated at many interconnected levels to hopefully provide the best possible therapy to cancer patients, in which nutritional interventions could support individualized pharmacological therapy (Faubert, Solmonson and DeBerardinis, 2020; Martínez-Reyes and Chandel, 2021).

Focusing on tumor cells nutrient uptake, the observation for extensive need for glucose in tumor cells was made by Otto Warburg in the early and mid-20th century. In his experiments he found that tumor cells do not metabolize glucose to its full energetic potential via mitochondrial OXPHOS in the presence of oxygen (respiration) producing 36 mole ATP per mol glucose molecule. Those cells rather favored glycolytic pathways (fermentation) producing 2 mol ATP per mol glucose (aerobic fermentation, “Warburg effect”) and lactate (O. Warburg, 1956; Pfeiffer, Schuster and Bonhoeffer, 2001). While originally this metabolic phenomenon was assumed as causative for tumor development and attributed to deleterious mitochondria (“grana”) with “irreversible injury of respiration”, today the question of metabolic alterations in tumor cells being cause or effect is still under debate (DeBerardinis and Chandel, 2016; Faubert, Solmonson and DeBerardinis, 2020). Initially, the central argument to explain the Warburg effect was the provision of biosynthetic building blocks needed for cellular growth. However, deeper analyses of this hypothesis became later feasible through increasing sensitivity and accuracy of metabolic assays, which utilize latest biotechnological methods e.g., mass spectrometry, nuclear magnetic resonance, or carbon tracing studies. Key experiments by Thompson and DeBerardinis described that, besides a high glucose consumption, transformed cells also exhibit a large rate of glutamine consumption (“glutamine addiction”) (DeBerardinis *et al.*, 2007; Wise and Thompson, 2010), thereby, beyond glucose, extending the pool of potential metabolic substrates of cell expansion and division. Later in 2016, Hosios et al. analyzed nutrient contributors to cell mass and described, that although glucose and glutamine have the highest consumption rate in tumor cells, the majority of proliferative cell mass actually derives from non-glutamine amino acids (Hosios *et al.*, 2016). Still, they address, that the majority of proteins are dependent on glutamine availability. However, recent studies focusing on intracellular nutrient and energy distribution enable analyses of nutrient fluxes in previously unmatched detail (Bartman *et al.*, 2021). For these reasons, current metabolic research is tending to analyze intracellular nutrient fluxes, rather than just nutrient uptake or consumption. Accordingly, Bartman et al. demonstrated that TCA flux is markedly reduced in tumor tissues and glycolytic flux measurements confirmed a switch towards glycolysis acceleration (Bartman *et al.*, 2021). Interestingly, the overall ATP production

in murine tumor models was reduced when compared to healthy tissue, suggesting an overall dampening of metabolic activity in tumor tissue. This finding opposes previous assumptions of tumors being hyper-metabolic. Still, in this study it was calculated that the majority of ATP is produced via OXPHOS. But, confirming Warburg, also in this recent study tumor cells derived an estimated 11-30% of their ATP production from glycolysis, while healthy tissues derived only 1.8% (Bartman *et al.*, 2021).

Despite the question for the dominant nutrient source for biomass and energy production, it seems clear that tumor cells possess selective advantages mediated through metabolic reprogramming. It is also accepted that tumors and even distinct regions of the same tumor harbor an extensive amount of metabolic flexibility and heterogeneity leading to an emerging view on cancer metabolism as highly adaptable and context-specific. To date, scientists thoroughly investigate how metabolic phenotypes evolve as cancer progresses, with the goal of a more nuanced and therapeutically actionable view of cancer. Taken together, intervening in metabolic changes within tumor cells could represent promising strategies to counter or revert malignant transformation. Interestingly, p53 is intertwined into numerous of those metabolic, tumorigenic adaptations acting either as transcription factor influencing gene expression programs or directly via protein-protein interactions within key metabolic pathways.

p53 in metabolism

P53's role in metabolism has been summarized and extensively debated in many excellent reviews (Flöter, Kaymak and Schulze, 2017; Simabuco *et al.*, 2018; Lacroix *et al.*, 2020; Lahalle *et al.*, 2021). Connections of p53 to almost all relevant metabolic pathways have been revealed and include: nucleotide metabolism, glucose metabolism, lipid metabolism (Parrales and Iwakuma, 2016), amino acid and ammonia metabolism, mitochondrial maintenance, iron metabolism (Laubach, Zhang and Chen, 2021), redox control (Eriksson *et al.*, 2019), autophagy (White, 2016; Mathiassen, De Zio and Cecconi, 2017; Mrakovcic and Fröhlich, 2018), and AMP-activated protein kinase AMPK (Shackelford and Shaw, 2009; Hardie, 2015), AKT Serine/Threonine Kinase AKT, and Mechanistic Target Of Rapamycin Kinase mTOR (Budanov and Karin, 2008a; Feng, 2010) signaling.

In the most generalized sense, the MDM2-p53 hub is affected by high-order growth signaling and nutrient/energy sensors e.g., AKT and AMPK. Pro-proliferation signals (e.g., through AKT/PI3K signaling) exerts activating functions on MDM2, which in turn leads to continuous p53 degradation under nutrient-proficient conditions, enabling cellular proliferation. On the opposite end, failure in growth stimulation (via inhibited AKT/PI3K/mTOR signaling) may result in lower ATP/AMP ratios and activates the central energy sensor AMPK (Hardie, 2015). In turn,

AMPK has been shown to activate p53 via Ser15 phosphorylation (Jones *et al.*, 2005) leading to its nuclear translocation and transactivation that results in cell cycle arrest and adaptation of cellular metabolism to nutrient poor conditions.

In non-proliferative, quiescent cells that are only subjected to transient or mild metabolic fluctuations within biologically reasonable margins, p53 promotes aerobic respiration (OXPHOS) and dampens glycolytic activity on many levels. In this context, p53 seems to oppose the “Warburg effect” and benefits overall cellular health. As transcription factor, p53 targets a plethora of genes, many of which are coding for metabolic enzymes involved in either glycolysis or OXPHOS (excellently summarized in (Lacroix *et al.*, 2020)). In regards of glycolysis, p53 directly affects transcriptional regulation of glucose transporters GLUT1 (repressed, SLC2A1), GLUT3 (via NFkb) and GLUT4 (repressed, SLC1A4) (Kawauchi *et al.*, 2008), Excitatory amino acid transporter 1 SLC1A3 (promoting adaptation to glutamine starvation) (Tajan *et al.*, 2018), Hexokinase 2 (HK2, activated, catalyzes the first step in glycolysis) (Mathupala, Heese and Pedersen, 1997), TP53-induced glycolysis and apoptosis regulator TIGAR (activated, reduces cellular levels of fructose-2,6-bisphosphate and thereby downregulates glycolysis) (Bensaad *et al.*, 2006; Bartrons *et al.*, 2018), 6-Phosphofructo-2-kinase/fructose-2,6-biphosphatase 3 PFKBP3 and 6-Phosphofructo-2-kinase/fructose-2,6-biphosphatase 4 PFKBP4 (both repressed) (Franklin *et al.*, 2016; Ros *et al.*, 2017), Phosphoglucomutase-1 PGM1 (Kondoh *et al.*, 2005), Ras-related associated with Diabetes RRAD (inhibits translocation of GLUT1 to the plasma membrane) (Zhang *et al.*, 2014), and Mono-Carboxylate transporter 1 MCT1 (SLC16A1, repressed, regulates the transport of lactate across plasma membranes) (Boidot *et al.*, 2012). Thereby, p53 downregulates glucose influx into cells, limiting glucose availability, and exerts a fundamental role in metabolic intermediates interconversion, availability and distribution. On the other hand, in varying contexts p53 was shown to transcriptionally activate genes encoding for enzymes that enhance mitochondrial function and respiration: GLS2 (enhancing glutamine hydrolysis to produce glutamate which is converted into a-KG and used to drive ATP generation OXPHOS via NADH) (Hu *et al.*, 2010; Suzuki *et al.*, 2010); Synthesis of cytochrome c oxidase 2 SCO2 (regulates cytochrome c oxidase and is essential for mitochondrial respiration) (Matoba, 2006); Mitochondrial Transcription Factor A TFAM (Yoshida *et al.*, 2003) or Spermatogenesis-associated protein 18 SPATA18 (Mitochondria-eating protein MIEAP) (Kitamura *et al.*, 2011) (both, TFAM and SPATA18 are key for mitochondrial integrity and quality assurance); or Pyruvate carboxylase PC (linking mitochondrial metabolism to insulin secretion and glucose homeostasis in the pancreas (Li *et al.*, 2016). Furthermore, in respect of amino acid metabolism, serine starvation was shown to lead to p53-dependent metabolic remodeling in cancer cells and leads to

changes in energy metabolism as well as a p53-dependent cell cycle arrest and protection from reactive oxygen species (ROS) generation (Maddocks *et al.*, 2013). The same study reports an upregulation of *de novo* serine synthesis via Phosphoglycerate Dehydrogenase (PHGDH) (although p53-independently) and Phosphoserine aminotransferase 1 (PSAT1) (Maddocks *et al.*, 2013) in reaction to serine/glycine starvation. Interestingly, MDM2 also seems to have p53-independent roles in serine/glycine metabolism and promotes expression of serine metabolism genes PHGDH, PSAT1, and Phosphoserine phosphatase (PSPH) in an ATF3/4-dependent manner (Riscal *et al.*, 2016). Also, p53 aspartate-asparagine homeostasis is controlled via p53-dependent transcriptional mechanisms in an AMPK-dependent manner (Deng *et al.*, 2020) thereby involving p53 directly into amino acid anabolism.

Overall, through these transcriptional regulatory events, p53 coordinates systemic and organ-specific metabolic responses and most prominently limits glycolysis, controls amino acid production and transport, while supporting mitochondrial respiration and quality (Table 1).

Table 1 **Roles of p53 regulated transcripts acting on metabolism and cellular integrity.**

Mitochondrial function	Mitochondria genome replication	TFAM
	Mitochondria organization / mitophagy	SPATA18/MIEAP
Glucose metabolism	Glucose transport	GLUT1, GLUT3, GLUT4
	Pentose phosphate pathway	TIGAR, PFKFB4, PFKFB3
	Glycolysis	HK2, PGM1, RRAD
Amino acid metabolism	Amino acid transport	SLC7A3
	Lactate transport	SLC16A1
	Glutamine metabolism	GLS2
	Pyruvate metabolism	PC
	Serine metabolism	PHGDH
Redox / Apoptosis	Pro-oxidant	BAX, PUMA, FXDR, NOXA
	Anti-oxidant	GPx1, GLS2, TIGAR, TPINP1

In respects of p53's influence on mitochondria and mitochondrial respiration, heightened mitochondrial activity is known to instigate increased reactive oxygen species (ROS) through electron spillover (via NADH) in the election transport chain (ETC), as the capacity of ATP synthase is exceeded. Increased ROS burdens are also addressed via p53's transcriptional functions, influencing both pro- (under stress conditions) and anti-oxidant (under normal conditions) protein expression. In these scenarios, pro-oxidant conditions lead to apoptosis (through regulation of BAX, PUMA, FXDR, NOXA) while anti-oxidant conditions lead to cellular survival (GPx1, GLS2, TIGAR, TP53INP1) (Liu, Chen and St. Clair, 2008; Eriksson *et al.*,

2019). Oxidative stress defense is mediated via nicotinamide adenine dinucleotide, phosphorylated form (NADP), that in its reduced form NADPH buffers ROS (Agledal, Niere and Ziegler, 2010; Aquilano, Baldelli and Ciriolo, 2014; Eriksson *et al.*, 2019; Balsa *et al.*, 2020). Beyond ROS, NADPH also plays a major role in anabolic metabolism as reducing agent (electron donor) for *de novo* synthesis of fatty acids and cholesterol, proteins, and glucose (gluconeogenesis in liver and kidney) and therefore represents a shared substrate pool for ROS defense as well as anabolic metabolism. NADP/NADPH pool is maintained via NAD kinase (NADK) and produced from its precursor NAD+/NADH. NAD+/NADH in contrast to its phosphorylated form, is produced and utilized in katabolic metabolism, e.g. glycolysis, b-oxidation, TCA cycle (Agledal, Niere and Ziegler, 2010). Therefore, the NAD+/NADH and NADP+/NADPH pools might represent an important biomolecular switch from catabolic to anabolic metabolism, which is intertwined with p53 on transcriptional as well as post-translational in many ways. In this sense p53 is implied as decider between cellular growth or rest.

A critical supplier of cellular NADPH is the pentose phosphate pathway (PPP) which has been shown to be directly influenced by p53, through protein-protein interaction with the rate-limiting PPP enzyme glucose-6-phosphate dehydrogenase G6PD (Jiang *et al.*, 2011). Jiang et al. showed that binding of p53 to G6PD inhibits its activity and represses glucose shunting through PPP. In consequence, this leads to repressed NADPH production and in turn reduced macromolecular biosynthesis, thereby confirming p53's role as cell proliferation inhibitor. Interestingly, ROS-sensitive cells were associated with dysfunctional NADP+-dependent dehydrogenases, among which is G6PD. Cells exposed to oxidative stress reacted with a rapid increase in both G6PD expression and activity (Ursini *et al.*, 1997) to provide NADPH. Of course, limited NADPH production in the PPP context seems to oppose p53-mediated ROS defense, as NADPH is responsible for GSSG recycling. However, these conflicting observations underscores the fine interplay of p53's metabolic functions, on the one hand fostering pro-apoptotic functions under stress conditions and anti-apoptotic functions in unstressed conditions. Taken together, the interaction with G6PD establishes p53 as key node in nutrient-sensing cell fate decisions based on nutrient availability.

Beyond G6PD, other examples for key metabolic proteins directly interacting with p53 are Malate dehydrogenase, cytoplasmic (MDH1) (which was shown to bind p53 under glucose deprivation) (Lee *et al.*, 2009), and other proteins involved in nucleotide synthesis, e.g. GMPS (Reddy *et al.*, 2014) and Ribonucleotide reductase subunit 2 RRM2 (Xue *et al.*, 2003).

Given the large body of available data, tremendous efforts have been undertaken to integrate the information of how key metabolic regulators and p53-mediated regulations can be unified into one model and coordinate metabolism.

Fasting/starvation in cancer metabolism

As mentioned previously, in 50% of all cancers, either p53 protein or it signaling pathway is mutated or pathologically altered (Aubrey *et al.*, 2018). Hence intensive research on p53 signaling is continuing, as modulating this signaling pathway and/or its downstream nodes might be worthwhile targets in the treatment of at least 50% of all tumors. It is known that mutant p53 can also protect cancer cells from elimination mediated through its protective function against divers stresses (Eriksson *et al.*, 2017; Mantovani, Collavin and Del Sal, 2019). Therefore, in each clinical setting (i.e., recuperation of absent p53 signaling or establishing wild-type (wt) signaling of mutated p53) or cancer prevention setting it is crucial to invoke and differentiate between wanted and unwanted p53-mediated cellular responses. It has been shown that fasting or caloric restriction clearly has beneficial effects on organismal health (de Cabo and Mattson, 2019) e.g., delayed aging, protection against diabetes, obesity, heart disease, neurodegeneration, and importantly was shown to improve the effects of cancer therapy, that are mediated via the p53 pathway (Longo and Mattson, 2014; Nencioni *et al.*, 2018; Deligiorgi, Liapi and Trafalis, 2020). Investigating fasting-based combination treatments to improve anti-tumor therapy, we found in previous studies in hepatocellular carcinoma models that p53 is necessary to proper fasting responses (Prokesch *et al.*, 2017; Krstic *et al.*, 2022) and that metabolic changes in cancer cells are partly relayed through the p53 signaling pathway. In this metabolic context, several questions about the action of the p53 signaling pathway under starvation arise: (1) How a low nutrient state is relayed towards the MDM2-p53 hub; (2) how this leads to p53 stabilization and nuclear translocation; (3) what key p53 interactors on chromatin level (co-activator/co-repressor) exert the specific transcriptional effect; and finally, (4) what is the p53-specific transcriptome outcome in the context of nutrient starvation. These questions demand systems biology approaches, especially on the proteome and protein interactome level, that were utilized in this thesis and described below.

Protein networks and protein-protein interaction analysis

A plethora of cellular signaling events are mediated via protein-protein interactions (PPI), often manifested in large assemblies of proteins organized in macromolecular protein complexes and protein interaction networks. This high degree of spatial and temporal organization is a fundamental quality of cell biology and disturbances in protein network organization are often associated with detrimental outcomes (Richards, Eckhardt and Krogan, 2021). Protein

organization and re-organization are highly dynamic processes and foundational for cellular signal propagation. During those biochemical events, protein conformations, modifications, localizations, as well as compositions of macromolecular complexes rapidly change in response to environmental stimuli. Commonly described as “signal transduction”, this permanent flow of information is an integral part in any living organism. For each given protein, the full repertoire of PPIs, the so-called interactome, is the collection of its vicinal proteins at a given time point in a given cellular context. Today, the analysis of PPI networks relies on sophisticated technologies involving mass spectrometry (MS) and bioinformatic network modeling (Dunham, Mullin and Gingras, 2012; Lundberg and Borner, 2019; Richards, Eckhardt and Krogan, 2021). While it has been a tedious task to interrogate individual protein interactions one-by-one in separate experiments, modern proteomics methods enable researchers to interrogate protein interaction networks in an a more comprehensive and much quicker manner. There are numerous different approaches to analyze PPIs and each comes with certain advantages and disadvantages (Titeca *et al.*, 2019). To decipher p53 signaling under nutrient stress we have chosen two suitable affinity-based purification MS methods: To determine early signaling events towards p53 in response to starvation, we established a proximity-based biotin-labelling approach (BioID). To analyze p53s function as transcription factor during long-term starvation, we established an affinity-purification coupled to MS assay for the analysis of nuclear interactions of p53 (Mohammed *et al.*, 2016). The reasoning for choosing the respective methods will be discussed in the next chapters.

Proximity-dependent biotin identification (BioID)

BioID utilizes artificial fusion proteins consisting of a bait protein, which is fused to a promiscuous biotin ligase (BirA) (Kim and Roux, 2016; Branon *et al.*, 2018; Roux *et al.*, 2018). When overexpressing BioID fusion proteins, promiscuous biotinylation generated by the biotin ligase enables labeling of proteins proximate to the bait protein within a given cellular context. Biotin is a naturally occurring co-factor for carboxylase enzymes and biotin ligases mediate the reaction of attaching biotin as PTM to terminal amine groups within lysine residues in their target proteins (Chapman-Smith and Cronan, 1999). This reaction is mediated through an ATP-dependent activation of biotin to reactive biotinyl-5’-AMP and is originally responsible for repressing transcription initiation within biotin synthesis operons in *Escherichia coli* (*E. coli*) (Barker and Campbell, 1981). Mutations in BirA (e.g. BirA*, R118G mutation) renders this protein suitable for promiscuous biotinylation events, as (1) its original DNA binding capacity is lost and (2) activated biotinyl-5’-AMP quickly dissociates from its active site (Kwon and Beckett, 2000). This immediate substrate release produces a “cloud” of reactive biotinyl-5’-AMP around the BirA* protein. Therefore, BirA*- tagged bait proteins are suitable for labeling

primary amines (e.g. lysine) with biotin as artificial PTM in adjacent/interacting proteins within a labeling radius of 10nm (Kim *et al.*, 2014). In BioID experiments, exogenous biotin is a necessary substrate to initiate the biotinylation reaction. It is actively imported into cells, but freely diffuses between cytoplasm and nuclei (Zempleni, 2005). After BirA*- tagged bait protein overexpression and incubation with exogenous biotin, biotinylated interactors are pulled-down from cell lysates with streptavidin beads, utilizing the high binding affinity (K_d =10^{-14} M) between biotin and streptavidin (Green, 1975). As the artificial biotin PTM is covalent and irreversible, BioID provides major advantages over other proteomics-based methods analyzing PPIs. First, BioID is capable of capturing and conserving transient or weak PPI within macromolecular complexes within intact cellular architecture. Therefore, BioID detects interactions that are potentially lost or below detection limit with other affinity purification methods and thus facilitates studies of dynamic cellular processes with high sensibility. Second, protein interaction studies often rely on maintaining intact protein complexes during downstream sample processing for MS analysis, which is not necessary in BioID, due to the covalent nature of the biotin-lysine binding. Therefore, rather harsh cell lysis methods are applicable, leading to effective solubilization of most cellular compartments and proteins.

The biotinylation of endogenous proteins depends on other methodological factors e.g., exogenously added biotin concentration, ligase efficiency (reflected in labeling times), and ligase size. Ligation efficiency (or in other words protein kinetics) is important when interrogating dynamic protein interactions. BioID labeling generates a “cumulative history” of PPIs during the respective time window of biotin incubation. Therefore, ligases that are more efficient will allow shorter labeling periods to accumulate sufficient protein biotinylation for downstream MS analysis. In turn, this shorter labeling time windows enhances the temporal resolution of the experiment. With regards to ligase size, it is worth mentioning that using fusion proteins in cell biological experiments inevitably leads to sterically alterations in protein interaction interfaces and therefore will alter its native environment. To limit these effects, it is beneficial to use rather small protein tags or fused peptide sequences. To optimize both these factors, ligation efficiency and protein length of biotin ligases have been successively improved since their advent in proximity labeling (Roux *et al.*, 2012; Kim *et al.*, 2016). Latest developments (Branon *et al.*, 2018) relied on engineering of two promiscuous BirA* mutants (TurboID, miniTurbo) which are superior to previous biotin ligases in respect of labeling times to produce sufficient material for proteomics analysis (<2h) and size (28kDa). In comparison to earlier versions of biotin ligases, miniTurbo is superior with regard to precise temporal control of the labeling window (Branon *et al.*, 2018). Given our objective to use BioID to analyze early immediate reactions in p53 signaling, we decided to utilize miniTurbo in our experiments.

Cross-linking affinity purification mass spectrometry (XL-AP-MS)

As previously mentioned, p53 predominantly acts as transcription factor to regulate numerous target genes under cellular stress. In humans, approximately 4800 proteins have been described that harbor nucleic acid-interacting elements, 2800 of which are potential DNA interactors and 1600 are transcription factors (Leung *et al.*, 2019) (http://qinlab.sls.cuhk.edu.hk/ENPD/). In the chromatin context, DNA-binding proteins are known to be organized in large protein complexes that include general transcription factors, chromatin remodelers, co-regulators to coordinately act on cis-acting elements within promoters and enhancers. These protein complexes modulate genome architecture and ultimately determine gene transcription (Lange *et al.*, 2011).

In case of p53, it is assumed that it mostly acts as transcriptional activator, whereas p53-mediated direct gene repression is suggested to play a minor role, with repressive effects mediated by secondary events such as p53-upregulated co-repressors (Rinn and Huarte, 2011; Fischer, 2017; Sullivan *et al.*, 2018). Still, in both scenarios, p53 gene expression regulation depends on interaction with other proteins in chromatin complexes, that can be delineated by XL-AP-MS experiments as described herein to create a comprehensive p53 chromatin interaction map under nutrient deprivation.

In general, investigating chromatin complexes is a challenging task, as chromatin-bound, non-histone proteins are difficult to access and lowly abundant (Dunham, Mullin and Gingras, 2012; Wierer and Mann, 2016). Still, the development of improved protocols has rendered crosslinking affinity purification coupled to high-resolution MS a viable method to interrogate chromatin complexes (Ji *et al.*, 2015). Rapid immunoprecipitation MS of endogenous proteins (RIME) for analysis of chromatin complexes (Mohammed *et al.*, 2016) was specifically developed for this purpose and utilizes formaldehyde (FA) crosslinking with stringent downstream purification of isolated nuclei to obtain pure chromatin fraction and its associated proteins. Using FA in crosslinking assays (e.g., immunohistochemistry, chromatin immunoprecipitation (ChIP)) harbors the inherent advantage that FA freely diffuses through membranes and it reacts with a wide range of functional groups (e.g., on proteins and DNA). In addition, the small size of FA renders it suitable for crosslinking macromolecules that are in close proximity, ignoring physical distances between reactive residues (Hoffman *et al.*, 2015). These properties are optimal for conserving intact macromolecular complexes for downstream MS analysis, independent of distances between interacting residues. Furthermore, protein-specific pulldown of complexes is facilitated with high affinity and high specificity antibodies, similar to classical ChIP methods. In this sense, high quality antibodies are essential for affinity

purification methods, leading to highly reproducible, reliable results. RIME experiments are background controlled with isotype-matched antibody (IgG) to identify non-specific pull-down of MS-identified proteins. In combination with performing experiments in biological replicates, stringent background control allows for accurate identification of interaction partners with bioinformatic downstream analyses. Proper background control in MS experiments is a fundamental necessity as contaminants e.g., non-specific binding of proteins to antibodies, proteins or epitope tags that interact with solid phase support (e.g., magnetic beads), are always co-purified. Therefore, non-specific contaminants are accounted for in up-front reduction as well as post-analysis subtraction (Dunham, Mullin and Gingras, 2012; Mellacheruvu *et al.*, 2013).

Protein quantification and protein network modelling

Protein quantification strategies in MS have developed in close association with methodological improvements, when MS evolved from mere identification to quantification of proteins. In general, protein quantification in large sets of samples is facilitated with two principal methods, label-based and label-free quantification (Nesvizhskii, Vitek and Aebersold, 2007; Tyanova, Temu and Cox, 2016; Anand *et al.*, 2017; Titeca *et al.*, 2019). In contrast to label-based methods (e.g., isotope-based labeling: SILAC, ^{15}N, ^{18}O, ITRAQ, TMT) that require extra preparation steps and have limited numbers in samples to compare (as number of possible plexes are limited), label-free methods are experimentally simpler, are most cost-effective, and are not limited in the number of samples to analyze at the same time. To meet the needs for accurate analysis and validation of proteomic data, considerable effort is put into developing bioinformatic algorithms that deliver sound statistical evaluation, not only for quantitation but also in modeling protein interactions (Nesvizhskii, Vitek and Aebersold, 2007).

Different bioinformatic tools for accurate protein quantification have been published. The most common state-of-the-art label-free quantification methods are “Label-free Quantification by Delayed Normalization and Maximal Peptide Ratio Extraction”, or MaxLFQ (Cox *et al.*, 2014) and intensity based absolute quantification, and iBAQ (Schwanhäusser *et al.*, 2011), both of which are calculating with peptide/protein intensities (quantitative information). MaxLFQ is an algorithm that is tailored to calculate relative protein quantities across a set of samples in a MS run and is represented by a normalized intensity profile between all samples. Introduced by J. Cox et al., the MaxLFQ algorithm benefits from high-quality instruments with top-level mass resolution, a measure of the ability to distinguish two peaks of slightly different mass-to-charge ratios. Mass resolution is of central importance when it comes to correctly identify and quantify peptides and their intensities. Therefore, ever increasing mass resolution will continue to

increase correctly identified and quantified peaks and enable between-sample comparisons. MaxLFQ algorithm facilitates comparability and normalization between samples on the presence of a majority population of proteins that are not changing between different samples. As such, MaxLFQ is optimal for the analysis of total cell lysates with large populations of unchanged proteins and therefore has major advantages when analyzing protein abundances on a global proteome scale (Choi *et al.*, 2012; Cox *et al.*, 2014). Importantly, the prerequisite for an unchanged majority protein population between samples, excludes samples that underwent experimental preparation steps e.g., antibody-dependent affinity purification steps that lead to specific enrichment and to large disparities in sample composition. In affinity purification experiments, sample compositions are rather variable due to the nature of using different pulldown antibodies, which raises the needs for optimized bioinformatic tools for this application. A possible alternative for affinity purification experiments is employing iBAQ, which provides an approximation of protein copies within each sample. In combination with protein normalization steps by (1) linearly calculating abundances relative to any reference protein or total protein and (2) normalizing differences in protein lengths by dividing the sum of peptide intensities for a single protein by the number of its theoretically observable tryptic peptides between 6 and 30 amino acids, iBAQ is suitable to compare heterogeneous samples.

Beyond protein quantification, the fundamental challenge in modelling protein interaction networks from proteomics data is distinguishing between true and false-positive interactions (or contaminants). An algorithm especially developed for modeling protein interaction networks from MS analysis is called “significance analysis of interactome”, or SAINT (Breitkreutz *et al.*, 2010; Choi *et al.*, 2011). In contrast to MaxLFQ and iBAQ, SAINT probabilistic scoring was tailored to detect protein interactions and utilizes spectral counts to assess the probability of a true interaction between two proteins. The SAINT algorithm (similar to iBAQ) also normalizes spectral counts to the length of the proteins and to the number of spectra in each sample, therefore rendering samples of different composition comparable. Improvements in mass spectrometry instrumentation combined with various bioinformatics analysis strategies, allows us to answer the questions surrounding p53, nutrient deprivation as well as the associated protein interaction networks at the proteome level.

Chapter 2: Methodology

Cell culture

The hepatocellular carcinoma-derived cells (HepG2 wt) were purchased from American Type Culture Collection and kept in DMEM (gibco, 41966-029) (growth medium, GM) containing 4.5 g/l glucose supplemented with 10 % (v/v) heat inactivated fetal bovine serum (FBS; HyCloneTM, SV30160.03) and 1 % Penicilin/Streptamycin (gibco, 15140-122). The cells were cultured at 5% CO_2, 95% air at 37°C. Starvation was conducted after growth medium was removed, cells once washed with 10ml phosphate buffered saline (PBS; gibco, 10010-015), and cultured in HBSS (gibco, 14175-053) ("starvation medium", SM) containing 1 g/l glucose supplemented with 10 mM HEPES (gibco, 1560-080). HepG2 p53KO cells were derived using CRISPR-Cas9 system as described elsewhere (Krstic *et al.*, 2022).

Compound treatments

Compound treatments with different inhibitors were used with following concentrations:
Nutlin-3a (Biomol, Plymouth Meeting, PA, USA), 10μM
Cycloheximide (CHX; Caymen Chem 14126), 10μM
MG132 (Calbiochem 474790), 10μM
FRAX597 (Selleckchem, S7271), 10nM, 1μM, 2.5μM

Gene silencing

PAK2 gene silencing was conducted with DharmaconTM ON-TARGETplus siRNAs (SMARTpool format) (Horizon, Perkin Elmer). siCTRL ON-TARGETplus Non-targeting Control Pool (Cat#D-001810-10-05) or siPAK2 SMARTpools (Cat#L-003597-00-0010) were transfected with transfection reagent DharmeFECT 4 (Cat#T-2004-02, Horizon) at 100nM per well in growth medium according to the manufacturers protocol. After 24h of incubation growth medium was changed and cells maintained for 24h before harvesting in either hypotonic buffer for subcellular fractionation or RNA lysis buffer for qPCR.

Cell lysis

Lysis buffers were supplemented with 1x PhosSTOP (Roche, 04906837001) and 1x protease inhibitor cocktail (PIC) (cOmplete Tablets EASYpack, Roche, 04693116001). Before cell lysis cells were washed with PBS and total protein lysates obtained using the respective buffers provided in each protocol segment.

Western Blotting

Whole cell lysates

Cultured cells were collected with a rubber police man in radioimmunoprecipitation assay (RIPA) buffer containing 50 mM Tris-HCl, 150 mM NaCl, 2 mM EDTA, 50 mM NaF, 0.1 % SDS, 0.5 % Na-deoxycholate, 1 % NP-40, pH 7.2 – 7.4 containing PIC and PhosStop. Sonication was conducted in a cooled water bath ultrasound sonicator (Bioruptor, Diagenode) for 5 min (30 secs on/off cycles). Thereafter the cell lysates were centrifuged at 14500 rpm for 15 min and 4 °C. The clear supernatants were used with a bicinchoninic acid assay (BCA; Thermo Fisher Scientific) to measure protein concentrations. Western blotting was conducted as described in (Prokesch et al. 2016), using 20-50 µg protein per lane.

Subcellular fractionation

Nuclear and cytoplasmic fractions were obtained using a previously described method (Baldwin, Rockland). In short, the cells were collected in hypotonic cytoplasmic lysis buffer containing 10 mM HEPES, 60 mM KCl, 1 mM EDTA, 1 mM, pH 7.6 containing PIC and PhosStop and incubated in an Eppendorf tube on ice for 10 min. After adding 10% IGEPAL to a final concentration of 0.5 %, the cells were immediately vortexed, incubated for 1 min on ice, and vortexed again before being centrifuged at 1500 rpm for 4 min. The clear supernatant (cytoplasmic fraction) was transferred to a new tube. The nuclei cell pellet was washed one time with cytoplasmic lysis buffer (without PIC/PhosSTOP), centrifuged again and resuspended by pipetting in one fifth of cytoplasmic buffer volume nuclear extraction buffer 20 mM Tris-HCl, 100 mM NaCl, 1.5 mM $MgCl_2$, 0.2 mM EDTA, 0.05 % SDS and 25 % (v/v) glycerol, pH 8.0 containing PIC and PhosStop. The nuclei with nuclear extraction buffer were sonicated for 5 min (30 secs on/off cycles) in a cooled water bath ultrasound sonicator (Bioruptor, Diagenode). After 5 cycles of sonication 100 U/ml benzonase (Chem Cruz, sc-202391) was added to each sample and incubated for 1 – 2 hours on ice. During the incubation time the pellet was resuspended periodically (every 15 min). After digestion, the samples were centrifuged for 15 min at 14500 rpm and 4 °C to precipitate cell debris. The supernatant transferred to a new tube and used as nuclear fraction.

RNA isolation and reverse transcription

RNA was isolated with PeqGOLD Total RNA Kit (C-Line) (peqGOLD VWR, 12-6634-02) according to the manufacturer's manual in RNA-Lysis-Puffer T (peqGOLD VWR, 12-TRK-88). The concentrations and purity of the samples were determined with a NanoDrop® ND-1000 (peqlab Biotechnologie GmbH). Reverse transcription was conducted using a High-Capacity cDNA Reverse Transcription Kit (Applied Biosystems by Thermo Fischer Scientific, 4368814)

according to manufacturer's protocol using 1000ng RNA in 20µl reaction volume. Cycler was programmed to 10 min at 25 °C, 120 min at 37 °C, 5 min at 85 °C, and cooled to 4 °C. cDNA was diluted afterwards to a concentration of 1 - 20 ng/µl and stored at -80 °C.

Real time quantitative PCR (qPCR)

qPCR was performed in 96 well plated or 384 well plates (BioRad) with a cDNA concentration between 1 - 2 ng/µl. Primers (2µl of primer pair mixtures at 800nM each) were pipetted into well and master mixes containing 5µl Blue SybrGreen qPCR (Biozym) and 2.5µl cDNA. qPCR was performed in CFX96 or CFX384 Real-Time System (C1000 Thermal cycler, BioRad). Program: 1 cycle (10 min) at 95 °C; 40 cycles: 15 sec at 95 °C, 1 min at 60 °C, 1 min at 72 °C; 1 cycle: 30 sec at 95 °C, 30 sec at 60 °C, 30 sec at 95 °C). qPCR data was analyzed with Bio-Rad CFX Manager 3.1 software. Primer list is provided in Table 7.

Molecular cloning

The vector inserts (p53 wt sequence or EGFP wt sequence) for V5-p53-miniTurbo-NES and V5-EGFP-miniTurbo-NES were amplified from Flag-p53 (Addgene #10838; Primer: F: 5'-ACAGCGCTAGCGAGGAGCCGCAGTCAGATC-3' R: 5'-ACAGCGCTAGCGGATCCGTCTG AGTCAGGCCCTTCTGT-3') or EGFP (Addgene #13031; Primer: F: 5'- ACAGCGCTAGCGT GAGCAAGGGCGAGGAG-3' R: 5'-ACAGCGGCTAGCGGATCCCTTGTACAGCTCGTCC ATGCCGAGAG-3'), and cloned into the in V5-miniTurbo-NES vector (Addgene #107170) at the NheI site. After cloning the vectors sequences were controlled and confirmed by Sanger sequencing.

Proximity-biotinylation (BioID)

HepG2 p53KO cells were grown to 100% confluency in T75 flasks (collagen-coated; approx. 1.5×10^7 cells) and transfected (VIAfect transfection reagent, E4981, Promega) with either V5-EGFP-miniTurbo-NES or V5-p53-miniTurbo-NES. 24 hours after transfection, cells were washed with PBS and cell culture media changed to either GM or SM both containing 250 µM biotin to induce biotinylation (medium composition described in subsection cell culture) and kept in this medium for 2 hours. For each group (GM_p53, GM_EGFP, SM_p53, SM_EGFP) we analyzed 3 biological replicates (12 samples in total). Samples were harvested and processed as previously published (Roux, 2018). Briefly, the cells were lysed in lysis buffer (8 M urea, 50 mM Tris-HCl, pH 7.4) containing PIC and 1 mM dithiothreitol (DTT). After addition of 20 % Triton X-100 to a final concentration of 1 % and sonication for 10 min (30 secs on/off cycles) in a cooled water bath ultrasound sonicator (Bioruptor, Diagenode), samples were subjected to affinity purification with streptavidin beads (Invitrogen, Cat.#65001) on a rotator at 4°C over night. On the next day, the streptavidin beads with captured biotinylated proteins

were 10 times washed with washing buffer containing 50 mM Tris-HCl, pH 7.4, 8 M urea and one final washing steps performed with 50 mM Tris-HCl pH 7.4 and 50 mM AMBIC containing 1 mM biotin to block unbound streptavidin moieties on the beads. The beads were reconstituted in 100 mM Tris-HCl pH 8.5, 2 % sodium deoxycholate (SDC) and reduced/alkylated with 5 mM TCEP/30 mM chloroacetamide for 10 min at 56 °C. After that, the proteins were quantified using a BCA assay and digested with 1:50 trypsin and 1:100 Lys-C overnight at 37 °C under continuous shaking. Digestion was stopped by adding 1 % trifluoroacetic acid (TFA) to a final pH of 2, where SDC was completely precipitated. SDC and the beads were removed by centrifugation for 10 min at 14000 rpm and the supernatant, containing peptides was desalted on an Oasis HLB plate (Waters). Peptides were dried and dissolved in 2 % formic acid before LC-MS/MS analysis.

Mass spectrometry run

MS was performed using an Ultimate3000 high-performance liquid chromatography system (Thermo Fisher Scientific) coupled to an EXPLORIS 480 mass spectrometer (Thermo Fisher Scientific) for 1000 ng of each sample. Buffer A consisted of water acidified with 0.1 % formic acid; Buffer B consisted of 80 % acetonitrile (ACN) and 20 % water with 0.1 % FA. First, the peptides were trapped for 1 min at 30 µl/min with 100 % Buffer A on a trap (0.3 × 5 mm with PepMap C18, 5 µm – 100 Å Thermo Fisher Scientific); after trapping, the peptides were separated in a 50 cm analytical column packed with C18 beads (Poroshell 120 EC-C18, 2.7 µm, Agilent Technologies) in a gradient of 9 – 40 % B in 40 min at 400 nL/min. For column cleaning Buffer B was raised to 55 % in 5 min and increased to 99 %. The peptides were ionized using a spray voltage of 2 kV and a capillary heated at 275 °C. The mass spectrometer setting acquired full-scan MS spectra (350–1400 m/z) for a maximum injection time of 120 ms at a mass resolution of 60,000 and an automated gain control (AGC) target value of 300 %. For a total cycle of 1 second the most intense precursor ions were selected for tandem MS (MS/MS). HCD fragmentation was performed in the HCD cell, with the readout in the Orbitrap mass analyzer at a resolution of 15,000 (isolation window of 1.4 Th) and an AGC target value of 200 % with a maximum injection time of 25 ms and a normalized collision energy of 28 %.

BioID data analysis

All raw files were analyzed by MaxQuant v1.6.17 software using the integrated Andromeda Search engine and aligned against the Human UniProt Reference Proteome (October 2020 release with 75,088 protein sequences). MaxQuant was used with the standard parameters (“Label-Free Quantification”, “iBAQ” and “Match between runs” were selected with automatic values) with only the addition of Deamidation (N) as variable modification. Data analysis was performed with Perseus v1.6.16: proteins reported in the file “proteinGroups.txt” were filtered

for reverse, potential contaminants and identified by site. For the quantitation, we used the iBAQ values calculated by MaxQuant and we kept only proteins found in at least 2 biological replicates in each group. Iintensities were log10 transformed and missing values were imputed by Perseus with the automatic settings (width: 0.3, down shift: 1.8, mode: separately for each column) leading to 2,500 proteins left for statistical analysis with ANOVA testing (Benjamini-Hochberg FDR 0.05), z-score (mean per row) and hierarchical clustering (distance: Euclidian). Clusters were selected if enriched over EGFP background control under both nutrient conditions. Volcano bots were generated with Perseus 1.4.16 using the setting t-test, GM_p53 vs SM_p53, FDR0.05.

KEGG overrepresentation analysis was performed in webgestalt.org (Liao *et al.*, 2019) functional database 'pathway – KEGG' against 'genome protein-coding' reference list with 272 high confidence p53 interactors originating from the hierarchical clustering analysis (3 clusters enriched over EGFP background, Fig 6B).

In a second screen with MaxQuant, the annotated proteins from the initial search were screened for biotinylated peptides only and were identified by adding the modification Biotin(K)="C(10) H(14) N(2) O(2) S" (+226.077598) possible on any K or protein N-term as search criteria. The resulting biotinylated peptides were filtered for occurring only in the p53 samples. Unique peptides found only in p53 samples were analyzed in Perseus v1.6.16: peptides from "peptideGroups.txt" were first filtered for reverse, potential contaminant, identified by site and afterwards only for occurring in p53 samples.

For SAINTscore analysis, the peptide counts for each sample were retrieved from MaxQuant output file "proteinGroups.txt" and prepared as input file for analysis in the Contaminant Repository for Affinity Purification (CRAPome, lit). Analysis in CRAPome was conducted with experiment type: Proximity Dependent Biotinylation; Quantitation type: SPC without selecting CRAPome internal controls, instead only experimental controls as background (GM_p53, SM_p53, and CONTROL) EGFP control groups were merged to a single group, as we specifically look for proteins enriched over background control in both conditions (GM and SM), similar to the hierarchical clustering analysis. Interaction scoring was conducted with standard analysis options. For generating dot plots, the CRAPome output file was downloaded via the External Tools section and used as input file in ProHits-viz (Knight *et al.*, 2015).

Fluorescence microscopy

HepG2 p53KO cells were seeded on collagen-coated glass 4-well chamber slides and transfected with overexpression vectors (V5-p53-miniTurbo-NES or V5-EGFP-miniTurbo-NES) with ViaFECT (Promega) according to the manufacturer's protocol. After 28 hours, cells were washed two times with PBS and fixed with 1 % paraformaldehyde (PFA; Thermo

scientific) for 15 min at room temperature. PFA was aspirated and cells were washed two times with PBS. Then cells were blocked using Ultravision Hydrogen Peroxide Block (Thermo scientific, Rockford, USA) for 5 min at RT. The fixated cells were incubated with primary antibodies (p53 DO1) diluted in Antibody diluent (Dako, California, USA) for 45 min in the dark. Cells were washed two times with PBS and incubated with secondary antibody Anti-rabbit IgG (H+L) Alexa Fluor 555 (Cell Signaling) for 30 min in the dark. Secondary antibodies were diluted 1:1000 in Antibody diluent. For subcellular localization experiments, GFP-p53 (Addgene, Cat.#12091) overexpressing cells were treated with MG132 for 2h prior fixation and processed without application of primary or secondary antibodies. In each protocol, after another two PBS washing steps, nuclei were counterstained with DAPI 1:2000 (Thermo scientific) diluted in PBS for 5 min at RT. Finally, chambers were removed from the slides and mounted with ProLongTM Gold antifade reagent (Invitrogen) and a cover slip. Slides were stored in the dark and analyzed on a PALM Microbeam Laser Microdissection microscope (Zeiss, New York, USA) at 40x magnification. Images were analyzed using Zen software 2.3.

Expression and purification of recombinant proteins

Expression constructs for the fragments of p53 (Uniprot ID P04637) corresponding to amino acid 1 to 94 ($p53^{TAD}$) and 94 to 312, as well as for PAK2 (Uniprot ID Q13177) corresponding to amino acid 1 to 212 were generated by synthesis of the corresponding optimized cDNA-constructs of p53 or PAK2 respectively and insertion of these cDNA into a pETM11-ZZ-His_6 vector via NcoI/BamHI restriction digest.

For expression of recombinant unlabeled or 15N labelled ZZ-His_6 proteins, the bacterial expression vectors were transformed into Escherichia Coli BL21-DE3 Star strain cells. Cells were either grown in lysogeny broth medium for unlabeled proteins or minimum medium supplemented with 6g $^{12}C_6H_{12}O_6$ and 1 g $^{15}NH_4Cl$ at 37 °C until they reached an OD600 of 0.8, when protein expression was induced by addition of 0.5 mM IPTG. After proteins were expressed at 20 °C for 16 hours, cells expressing disordered fragments ($p53^{1-94}$ and $PAK2^{1-212}$) were harvested in denaturing buffer (50 mM Tris-HCl pH 7.5, 150 mM NaCl, 2 mM Imidazol, 6 M Urea) and cells expressing folded fragments ($p53^{94-312}$) were harvested in non-denaturing harvesting buffer (50 mM Tris-HCl pH 7.5, 150 mM NaCl, 2 mM Imidazol, 2 mM tris(2-carbocyethyl)phosphine)), followed by sonication and centrifugation at 6198 rcf for 45 min. Proteins were purified from the lysate using Ni-NTA agarose (Qiagen) and the ZZ-His_6 tag was cleaved by 2 % (w/w) His_6-tagged TEV protease treatment for 16 hours at 4°C. After a desalting step (HiPrep 26/10, GE Healthcare) on an ÄKTA Pure system (GE Healthcare) into a low imidazole buffer (50 mM Tris-HCl pH 7.5, 150 mM NaCl, 2 mM Imidazol), the cleaved protein was separated from the uncleaved protein and the His_6 tagged TEV protease by Ni-NTA affinity

chromatography. Finally, the proteins were purified using size exclusion chromatography (Superdex 75 Increase, GE Healthcare).

Nuclear magnetic resonance (NMR) binding assay

For binding studies all proteins were equilibrated in the same buffer containing 20 mM Hepes pH 7.0, 50 mM NaCl, 2 mM TCEP. Samples for NMR measurements contained 100 µM ^{15}N labelled p53$^{94-312}$ in presence of 0 µM, 50 µM, 100 µM or 200 µM unlabeled PAK2$^{1-212}$ and 10 % D_2O. For titrations using ^{15}N labelled PAK2$^{1-212}$ 50 µM were used in presence 0 µM, 50 µM and 100 µM p53$^{94-312}$ and 10 % D_2O. $^{1}H^{15}N$ HSQC spectra of the aforementioned samples were recorded at 25 °C on a Bruker 600 Mhz Avance Neo NMR spectrometer equipped with a TXI room temperature probe.

Rapid immunoprecipitation mass spectrometry of endogenous proteins (RIME) for analysis chromatin complexes

HepG2 wt cells were grown to 100% visual confluency and treated with either GM or SM for 24 hours. Crosslinking with 1 % FA (prepared in either SM or serum–free GM) was conducted for 8 min and the reaction quenched with glycine at a final concentration of 0.1 M. Cells were washed twice in the flask with ice-cold PBS. Then, cells were immediately frozen at -80 °C and stored in flasks until use. Cell lysates und nuclei were prepared as previously described (Mohammed et al. 2016). IP was conducted using either p53 DO1X (Santa Cruz, sc-126 X) antibody or IgG_{2A} isotype control (Cell Signaling, 61656S). Beads with bound proteins were thoroughly washed with AMBIC, and proteins were digested on-bead with trypsin (1:50) o/n and for an additional 4 hours the next day. Derived peptides were desalted with C18 ultra micro spin columns and analyzed with LC-MS/MS.

Mass spectrometry run

One-tenth of each sample was measured by nano-HPLC (Dionex Ultimate 3000) equipped with an Aurora Series Emitter nanocolumn with CSI fitting (C18, 1.6 µm, 120 Å, 250 x 0.075 mm) (IonOpticks, Melbourne, Australia). Separation was carried out at 50 °C at a flow rate of 300 nl/min using the following gradient. Buffer A: 0.1 % formic acid in water and Buffer B: acetonitrile containing 0.1 % formic acid: 0-18 min: 2 % B; 18-100 min: 2-25 % B; 100-107 min: 25-35 % B, 107-108 min: 35-95 % B; 108-118 min: 95 % B, 118-118 min: 95-2 % B; 118-133 min: 2 % B. The Bruker maXis II ETD mass spectrometer was operated with the captive source in positive mode with following settings: mass range: 150 - 2200 m/z, 4 Hz, precursor acquisition control top20 (CID), capillary 1600 V, dry gas flow 3 L/min with 150 °C, nanoBooster 0.2 bar.

RIME data analysis

The MS/MS data were analyzed for protein identification and label-free quantification using MaxQuant 1.6.1.0 against the public database Swiss-Prot with taxonomy *Homo sapiens* and common contaminants (downloaded on 16.04.2019, 20482 sequences). Detailed search criteria were used as follows: trypsin, max. missed cleavage sites: 2; oxidation on Met as variable modification; search mode: MS/MS ion search with decoy database search included; precursor mass tolerance +/- 0.006 Da; product mass tolerance +/- 80 ppm; acceptance parameters for identification: 1 % PSM FDR; 1 % protein FDR and 1 % site decoy fraction. In addition, a label free quantitation and iBAQ values including the match between runs feature of MaxQuant was performed (Cox et al. 2014) requiring a minimum of 2 ratio counts of quantified razor and unique peptides while omitting the normalization step. Data processing was performed using Perseus software version 1.6.6.0, contaminants and reverse proteins created during database search were removed. Intensities were log10 transformed in order to lower the effect of the outlier values, filtered for 3 valid values in either GM_p53 or SM_p53, or at least 4 valid values in total, allowed no values in the IgG control groups. Missing intensities were replaced with random values taken from the Gaussian distribution of values using default parameters (width: 0.3, down shift: 1.8, mode: separately for each column), in order to simulate a value for low abundant proteins. Two-sample t-tests and volcano blotting were used to identify altered proteins between GM and SM conditions. PCA analysis and multi-scatter plot were generated in Perseus.

For SAINTscore analysis, the peptide counts for each sample were retrieved from MaxQuant output file “proteinGroups.txt” and prepared as input file for analysis in the Contaminant Repository for Affinity Purification (CRAPome, lit). Analysis in CRAPome was conducted with experiment type: Endogenous pull-down; Quantitation type: SPC without selecting CRAPome internal controls, instead only experimental controls as background (GM_p53, SM_p53, and IgG CONTROL) IgG control groups were merged to a single group, as we specifically look for proteins enriched over background control in both conditions (GM and SM). Interaction scoring was conducted with standard analysis options. For generating dot plots and comparison of average spectral counts, the CRAPome output file was downloaded via the External Tools section and used as input file in ProHits-viz (Knight *et al.*, 2015).

Co-Immunoprecipitation (co-IP)

UGP2-FLAG (Genscript, OHu02074D) and/or HA-p53 (Genscript, OHu20059C) were transiently overexpressed in HepG2 p53KO cells with ViaFECT (Promega) according to the manufacturer’s protocol. After 24 hours of transfection, cell culture media was changed to either GM or SM and cells maintained under the respective medium for another 24 hours. After

that, cells were washing with ice-cold PBS and lysed in co-IP buffer 25 mM Tris-HCl, 150 mM NaCl, 1 mM EDTA, 1 % IGEPAL, 5 % glycerol; pH 7.4 containing PIC and PhosSTOP. Cells were passively lysed on ice for 30 min and sonicated for 5 min (30 secs on/off cycles) in a cooled water bath ultrasound sonicator (Bioruptor, Diagenode) at 4 °C. The lysates were centrifuged at 14500 rpm for 5 min and 4 °C. Protein concentration was measured with a BCA protein assay kit. 500 µg of protein lysates was normalized to equal volumes with co-IP buffer and used for precipitation as previously mentioned. For pulldown, 30 µl Flag-beads slurry (Sigma, M8823) was used per mg protein, and equilibrated in 500 µl co-IP buffer for 3 times before use. The protein lysates and beads were incubated over night at 4 °C under reciprocal shaking (BioSan MultiBio RS-24). On the following day, flow-through (supernatant) was collected and used for control blots. Beads were washed 3 times with ice-cold co-IP buffer and proteins eluted from the beads with elution buffer (100 mM glycine, pH 3) under horizontal shaking at room temperature for 5 min.

RNA-seq experiments and data analysis

SEQ libraries (TruSeq® Stranded mRNA Library Prep) of FLAG-p53 (pcDNA3 flag-p53, Addgene) re-expressing cells and vehicle control cells (pcDNA4/HisMax, Invitrogen) were prepared from purified mRNAs of HepG2 p53KO re-expressing the previously mentioned vectors cells under untreated (GM) or treated (SM) conditions for a total of 4 x 3 (12) libraries. Raw sequencing data was obtained from an Illumina NextSeq 550 and mapped to the human genome (hg18) using STAR alignment (Dobin et al. 2013). Differentially expressed genes were found using DEseq2 package R, data was transformed (VST), Wald-Test performed on individual genes, and Benjamini-Hochberg corrected for multiple testing. Genes with an adjusted P-value≤ 0.05 and minimum 2-fold differential expression were used for analysis (Venn diagrams).

Chapter 3: Results

p53-MDM2 regulatory cycle is disrupted upon nutrient starvation in HepG2

Based on our previously published observations that p53 is stabilized in different in vivo and in vitro systems (Nössing, 2017; Prokesch *et al.*, 2017) after 24h nutrient starvation, we asked the question how this process relates to MDM2 levels and what role subcellular localizations of both proteins play during this process. We first tested the effect of pharmacological activation (nutlin-3a) of p53 in in whole cell lysates growth (GM), 24h starvation (SM) medium, or re-feeding (RF) for 6h with GM after 24h GM treatment (Figure 1). Under growth medium conditions both, p53 and MDM2 protein levels markedly increased upon nutlin-3a treatment (Figure 1A top). Conversely, 24h starvation with concomitant nutlin-3a treatment led to an increase in p53 protein levels comparable to GM conditions, but the total amount of MDM2 protein was notably diminished. This pattern was reversible after 6h re-feeding. Quantitative real-time PCR revealed diminished Mdm2 mRNA levels in the starvation plus nutlin-3a treatment group, which could be causative for reduced Mdm2 protein levels under starvation (Figure 1A bottom). Considering the p53- dependent auto-regulatory transcriptional mechanism at the Mdm2 promotor, this result suggests that 24h starvation abolishes p53 activity at the Mdm2 promotor. In contrast, other p53 target genes (i.e., CDKN1A (protein name: p21), GADD45A, and TIGAR) remained responsive to nutlin-3a treatment under feeding and starvation conditions, albeit to a lower extent under starvation. Re-feeding largely reinstates the nutlin-3a responsiveness of MDM2 and TIGAR expression levels are highly responsive to 6h RF and are even more pronounced under nutlin-3a treatment or these results indicate disruption of the p53-MDM2 hub by starvation, with differential transcriptional output on p53 target genes.

As described earlier, subcellular localization plays a central role in p53-MDM2 regulation. To address this circumstance, we established a subcellular fractionation protocol to trace p53 and MDM2 protein abundances in nuclei and cytoplasm with different nutrient status (Figure 1B). We show that mainly nuclear p53 accounts for the increase in p53 levels under starvation, whereas cytoplasmic levels remain stable. MDM2 protein is markedly reduced after 24h starvation in cytoplasmic fraction and this reduction is even more pronounced in the nuclear fraction, although the overall MDM2 levels lower in nuclear fractions. Upon addition of nutlin-3a in either group (GM or SM), p53 protein abundance increased over the non-treated group and much less so for the MDM2 protein under starvation: MDM2 levels in the combined starvation/nutlin-3a treated group were markedly reduced in cytoplasm and nuclei. This strongly indicates that nutlin-3a-induced dissociation of p53 and MDM2 is ineffective after 24h

starvation, as MDM2 protein is excluded from the nucleus. Re-feeding leads to a pronounced re-localization of MDM2 to nuclei, most probably to downregulate elevated p53 proteins to reinstate normal physiological p53 levels. Still, 6h of re-feeding did not reduce p53 to basal levels, which indicates that full recovery from nutrient stress extends this period. To check if MDM2 protein is primed for proteasomal degradation upon a starvation stimulus we treated starved HepG2 cells for 1, 3, or 5h with MG132, a potent proteasomal inhibitor (Figure 1C). While MDM2 levels diminished in the vehicle control group over 5h of treatment, they remained at high levels in the MG132 treated group suggesting that the MDM2 is proteasomal degraded upon a starvation stimulus.

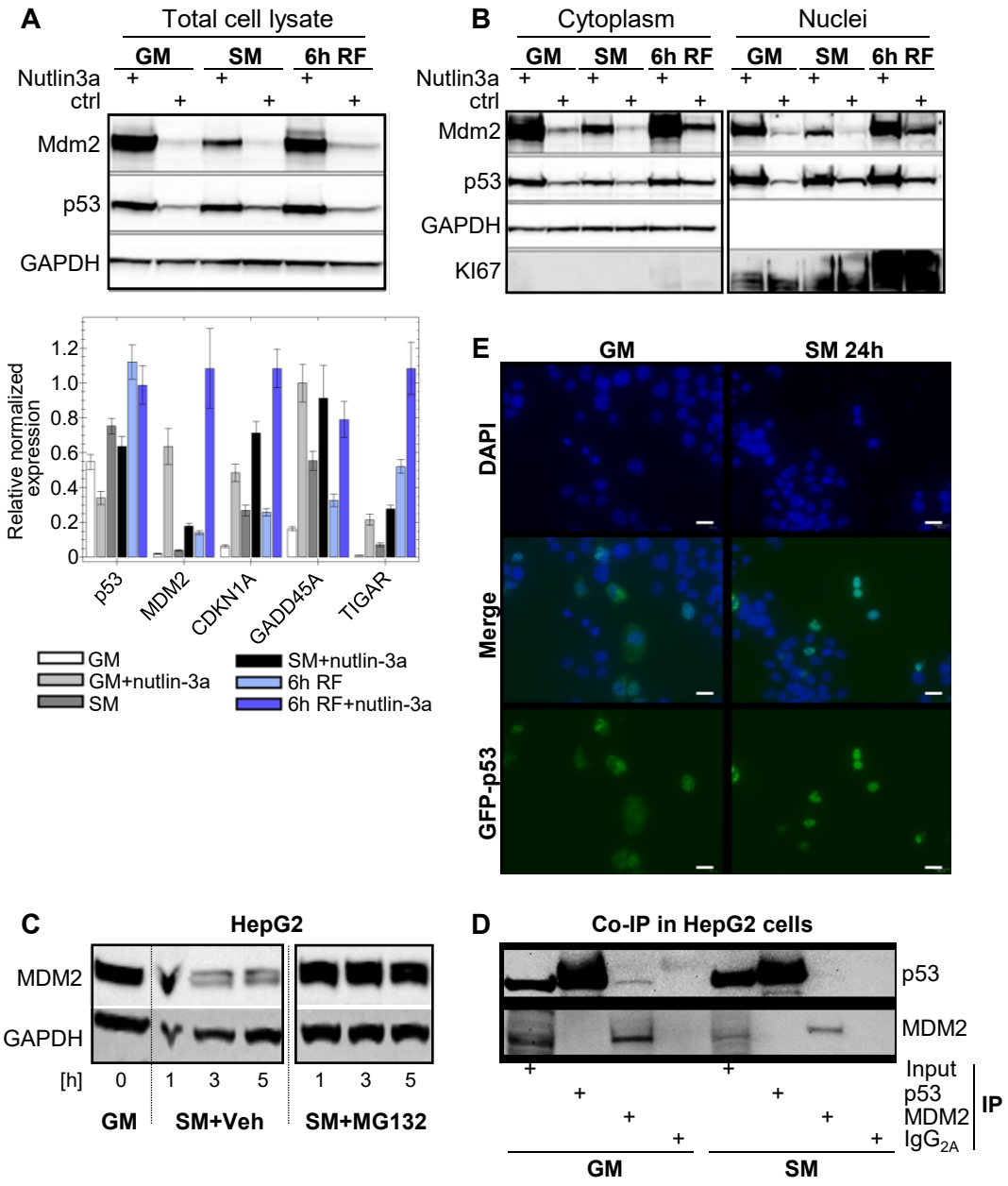

Figure 1 **p53-MDM2 regulatory hub reacts reversibly to metabolic stimuli (starvation, re-feeding).** **A** (top) Immunoblot of whole cell lysates kept in GM, SM, or 6h RF HepG2 cells to detect p53 and MDM2 levels in nutlin-3a treated/untreated conditions. GAPDH loading control. (bottom) qPCR of RNA extracts from samples to determine expression of p53, MDM2, and p53 target genes. **B** Subcellular fragmentation into cytoplasmic and nuclear fraction detecting p53 an MDM2 abundances under GM, SM, or 6h RF conditions and nutlin-3a treated/untreated conditions. Loading control for cytoplasmic fraction GAPDH. Quality control for nuclear fraction KI67. **C** Immunoblot showing MDM2 protein after 1,3, and 5h of starvation treated with MG132. GAPDH loading control. **D** Co-immunoprecipitation of p53 and MDM2 under GM and SM conditions. Pulldown-Antibodies: p53(DO1), MDM2 (SMP14), IgG2A isotype control. **E** Immunofluorescence microscopy in GM and SM HepG2 cells after transfection with a GFP/p53-fusion vector and 2 h MG132 treatment (proteasomal inhibitor) to stabilize proteins. Scale bars indicate 20 µm. Partly reproduced from Galhuber et al. 2022 covered under the CC BY license.

Furthermore, we assessed the p53/MDM2 interaction in a co-immunoprecipitation (co-IP) experiment and found that both proteins interact under GM conditions (co-IP of p53 upon MDM2 pull-down), but to lesser extent under SM conditions (Figure 1D). Of note, we successfully established a co-IP using a MDM2-specific antibody (SMP14), while the reverse pulldown using a p53-specific antibody did not yield the expected result. This might be explained with overlapping interaction domains in the p53/MDM2 interaction (Kussie *et al.*, 1996) with the p53-specific epitope of DO1 antibody (amino acid residues 11-25). In addition, we tracked the p53 localization with immunofluorescence imaging and confirmed GFP-p53 signal in the cytoplasm under GM, while this signal shifted to nuclei under SM conditions (Figure 1E).

To dissect the p53-MDM2 shuttling dynamics between nucleus and cytoplasm with increased temporal resolution we designed a time course experiment that utilized either nutlin-3a (Figure 2A) or cycloheximide (CHX) (Figure 2B) treatment, nutrient deprivation, and subcellular fractionation. CHX is an inhibitor of protein synthesis interfering with ribosomes, which enables observation of protein degradation over time (protein half-life). In this experiment, we treated HepG2 cells with GM or SM for 24h, after which we added nutlin-3a or CHX to the cultures and fractionated the cells after 0h, 1h, 3h and 5h.

Nutlin-3a treatment (Figure 2A) lead to a pronounced activation of p53 and MDM2 over time in both cytoplasm and nuclei, which further translates into downstream p53 target gene activation (p21). Strikingly, the capability of MDM2 induction, and translocation to nuclei in particular, seem to be blunted under SM conditions, which reflects the results from whole cell lysates (Figure 1A). In addition, nuclear p21 protein levels are much lower under starvation conditions in comparison to GM. The protein degradation assay with cycloheximide revealed a decline of p53 and MDM2 protein over the investigated period under GM conditions, underpinning the earlier described permanent protein turnover. Sustained nuclear p53 stabilization was observed upon 24h nutrient deprivation and the MDM2 protein exclusion from the nucleus was confirmed, overlapping with the results from the nutlin-3a time course experiment.

Taken together these results raised the question which regulatory mechanisms, beyond dissociation of p53 and MDM2, lead to their spatial separation and nuclear p53 stabilization under starvation? To investigate these mechanisms, we used different mass spectrometry based-protein analysis methods.

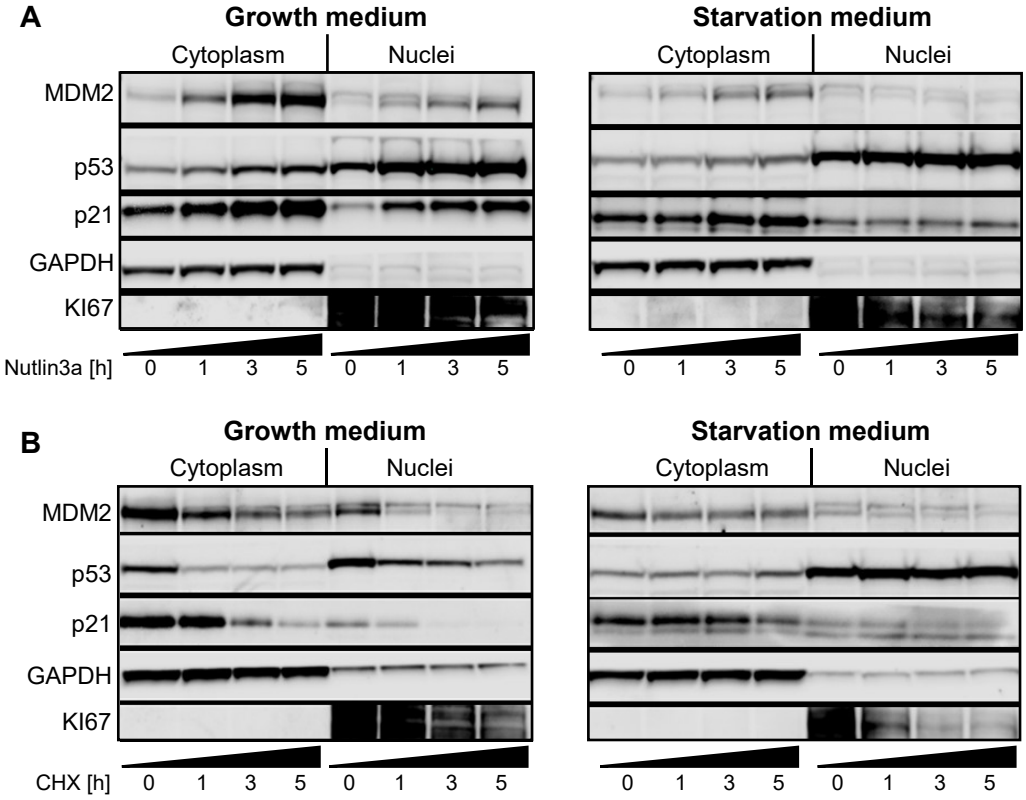

Figure 2 **Nuclear p53 is neither inducible nor degradable after 24h nutrient starvation.** Western blot of protein degradation assay showing regulation of p53, MDM2, and p21. HepG2 cells were kept in growth medium (left panel) or starvation medium (right panel) for 24 hours before they were treated with mutlin-3a (**A**) or cycloheximide (**B**) for the indicated times. Loading controls: cytoplasm GAPDH, nuclei KI67. Reproduced from Galhuber et al. 2022 covered under the CC BY license.

Proximity-dependent biotin identification (BioID) reveals cytoplasmic p53 interactome changes in response to nutrient depletion

To decipher signaling transduction towards p53 in response to nutrient starvation we generated a comprehensive p53-centered cytoplasmic protein interaction map using BioID (Workflow Figure 3). Initially, we also intended to apply BioID for nuclear p53 interaction but were facing numerous unresolvable challenges during fusion protein preparation (details for BioID principles see below). Although we successfully cloned and confirmed the correct sequence for nuclear p53 fusion protein, we were unable to obtain fusion protein with the predicted size (western blotting). Based on this uncertainty, BioID was only conducted to find cytoplasmic p53 protein interaction partners.

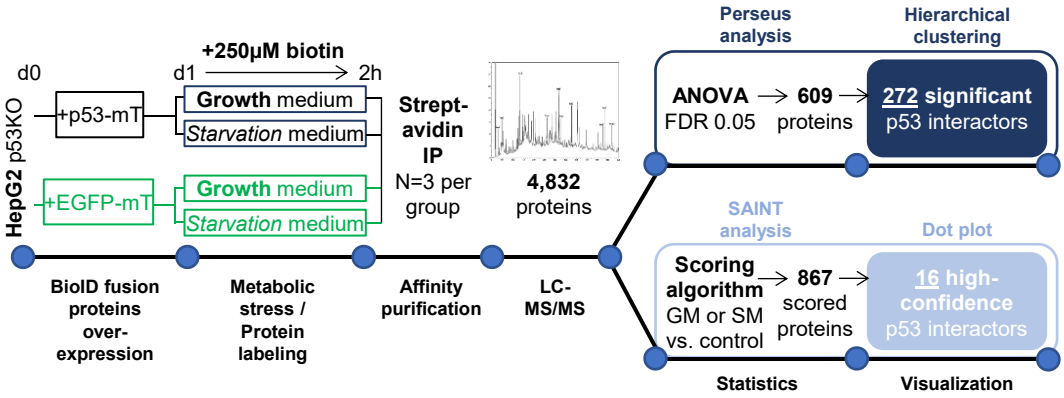

Figure 3 **BioID workflow showing experimental setup and statistical anayses.** d0…day 0 (start of experiment); d1…24h after start. Details of results shown in the following figures. Reproduced from Galhuber et al. 2022 covered under the CC BY license.

Generation and validation of fusion proteins

In general, BioID experiments require the fusion of the biotin ligase to either the N- or the C-terminus of the bait protein, which is crucial for the experimental outcome. Given that p53 harbors its main transactivation domains at the N-terminus, we chose to fuse the biotin ligase to the C-terminus of p53 (henceforth called p53-miniTurbo). In our view, this should minimize potential sterical hindrance at the N-terminal p53 transactivation domains (Raj and Attardi, 2017) and facilitate the best possible experimental representation of endogenous p53 regulation and early interaction at the transactivation domains. In addition, considering canonic mechanisms for p53 regulation where subcellular localization plays a central role, we conceived it crucial to distinguish between cytoplasmic and nuclear p53 interaction. Therefore, we performed targeted studies using fusion proteins harboring a nuclear export signal (NES) to focus on cytoplasmic interactions early after nutrient withdrawal. Importantly, our experimental design includes EGFP negative controls (henceforth called EGFP-miniTurbo) to determine and subtract unspecific background labelling during downstream bioinformatic analyses. For our cytoplasmic interaction setup, we cloned fusion constructs that contain the coding sequences of either p53 or EGFP fused upstream of a C-terminal miniTurbo/NES module (Figure 4A) and confirmed correct orientation and bait protein sequence by sanger sequencing (not shown). We transiently transfected HepG2 p53KO cells (generated in our lab with CRISPR/Cas9) (Nössing, 2017) with the fusion constructs and confirmed their correct subcellular localization in the cytoplasm with fluorescence microscopy (Figure 4B). Furthermore, we validated the predicted size, localization, and responsiveness to nutrient stress of the fusion proteins by immunoblotting after subcellular fragmentation (Figure 4C). Both proteins appear at the predicted height (p53 miniTurbo 75.1kDa and EGFP-miniTurbo

58.3kDa) and are predominantly localized in the cytoplasm. Beyond that, p53-miniTurbo mimics endogenous p53 responsiveness (Figure 1A, C) and is inducible by a starvation stimulus.

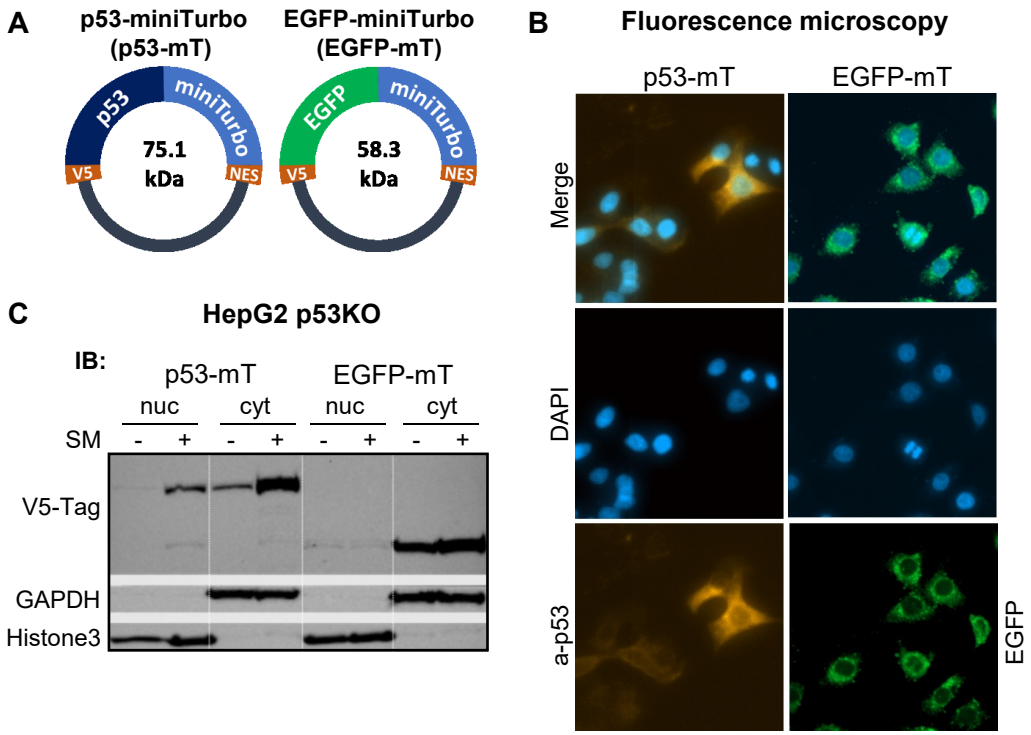

Figure 4 **Cloning and validation of fusion proteins for BioID. A** p53 and EGFP cloned into the multiple cloning site (MCS) of V5-miniTurbo-NES. Resulting in fusion proteins with the indicated sizes and harboring a N-terminal V5-Tag and C-terminal miniTurbo/NES module. **B** Fluorescence microscopy with p53-specific antibody (top panels) or EGFP (bottom panels) counterstained with DAPI. **C** Immunoblot after overexpression of p53-miniTurbo or EGFP-miniTurbo, treatment with SM for 2h and subsequent subcellular fractionation. Overexpression plasmids were detected using V5-Tag-specific antibody. Loading control for cytoplasm or nuclei: GAPDH, Histone 3 Reproduced from Galhuber et al. 2022 covered under the CC BY license.

Titration of optimal biotin concentration, labelling duration, and streptavidin pulldown

After validating our fusion constructs, we tested for optimal biotin concentrations and labeling times. Previous reports compared biotin concentrations between 50µM and 500µM with labeling times between 10min and 24h, revealing considerable differences on total biotin labeling (Branon *et al.*, 2018). Optimizing these parameters aims to balance between producing sufficient biotinylated proteins for MS analysis while omitting “over-biotinylation” leading to spurious results. Therefore, we titrated 125µM, 250µM, and 500µM exogenous biotin in either GM or SM for 2, 4, and 6h in HepG2 p53KO cells overexpressing p53-miniTurbo (Figure 5A). We normalized overall biotinylation detected with Streptavidin-HRP antibody to p53-miniTurbo expression levels (detected with p53-specific directly HRP conjugated

antibody) and found that total biotinylation is trending upwards with increased time- and concentration. In parallel, we tested for detectable changes in endogenous p53 localization upon a starvation stimulus (Figure 5B) and found that after 3h p53 is stabilized in the nuclear fraction. These observations paired with the intention to capture early signaling events towards p53, we chose 250µM biotin for 2h as experimental parameters. In a last step of protocol validation, we optimized the streptavidin bead amounts to ensure complete pulldown of biotinylated proteins after labeling (Figure 5C). Constant protein amounts (250µg) from HepG2 p53KO cells overexpressing p53-miniTurbo were pulled down with increasing amounts of streptavidin beads (0.5mg, 1mg, 2mg) resulting in clean flow through with the highest bead to protein ratio (2mg), that was subsequently used for the pulldown protocol for MS analysis.

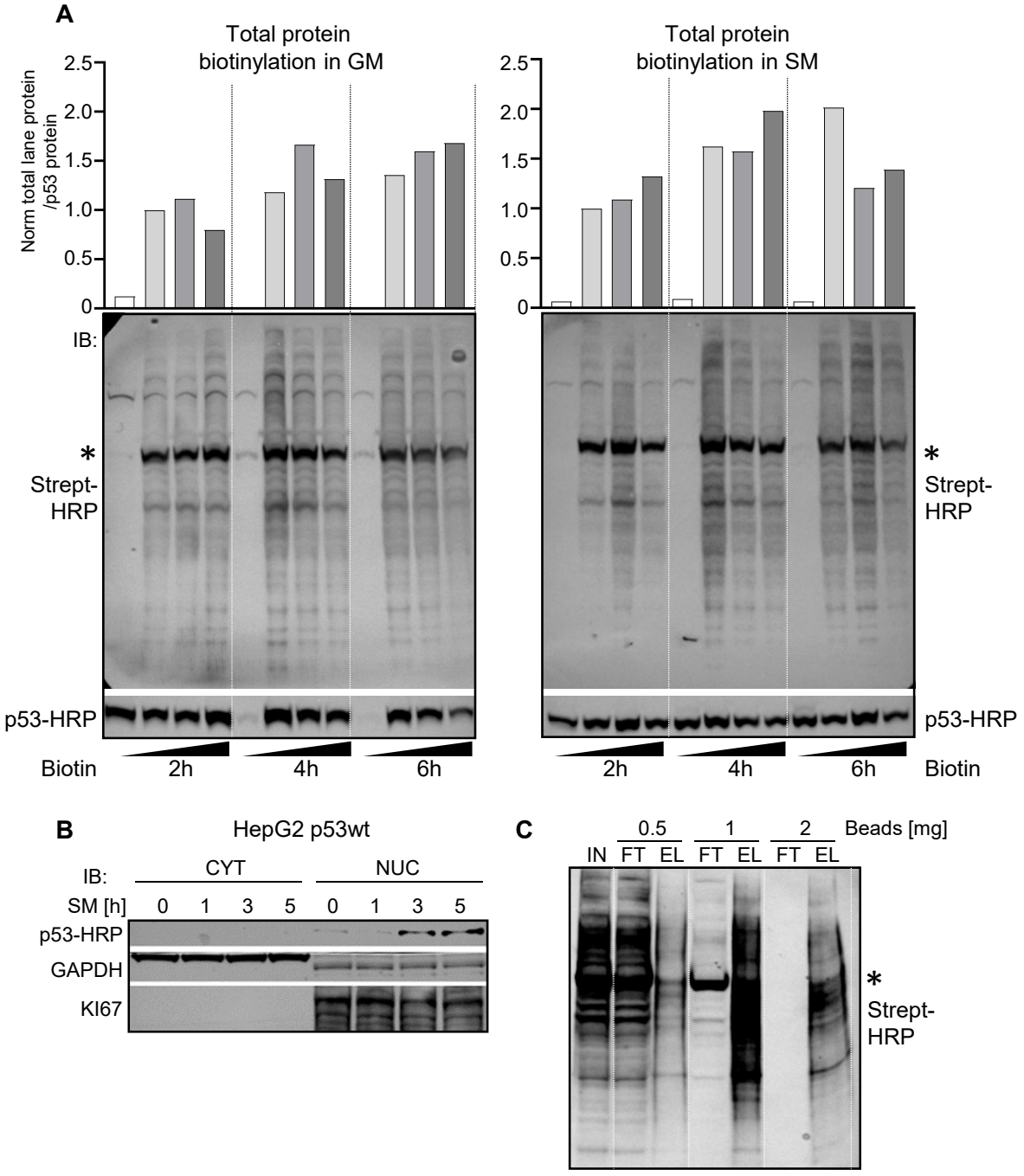

Figure 5 **Biotin titration and optimization of labeling window and streptavidin beads concentration for BioID. A** Total protein biotinylation after overexpression of fusion proteins (indicated with *) under GM (left panel) or SM (right panel) conditions with increasing biotin concentrations (black wedge from left to right: 0µM, 125µM, 250µM, 500µM) analyzed with streptavidin-HRP (bottom row). Asterisks indicate auto-biotinylated p53-miniTurbo. (Top row) total protein biotinylation normalized to overexpressed p53-miniTurbo reveals concentration- and time-dependently increased biotinylation. **B** Immunoblot showing HepG2 p53wt cells subjected to 5h SM and subsequent subcellular fractionation. p53 antibody indicates nuclear accumulation between 1 and 3h SM. Loading controls: GAPDH, KI67. **C** Immunoblot showing protein lysates from p53-miniTurbo overexpressing HepG2 p53KO cells pulled down with increasing amounts of streptavidin beads. Using 2mg beads completely pulls-down biotinylated proteins from 250µg total protein lysate. IN…input, FT…fow through, EL…eluate. Asterisk indicates auto-biotinylated p53-miniTurbo. Reproduced from Michenthaler, H. 2020 with permission of

Quantitative mass spectrometric analysis of cytoplasmic p53 interactome

We performed our experiments in triplicates (total 12 samples; 3 samples of each p53-miniTurbo GM, p53-miniTurbo SM, EGFP-miniTurbo GM, EGFP-miniTurbo SM) and used MaxQuant and Perseus for bioinformatics analysis. Additionally, we analyzed six untransfected HepG2 p53KO background controls, 3 samples each for GM and SM conditions, processed with our protocol including streptavidin pulldown. In the transfected samples, we detected 4832 proteins with MaxQuant and processed iBAQ values with Perseus. We filtered for proteins found in at least two biological replicates in each group resulting in 2500 proteins. After imputing missing values, we subjected those 2500 proteins to ANOVA testing, z-scoring, hierarchical clustering and generated a heatmap to reveal differentially biotin-labeled proteins (Figure 6A). ANOVA testing resulted in 609 proteins showing a significant abundance change in a least one group (ANOVA, FDR=0.05; Figure 6A left). From those proteins we manually selected clusters that are enriched in p53-miniTurbo groups over EGFP-miniTurbo groups (Figure 6A middle panel) and derived the according profile blots (Figure 6A right-most panel). A total of 137 proteins were significantly enriched under p53-miniTurbo GM conditions compared to p53-miniTurbo SM conditions (cluster 1; termed “GM_up”), 37 proteins were significantly enriched under p53-miniTurbo GM and SM conditions (cluster 2; termed “GM&SM_up”), and 98 proteins were significantly enriched under p53-miniTurbo SM (cluster 3; termed “SM_up”). Importantly, in all three clusters EGFP background labeling was unchanged between GM and SM conditions, underscoring that the enriched proteins are selective for p53-miniTurbo groups. Collectively, we find 272 proteins enriched over EGFP background, which we overlapped with BioGRID data of known physical p53 interactors (BioGRID: TP53 filtered for category evidence: Interactors with ONLY Physical Evidence (LTP or HTP); LTP low through put, HTP high through put). Ninety-four proteins were found in the database for known physical p53 interactors, while 177 proteins are putative novel p53 interactors or are localized within labeling range of p53-miniTurbo (Appendix Table 2). This large ratio (94/272 proteins: 34%) of detecting previously described p53 interactors strongly argues for the validity of our BioID approach. To assess differential protein abundances (fold changes between GM and SM conditions) we filtered the dataset for cluster 1 to 3 (272 proteins) and generated a volcano blot (Figure 6B).

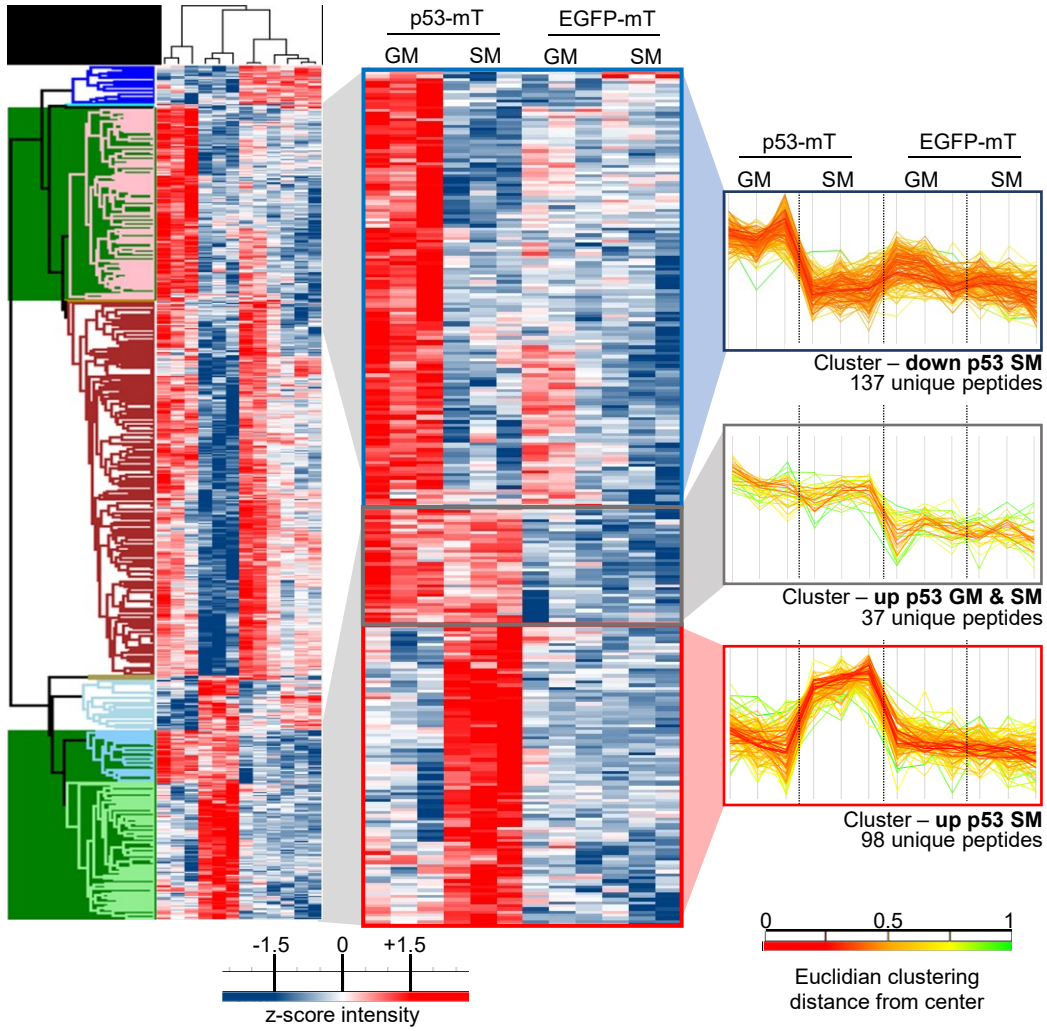

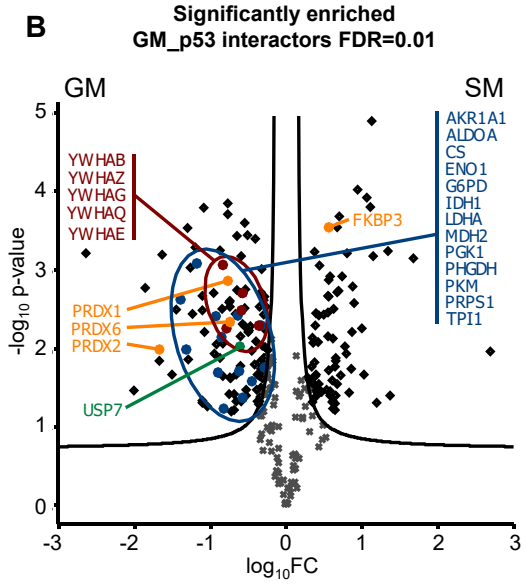

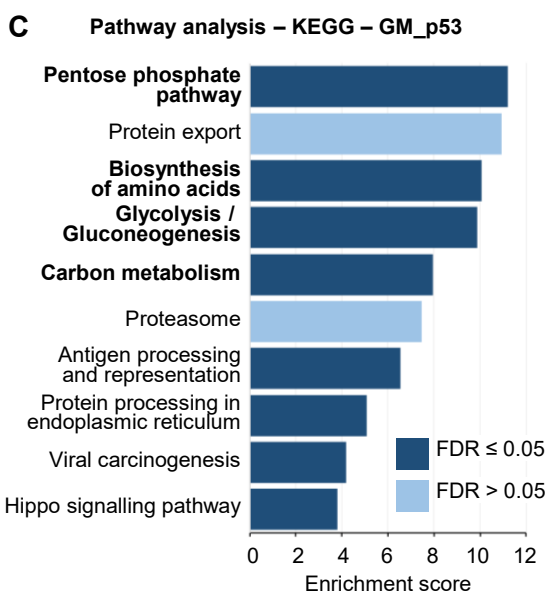

(Figure legend on next page)

Figure 6 **p53-dependent cytoplasmic interactome. A** Mass spectrometric data of 3 samples per group were analysed with ANOVA, z-scoring and hierarchically clustered (left, mid) (Euclidian distance, linkage: average). Blue colour indicates decreased abundance; Red colour indicates increased abundance. Clusters that show enriched p53 interaction over background controls (EGFP) were selected (indicated with green background) and their normalized proteins abundances (z-scores) are shown in profile blots (right). Red to green colour scale indicates Euclidian distance from centre. **B** Volcano blot showing 272 proteins enriched over EGFP background taken from profile blots in A. FDR=0.01. Proteins left from cut-off curve enriched in p53_GM samples. Proteins right from cut-off curve enriched under p53_SM conditions. Blue proteins refer to metabolic pathways analysed with KEGG overrepresentation analysis. Orange (PRDX1, PRDX2, PRDX6, FKBP3), green (USP7) and red (14-3-3) proteins were previously described in connection with p53 regulation/ubiquitination. **C** KEGG pathway overrepresentation analysis of proteins vicinal to p53 under GM conditions. Reproduced from Galhuber et al. 2022 covered under the CC BY license.

With Peroxiredoxin 1, 2, and 6 (PRDX1, PRDX2, PRDX6) we find a noticeable group of proteins vicinal to p53 under GM conditions. All three peroxiredoxins are known p53 interactors and PRDX2 was recently described to promote ubiquitination and degradation of p53 (Wang *et al.*, 2021), matching our assumption for permanent p53 protein turnover under basal conditions. We find Ubiquitin specific peptidase 7 (USP7 also known as HAUSP), highly interacting with p53 in GM_up group. USP7 is (after MDM4: 72 evidences)) the second most described TP53 interactor in the BioGRID database (USP7: 40 evidences) and well-known for its modulating function in the p53/MDM2 interplay (Reddy *et al.*, 2014; Tavana and Gu, 2017). Moreover, with 14-3-3 proteins (YWHAB, YWHAE, YWHAG, YWHAQ, and YWHAZ) we find several members of this adaptor protein family implicated with p53 regulation and a large spectrum of other general and specialized signaling pathways (Falcicchio *et al.*, 2020). To investigate enriched pathways within the protein clusters, we subjected cluster 1-3 to KEGG pathway overrepresentation analysis (Webgestalt) and analyzed for local network clusters with STRING (www.string-db.org). Intriguingly, KEGG overrepresentation analysis revealed proteins vicinal to p53 under GM conditions that are mapped to fundamental metabolic pathways, e.g. pentose phosphate pathway, biosynthesis of amino acids, glycolysis/gluconeogenesis, or carbon metabolism (Figure 6C), which suggests a close association of cytoplasmic p53 with key metabolic pathway enzymes. In addition, deriving local STRING network clusters with the GM_up group, we find 14-3-3 domain proteins, RHO GTPases, and metabolic pathway proteins enriched (Figure 7).

In the SM_up group (97 proteins) we also find proteins previously associated with p53. Peptidyl-prolyl cis-trans isomerase FKBP3 (also named FKBP25), was shown to promote MDM2 auto-ubiquitination and therefore p53 stabilization (Ochocka *et al.*, 2009). Interestingly, interaction of p53 with prolyl isomerases also affects cellular pathways downstream to p53 phosphorylation events. For example, p53 isomerization around phosphorylated p53 Ser46 via peptidyl-prolyl cis-trans isomerase NIMA-interacting 1 (PIN1) is known to increase and even

potentiate p53 transactivation potential (Mantovani *et al.*, 2015; Liebl and Hofmann, 2019). Surprisingly, with peptidyl-prolyl cis-trans isomerase NIMA-interacting 4 (PIN4) and peptidyl-prolyl cis-trans isomerase CWC27 homolog (CWC27) we find two more peptidyl-prolyl cis-trans isomerases in the SM_up group, suggesting previously undescribed proteins that potentially enhance p53 activation. With High mobility group proteins (HMGA1, HMGA2, HMGB1, HMGB2, HMGB3, HMGN1) we find several members of this family associated with p53 under SM conditions. HMG family members are essential proteins in genome architecture and dynamically change their association with DNA to modulate chromatin and transcriptional activity. Beyond that, HMG class of proteins also act as signaling regulators in the cytoplasm (Ozturk *et al.*, 2014; Mallik, Kundu and Chaudhuri, 2018) which could explain that we find HMG proteins associated with cytoplasmic p53. Also accumulated in the SM_up group is Transcription factor A, mitochondrial (TFAM). It functions in mitochondrial transcription regulation, is a known physical p53 interactor (Yoshida *et al.*, 2003) and regulates mitochondrial genes expression upon metabolic stress (Celestini *et al.*, 2018). TFAM, in analogy to HMG class proteins, harbors two HMG box domains, extending the pool proteins with p53 association containing HMG box domains.

Subjecting the 97 enriched p53 interactors in the SM_up group did not yield significant KEGG pathways or local STRING network clusters enrichment, revealing this group of proteins as more heterogeneous than GM_up interactors.

A

#term ID	term description	observed/ background gene count	strength	FDR	matching proteins in your network (labels)
CL:9278	14-3-3 domain, and regulation of TORC2 signaling	5/10	1.86	0.0247	YWHAE, YWHAG, YWHAB, YWHAQ, YWHAZ
CL:17048	RHO GTPases Activate WASPs and WAVEs, and actin filament organization	12/105	1.22	4.48E-05	VCL, PFN1, DSTN, ACTR3, ACTB, TAGLN2, FLNA, CAP1, ACTR2, FSCN1, WDR1, ACTG1
CL:17047	Mixed, incl. regulation of actin polymerization or depolymerization, and calponin homology (ch) domain	13/118	1.2	2.96E-05	VCL, PFN1, DSTN, ACTR3, ACTB, TAGLN2, FLNA, CAP1, ACTR2, FSCN1, WDR1, CFL1, ACTG1
CL:11549	Carbon metabolism, and Pyruvate metabolism	10/96	1.18	0.0021	TPI1, ENO1, PKM, MDH2, CS, PGK1, G6PD, ALDOA, IDH1, LDHA
CL:11548	Carbon metabolism, and Starch and sucrose metabolism	12/124	1.15	0.0002	PYGL, TPI1, ENO1, PKM, MDH2, CS, PGM1, PGK1, G6PD, ALDOA, IDH1, LDHA
CL:17049	RHO GTPases Activate WASPs and WAVEs, and actin filament organization	9/96	1.13	0.0247	VCL, PFN1, DSTN, ACTR3, ACTB, CAP1, ACTR2, FSCN1, ACTG1
CL:11547	Mixed, incl. carbon metabolism, and starch and sucrose metabolism	13/157	1.08	0.0002	PYGL, TPI1, ENO1, AKR1B1, PKM, MDH2, CS, PGM1, PGK1, G6PD, ALDOA, IDH1, LDHA

B

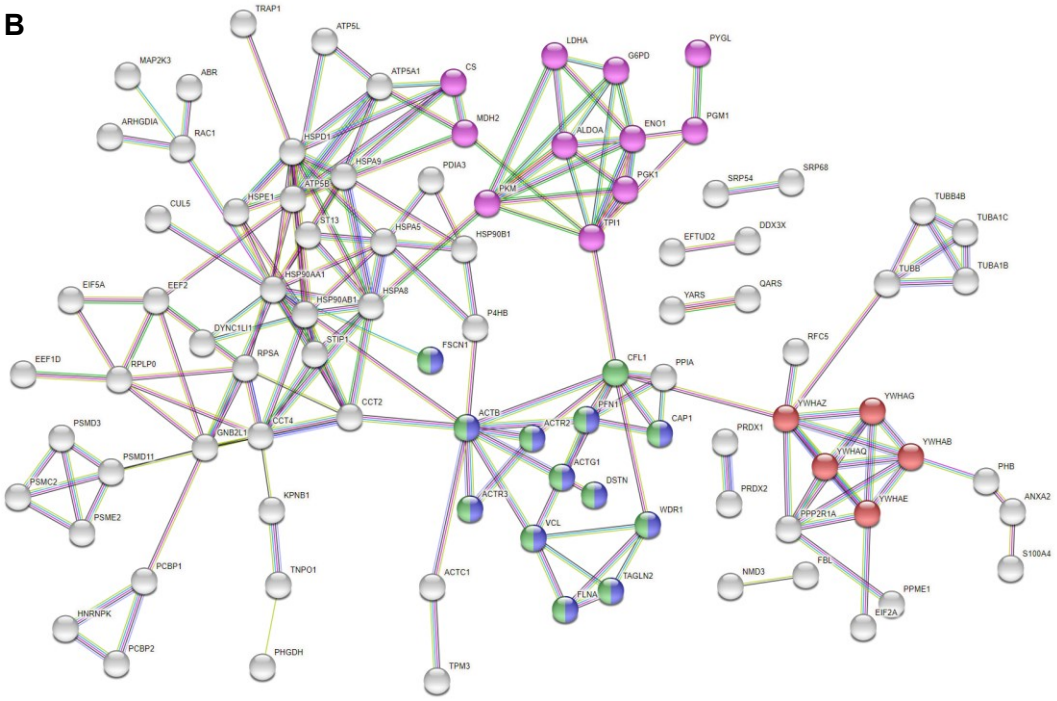

Figure 7 **Local STRING network clusters within GM_up group (137 proteins). A** Clusters with highest strength (enrichment) and FDR (5%) are listed. STRING Basic settings: full STRING network. High confidence interaction score: 0.900. Disconnected nodes in the network are hidden. **B** Local network clusters are indicated in a protein interaction map. Pink…CL:11548, Blue…CL:17048, Green…CL:17047, Red…CL:9278.

As another level of controlled analysis, we compared the 272 proteins enriched over EGFP background control (volcano blot Figure 6B) with their abundance in untransfected HepG2

background controls, which we included in our MS runs to check for protein expression levels in HepG2 p53KO cells. Overall, protein abundances were not significantly altered between GM and SM in untransfected background controls (Figure 8A). Of 272 proteins from groups GM_up, SM_up, and GM&SM_up we found 236 in untransfected HepG2 cells, whereas 36 proteins are not occurring in at least 2/3 replicates in these control groups (Appendix Table 3). Based on their absence in untransfected background controls, we interpret this group of proteins highly likely p53 interactors, when biotin-labelled in p53-miniTurbo groups and significantly enriched over EGFP-miniTurbo background controls. Among these 36 proteins, we find 10 previously described p53 interactors (BioGRID), e.g. previously described USP7, as well as 26 highly probable candidate interactors (Figure 8B).

A

BioID –
Total protein changes
untransfected controls

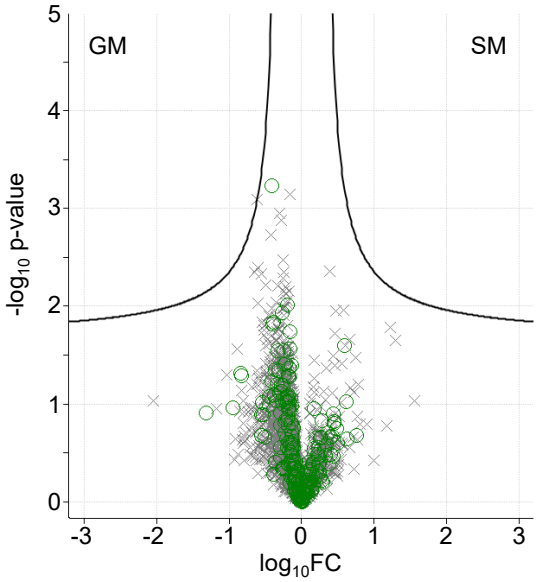

B

Proteins significantly enriched
in p53-miniTurbo over EGFP background
lacking in untransfected controls

AGFG1	HNRNPF	PCBP1	TAF15
CCDC9	IGBP1	PDLIM5	TNS3
CCNL2	KIAA1522	PSMC2	TP53
CPLX2	KIAA1598	RBM17	TPM3
DNAH10	LYPLA2	RPAP3	TTC1
DYNC1LI1	MED15	SCAF11	UBAP2
EIF4H	MRE11A	SEC23A	USP7
FUBP1	NUDC	SMAP; C11orf58	WDR13
HN1L	PAK2	ST13; ST13P5; ST13P4	YAP1

Figure 8 **Protein abundances in GM and SM conditions in untransfected HepG2 background controls. A** Volcano blot showing differentially identified proteins between GM and SM conditions in HepG2 cells processed with our standardized protocol for BioID. 2500 proteins found in at least 2/3 replicates. Green circles indicate 236 proteins enriched in p53-miniTurbo samples over EGFP-miniTurbo samples in Biotin ligase overexpressing cells. (Perseus: cutoff curve, FDR0.01, s0:0.1) **B** List of 36 proteins not detected in untransfected controls but enriched in p53-miniTurbo vs EGFP-miniTurbo groups. Grey boxes indicate previously described p53 interactors (BioGRID). White boxes indicate novel p53 interactors. Reproduced from Galhuber et al. 2022 covered under the CC BY license.

High-confidence p53 cytoplasmic interaction network

To assess for high-confidence p53 proximity interactors and generate proximity maps from our BioID dataset we employed SAINTscore analysis (Choi *et al.*, 2011; Gingras *et al.*, 2013). To delineate the p53 proximity network we scored spectral counts (sum of each individual peptide

per group) in each p53_GM and p53_SM samples against the pooled EGFP_GM and EGFP_SM controls. In handling the background controls as one group, we ensure that identified interactors in p53 groups are enriched over both EGFP_GM as well as EGFP_SM. SAINTscore ≥0.9 were considered as high-confidence interactions (Figure 9A, B).

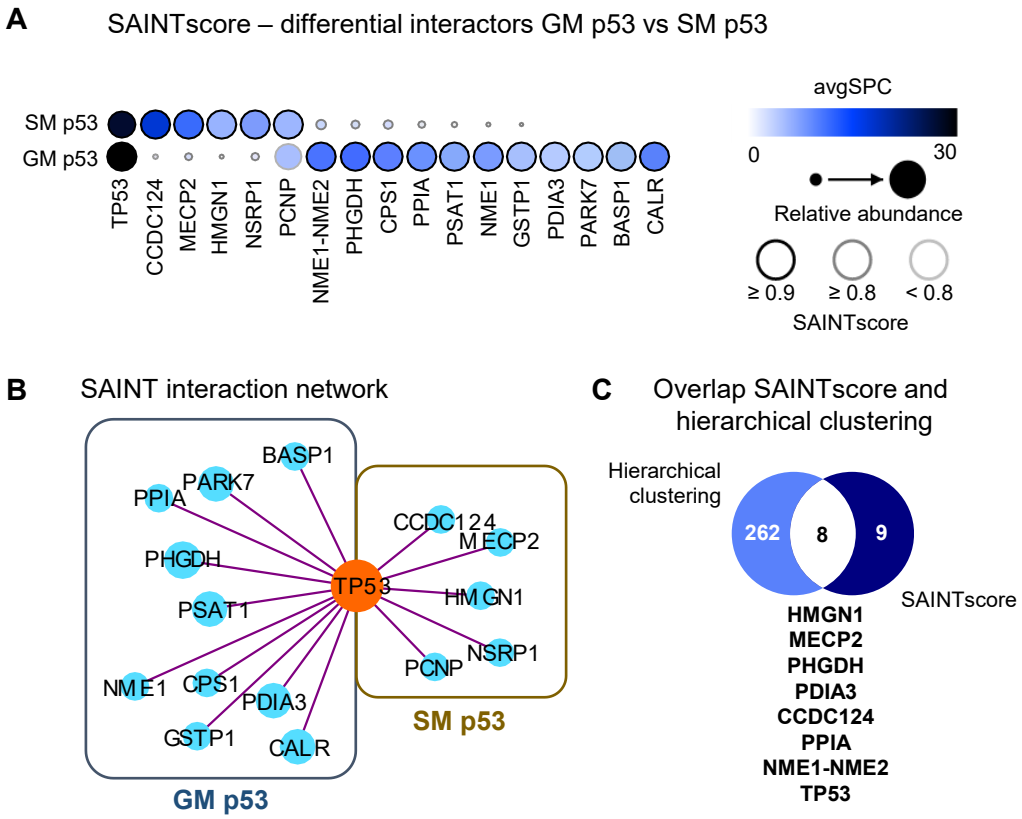

Figure 9 **SAINTscore analysis. A** Dot plot of interaction partners identified with BioID (SAINTscore ≥0.9 black circles for high confidence interactors) **B** Interaction network of proteins interacting under growth medium or starvation medium with p53. Green circles indicate proteins that are associated with serine biosynthesis. **C** Overlap of proteins found with two complementary analysis methods (Hierarchical clustering *Figure 6* and *Figure 7* vs SAINTscore). Reproduced from Galhuber et al. 2022 covered under the CC BY license.

Eight proteins found with hierarchical clustering also qualified as high confidence interactors with SAINTscore (Figure 9C). With HMGN1 and Methyl-CpG-binding protein 2 (MECP2) this overlapping group contains 2 proteins that are mostly associated with nuclear localization. These results either suggest that HMGN1 and MECP2 have previously undescribed cytoplasmic roles, or that the biotin labelling results from a spill over of fusion protein into the nucleus. Furthermore, we confirm candidate proteins from the hierarchical clustering related to metabolic functions or protein translation. D-3-phosphoglycerate dehydrogenase (PHGDH) (SAINT probability (SP): GM 0.96, SM 0.02), an enzyme centrally involved in amino acid metabolism, catalyses both, the first step of the serine biosynthesis pathway and the reversible

oxidation of 2-oxoglutarate to the oncometabolite 2-hydroxyglutarate (Fan *et al.*, 2015). Intriguingly, with SAINTscore analysis, we also find the protein the catalyses the second step of serine biosynthesis, Phosphoserine aminotransferase (PSAT1) (SP: GM 0.93 SM0.07). If the p53/PHGDH or p53/PSAT1 interaction is functional or relevant in a cellular context is not described to date. However, in the context of p53, combined depletion of nutritional serine with PHGDH inhibition suggests beneficial outcomes in cancer therapy (Tajan *et al.*, 2021) and p53 inhibits PHGDH expression on transcriptome level (Ou *et al.*, 2015). Therefore, p53/PHGDH protein interaction could function as a potential feedback mechanism in the context of differential nutrient availability.

An interesting starvation-specific candidate interactor is Coiled-coil domain-containing protein 124 (CCDC124). This protein was recently reported to resemble the mode of action of ribosomal hibernation factors and found accumulating at idle ribosomes (Wells *et al.*, 2020). CCDC124 shows RNA binding properties and acts as potential transcription coactivator (GO – molecular function) but seems to fulfil at least a dual cellular function as it also localizes at the centrosome and midbody during cytokinesis (Telkoparan *et al.*, 2013). This would imply that starvation either leads to p53 localization at hibernating ribosomes or that p53/CCDC124 interaction occurs at the centrosome/midbody. Centrosomal p53 was described previously and was recently found to act as mitotic fail safe or “centrosome-loss sensor” (mitotic surveillance pathway) to prevent chromosomal abnormalities during cytokinesis and induces p53-mediated cell cycle arrest (Lambrus and Holland, 2017; Contadini *et al.*, 2019). In this sense, the p53/CCDC124 interaction at the centrosome suggests another mode of how p53 prevents tumorigenic transformation. In particular, follow up experiments would first need to distinguish between p53/CCDC124 interactions at the ribosome or centrosome to enable further, more detailed research.

Overall, our analyses reveal many known p53 interactors as well as previously unknown associations. Of particular interest, we find a large number of metabolic enzymes as well as ubiquitin ligases as well as proteins associated with ROS control near p53 under GM conditions. Those complexes seem to dissociate under SM conditions that lead to significant interactions under SM conditions. To delineate those findings we suggest further functional studies with suitable biochemical or molecular biological methods.

Unique peptide and biotinylated peptide analysis

To get more detailed insights, we re-examined our proteomics data on peptide level. In total, we found 33808 peptides (untransfected controls, p53-miniTurbo, or EGFP-miniTurbo) which we overlapped based on their occurrence in a Venn diagram (Figure 10A). 3850 peptides

(11.38%) were detected in samples overexpressing p53-miniTurbo, while being not detectable in either untransfected background control or EGFP-miniTurbo (29958 peptides, 88.61%). Looking more closely at the p53-specific subset, we found different peptide counts in the six replicates (GM and SM, n=3 each) and assume that a higher number of peptides also means a higher probability of a true interactor. While the majority of the peptides occur in up to 3/6 replicates (97.32%), only 103 peptides are found in 4 or more p53-containing replicates (2.68%) (Appendix Table 5) originating from 70 different proteins (Figure 10B).

In a parallel analysis, we screened for biotinylated peptides in our proteomic dataset. We assumed that peptides harboring multiple potential biotinylation lysine (K) sites could fulfil two essential criteria. First, biotinylation at multiple K sites leads to stochastic binding and purification with only one biotin residue at the streptavidin beads, while secondly, the unbound biotin residues on the same peptide leaves traceable properties in MS bioinformatic analysis. Upon on-bead digestion, the streptavidin-bound biotinylation is enzymatically cut, while additional biotinylated K sites on peptides harbor a biotin PTM at lysines. Therefore, we screened for biotinylated peptides by adding the modification Biotin(K)="C(10) H(14) N(2) O(2) S" (+226.077598) possible on any K or protein N-terminus to our search space in a MaxQuant search. This search resulted in 65 peptides harboring biotinylated K residues, of which 10 peptides originating from 6 proteins were exclusively found in p53-miniTurbo overexpressing samples and not in EGFP or untransfected background controls (Figure 10C, Appendix Table 4). Confirming the use of a fusion protein, p53-miniTurbo auto-biotinylation resulted in the most observed biotinylated p53 peptides (found in 5/6 or 6/6 replicates p53GM or p53SM), while others were less abundant. Charged multivesicular body protein 4b (CHMP4B) was found in 3/6 replicates and Calponin-3 (CNN3), Src substrate cortactin (CTTN), Stomatin-like protein 2, mitochondrial (STOML2) each found in 1/6 replicates. Interestingly, it was demonstrated that CHMP4B (as a member of the ESCRT-III complex) is recruited to midbodies and is implicated in mediating the final stages of cytokinesis (Elia *et al.*, 2011). This finding strongly overlaps with the previously mentioned p53/CCDC124 interaction and suggests p53 interaction at the midbody/centrosome.

However, standing out in biotinylated peptide analysis are Serine/threonine-protein kinase PAK 2 (PAK2) found in 4/6 replicates and Transgelin (TAGLN) found in 5/6 replicates. Interestingly, when we overlap the set of unique peptides with the set of biotinylated peptides, we were able to reduce the pool of highly likely p53 interactors to CTTN, PAK2, and TAGLN (Figure 10D). PAK2 is also contained in the group of 36 proteins significantly enriched in p53-

miniTurbo over EGFP-miniTurbo sample and absent in untransfected background controls (Figure 8B, previous chapter).

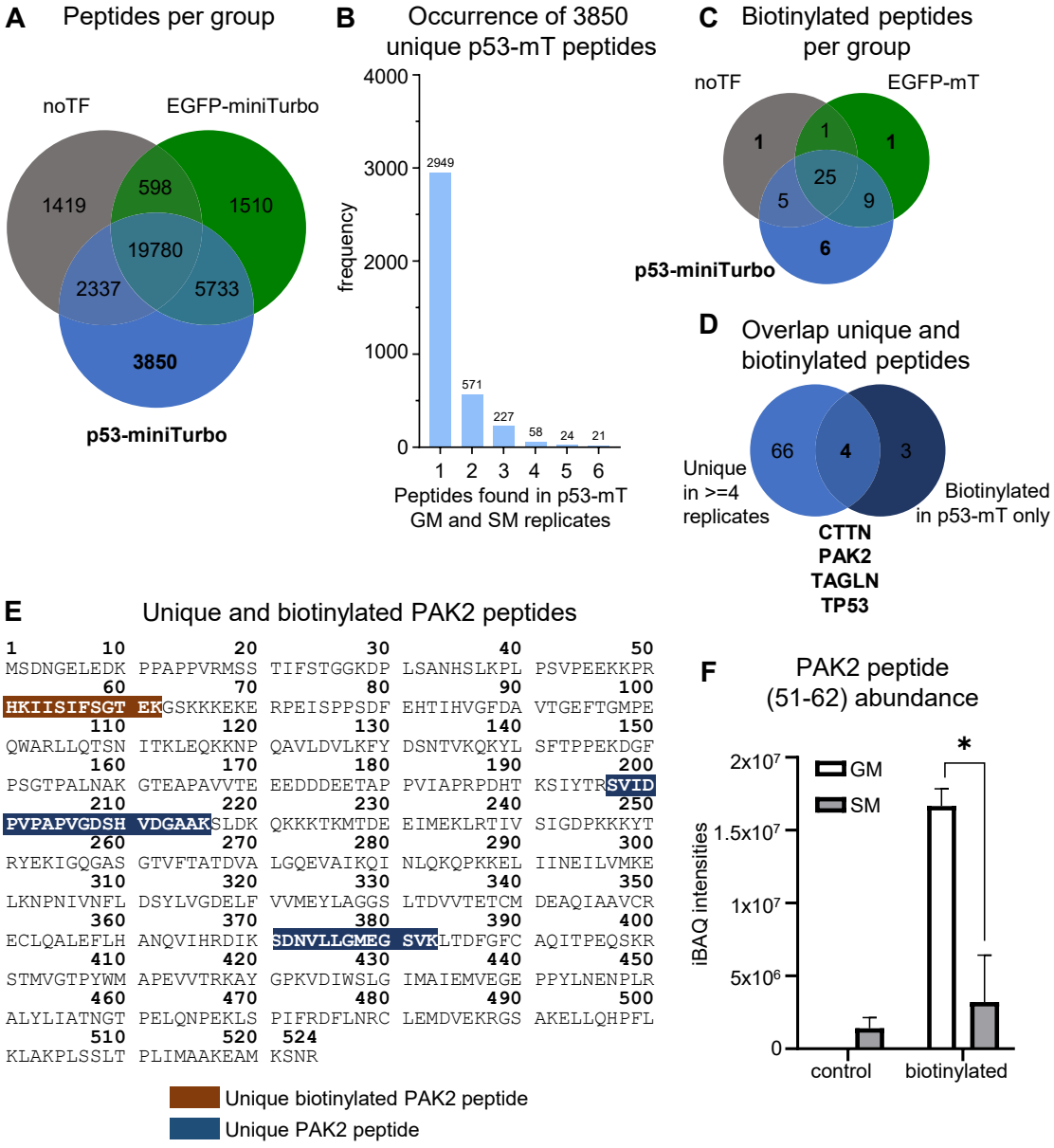

Figure 10 **Occurrence and distribution of peptides detected with MS. A** Overlapping groups of peptides found in either untransfected background control (grey), EGFP-miniTurbo (green), or p53-miniTurbo (blue) samples. **B** Histogram of total peptide counts in p53_GM and p53_SM samples from 1/6 to 6/6 samples. **C** Biotinylated peptides found in each group (colors as in A) **D** Overlap of peptides found enriched over background controls in more than or equal to 4 replicates and biotinylated peptides. **E** PAK2 protein sequence with indicated unique peptides (blue) as well as unique biotinylated peptide (brown), that are absent in untransfected controls and EGFP-miniTurbo samples. **F** Specific PAK2 peptide 51-62 abundance in control conditions and p53-mT conditions. Partly reproduced from Galhuber et al. 2022 covered under the CC BY license.

To investigate PAK2 in more detail we compared unique peptides and biotinylated peptides (Figure 10E) and we found that the amino acid sequence (51)HKIISIFSGTEK(62) qualified as unique peptide as well as biotinylated peptide. iBAC abundances in Figure 10F indicate that this peptide is present at very low levels in control conditions. More importantly, using p53-miniTurbo protein led to pronounced biotinylation levels under growth medium conditions that are significantly reduced under starvation.

Taken together, these observations render PAK2 a highly probable candidate interactor for p53 under growth medium conditions, which is lost under starvation conditions, leading to the hypothesis that loss of PAK2 interaction could reflect a prerequisite for subsequent p53 stabilization and translocation. First, to test for PAK2 for interaction with p53, we employed nuclear magnetic resonance (NMR) spectroscopy with collaborators at the Medical University of Graz.

NMR spectroscopy to assess p53 / PAK2 interaction

To analyze domain specific p53-PAK2 interaction we produced recombinant protein constructs of p53 transactivation domain 1-94 amino acids (aa) (p53 TAD), p53 DNA binding domain 94-312aa (p53 DBD), and PAK2 N-terminal domain 1-212aa. PAK2 N-terminal domain represents the auto-inhibitory/regulatory domain and was selected based on the differentially biotinylated peptide we found in our peptide analysis (Figure 10E), whereas PAK2 C-term domain (213-524aa) represents the kinase domain. We labelled each construct with 15N and titrated p53 DBD against PAK2 N-terminal domain as well as p53 TAD against PAK2 N-terminal domain (PAK2 N-term) (Figure 11A-C). In NMR spectroscopy, titration of different 15N labelled peptides leads to chemical shift perturbation (CSP) that indicate direct interaction of proteins. When titrating PAK2 N-term to a solution containing 15N- labeled p53 DBD we observed CSPs with increasing amounts of PAK2 N-term (Figure 11A).

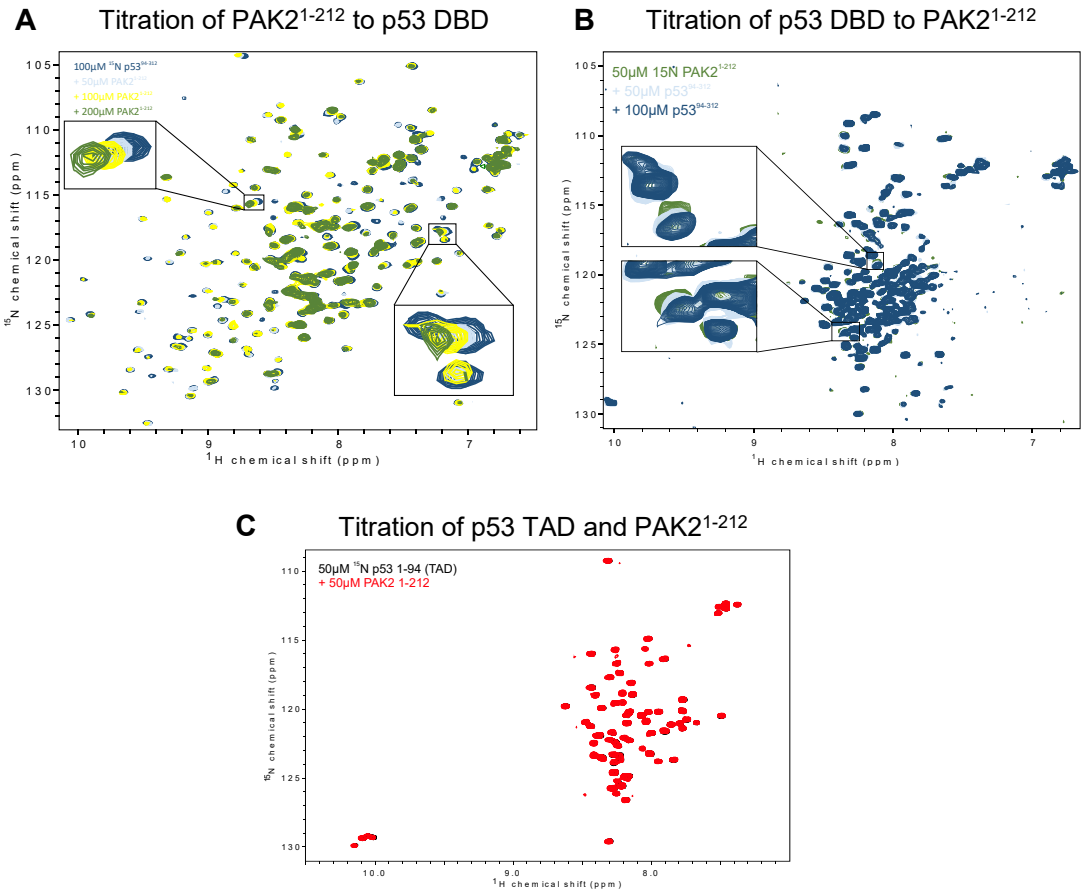

Figure 11 **NMR binding assay for p53 and PAK2. A** 1H, 15N HSQR NMR spectra of 15N-labelled recombinant p53 DBD (94-312) incubated with increasing concentrations of recombinant PAK2 N-terminal domain (1-212). Insets show clear concentration-dependent chemical shift perturbations. Bottom: intensity ration of p53 DBD residues in bound vs free state. **B** 1H, 15N HSQR NMR spectra of 15N-labelled N-terminal PAK2 domain (1-212) incubated with increasing concentrations of p53 DBD (94-312). Insets show clear concentration-dependent chemical shift perturbations. **C** NMR spectrum of 15N- labelled p53 transactivation domain (TAD, 1-94) with PAK2 N-terminal domain (1-212) showing no chemical shift perturbation. Reproduced from Galhuber et al. 2022 covered under the CC BY license.

Confirming this, we find CSPs in a reverse experiment when using 15N- labelled PAK2 N-term for titrating p53 DBD (Figure 11B). To test whether PAK2 also bind to p53 TAD we titrated PAK2 N-term into 15N- labelled p53 TAD, where we did not observe any CSP, indicating that PAK2 protein binding is specific for p53 DBD (Figure 11C). We limited our analyses to the PAK2 N-term domain and did not check for interaction with PAK2 C-term kinase domain.

PAK2/p53 protein interaction in HepG2 wt cells

Based on the potential interaction of PAK2 N-terminal domain with the p53 DBD, we probed the PAK2/p53 interaction in a cellular context and conducted co-IP experiments in HepG2 p53 wt cells, as well as p53/PAK2 overexpression experiments in HepG2 p53KO cells. Although

we have made huge efforts to prove co-IP p53/PAK2 in a cellular context, we have not succeeded in either approach.

To further investigate the relevance of the PAK2/p53 interplay *in vitro*, we first used a PAK2 inhibitor FRAX597 (Licciulli *et al.*, 2013) on HepG2 wt cells. FRAX597 acts as potent ATP-competitive inhibitor of group 1 PAKs, one of two subgroups in the PAK family ((Liu, Liu and Dong, 2021) with high specificity for PAK1-3 over PAK4-6. We treated HepG2 cells with 100nM FRAX597 and found that the well-known p53 target gene CDKN1A was significantly upregulated while MDM2 mRNA levels were mostly unaffected (Figure 12A top panel). In addition, p53 protein stabilization and target gene activation (CDKN1A) with even lower concentrations of FRAX597 (20nM) were reflected on protein abundances shown in Figure 12A (bottom panel).

To test if we could replicate the effects of pharmacological PAK2 inhibition with gene silencing, we established a PAK2 RNA interference protocol. Confirmingly, upon almost significant reduction in PAK2 mRNA levels ($p=0.052$) we find CDKN1A and, in contrast to FRAX597 treatment also MDM2 mRNA levels slightly increased (Figure 12B). Given our hypothesis that dissociation of PAK2 and p53 is a prerequisite for p53 nuclear stabilization we next treated HepG2 wt cells either with FRAX597 or gene silencing and subjected the cells to subcellular fractionation. Both approaches lead to cytoplasmic as well as nuclear p53 accumulation, more pronounced with FRAX597 inhibitor (Figure 12C, D), which could be explained with residual PAK2 activity in the silencing approach.

Therefore, these pharmacological and gene silencing interventions suggest a functional p53/PAK2 axis in HepG2 cells and, considering our experimental setup in the BioID experiments, renders PAK2 a highly likely p53 regulator in the context of a switch between nutrient abundance and deprivation.

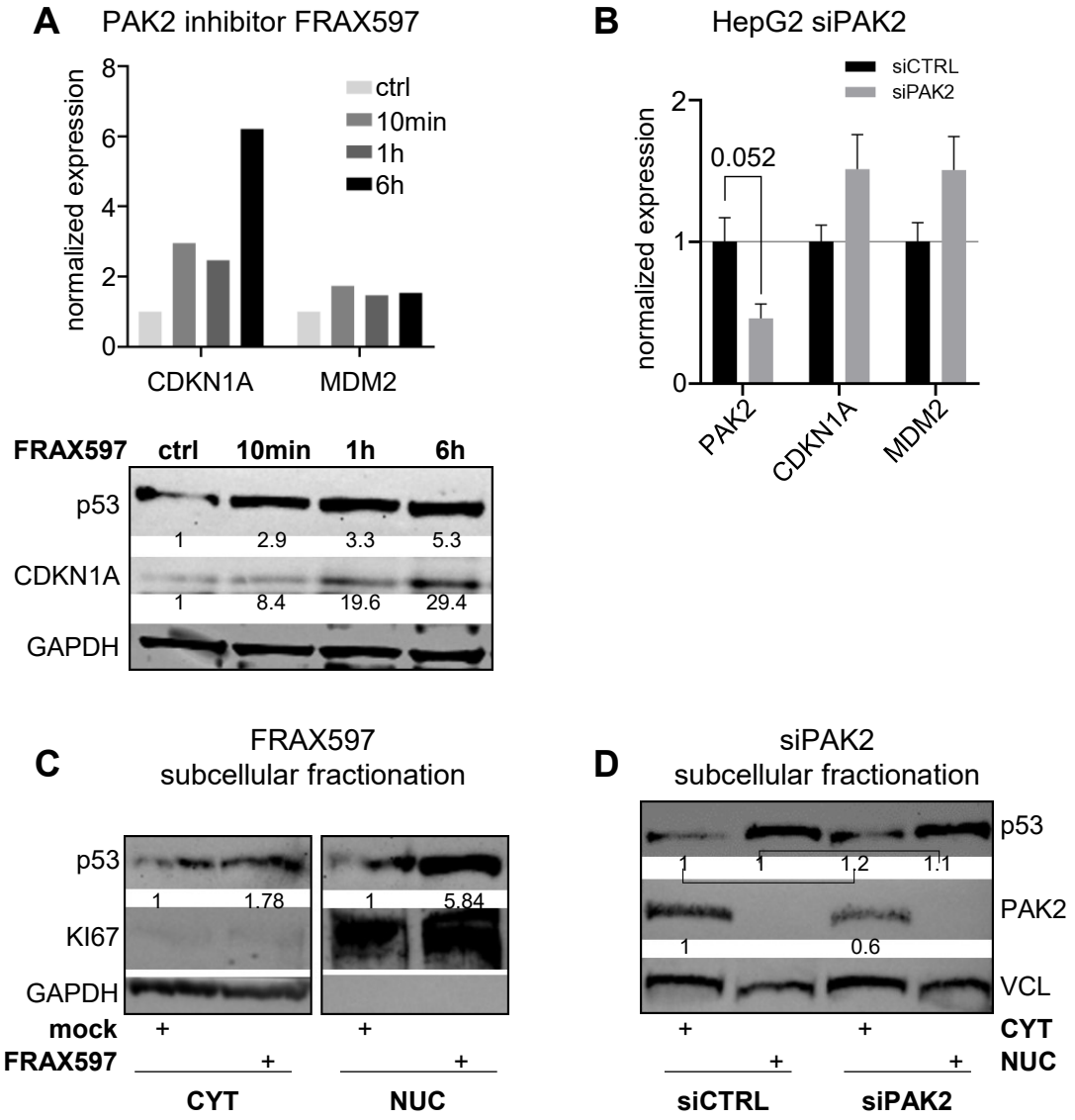

Figure 12 **Serine/threonine-protein kinase PAK2 upstream regulates p53. A** (top) RT-qPCR showing p53 target gene activation upon PAK2 inhibition with FRAX597 (100nM) in HepG2 cells. N=1. (bottom) Immunoblot showing time course experiment with PAK2 inhibitor FRAX597 (20 nM) over 6 hours of treatment. GAPDH loading control. **B** RT-qPCR showing p53 target gene activation upon PAK2 silencing in HepG2 cells. (Student's t test) **C** Subcellular fractionation after FRAX597 treatment (1µM) shows nuclear p53 accumulation. GAPDH loading control. KI67 nuclear quality control. **D** Subcellular fractionation after PAK2 gene silencing (siPAK2) shows cytoplasmic and nuclear p53 accumulation. Vinculin (VCL) loading control. In all western blots densiometric analysis is indicated with black numbers below bands Reproduced from Galhuber et al. 2022 covered under the CC BY license.

Cross-linking affinity purification mass spectrometry (XL-AP-MS)

Since we observed p53 nuclear translocation upon starvation, we next set out to identify starvation-specific nuclear p53 interactors. Those starvation-specific subsets could determine downstream transcriptional programs and ultimately define the p53-induced and starvation-specific transcriptional landscape.

To screen for nuclear p53 interactors we employed a XL-AP-MS as previously published (Mohammed *et al.*, 2016). HepG2 wt cells were treated with either GM or SM for 24h and cross-linked with 1% FA. We controlled for p53-specific crosslinking by comparing HepG2 wt cells with HepG2 p53KO cells and confirmed that high-molecular weight complexes (HMWC) accumulate in p53-proficient cells particularly under starvation, while these complexes are absent in p53KO cells (Figure 13A). HMWC are large clusters of proteins, in the case of nuclear p53 most probably chromatin interactors, that are crosslinked and not separable during electrophoresis. Crosslinked nuclei with p53-containing HMWCs were isolated and subjected to LC-MS/MS after p53-specific pulldown (Workflow see Figure 13B).

In total we identified 1,008 peptides which were annotated to their corresponding proteins with MaxQuant and quantified with iBAQ values (Schwanhäusser *et al.*, 2011). The Pearson correlation between biological replicates was on average 0.94 and the different biological replicates clustered together in a principal component analysis (Figure 13C). We successfully pulled down p53 containing complexes, which is confirmed by identifying p53 peptides in both GM and SM conditions, which we not found in IgG isotype controls (Figure 13D). Based on our initial protocol validation by western blotting (Figure 13A), we were also able to find more crosslinked complexes in SM conditions, reflected in higher average spectral counts for peptides in SM against GM samples (Figure 13E).

We subjected the identified peptides to SAINTscore analysis which yielded a dot plot of differential interactors between GM and SM, as well as a protein interaction map for p53 in SM (Figure 14A). Focusing on metabolic pathways the most striking finding is an association of p53 with UTP--glucose-1-phosphate uridylyl-transferase (UGP2) (SP: GM 0.61, SM 0.93) that is the only protein that catalyzes the conversion of glucose-1-phosphate into UDP-glucose in mammals. UDP-glucose has multiple biochemical functions and serves not only as precursor for glycogen synthesis (Adeva-Andany et al., 2016) but also in the hexosamine biosynthetic pathway resulting in glycosylation of proteins and lipids, with many implications in tumorigenesis and tumor progression (Varki, 2017; Akella, Ciraku and Reginato, 2019; Mereiter et al., 2019). Strikingly, according to protein interaction databases (IntAct, BioGRID) both proteins p53 and UGP2 share multiple reported physical interactions with ariadne RBR E3 ubiquitin protein ligase 2 (ARIH2) in different experimental approaches (Stelzl et al., 2005; Luck et al., 2020) that might represent a common ubiquitin ligase that targets both proteins. ARIH2 (also known as TRIAD1) was also reported in low throughput experiments (co-IP) to promote p53 stability by binding its C-terminus and initiating its dissociation from MDM2 (Bae et al., 2012). The combination of these results with our new observation may represent a

crucial finding linking glucose metabolism and the regulation of p53. Also, previous studies have detected UGP2 in nuclear fractions of lung cancer cells (Sun et al., 2019). Hence, co-localization (and maybe interaction) of UGP2 and p53 might open the possibility of previously unappreciated functions in transcriptional regulation or nutrient-related signal transduction. Beyond UGP2, another enzyme Galactokinase (GALK1; SP GM 0.89 SM 0.86) is enriched in both GM and SM conditions. GALK1 converts galactose into galactose-1-phosphate and with that facilitates it for conversion into UDP-galactose, that in turn is interconvertible to UDG-glucose. This observation makes the interplay of p53 with enzymes of sugar metabolism an exciting object of research. Anyhow, to confirm our RIME interaction data for UGP2, we conducted a co-IP experiment where we overexpressed HA-tagged p53 and FLAG-tagged UGP2 in HepG2 p53KO cells and kept the cells either in GM or SM. Importantly, we confirmed p53/UGP2 interaction in SM samples with a successful pulldown of HA-p53 using FLAG-beads specific for FLAG-UGP2 (Figure 14B). Of note, in all experiments conducted with FLAG-UGP2, its overexpression was very pronounced in SM conditions, while GM mostly showed very weak or absent protein abundance. This could imply that the lack of nutrients is not only a prerequisite for UGP2 stabilization but also for its interaction with p53. We additionally tested for other metabolism-associated candidate proteins from our XL-AP-MS experiment (e.g., IDH1 SP: GM 0.74, SM 0.91)) with co-IP but these data were not conclusive (MRE11A, RAD50, CTNNA1, TPI1 data not shown).

Along with metabolic enzymes, Sorbin and SH3 domain-containing protein 1 (SORBS1) emerged as another differential candidate interaction protein (SP: GM 0.29, SM 0.82) from our data set and was confirmed with co-IP (Figure 14C). SORBS1 was previously related to glucose metabolism in mouse experiments by regulating E3 ubiquitin-protein ligase CBL (CBL) phosphorylation and thereby facilitating the link of CBL to the insulin receptor, which is required for insulin-stimulated glucose transport (Baumann *et al.*, 2000). In line with that, Sorting nexin-1 (SNX1; SP GM 0.93 SM 0.99) and Sorting nexin-2 (SNX2; SP GM 0.63, SM 0.87) that we also found in our SM enriched dataset are part of insulin receptor binding (GO-term:0005158) and trafficking. Additionally, we find Sorting nexin-27 (SNX27; SP GM 0.73, SM 0.92) and Sorting nexin-5 (SNX5; SP GM 0.81, SM 0.78) that are involved in several stages of intracellular trafficking, i.e. endosome-to-plasma membrane transport (Van Weering *et al.*, 2012). In combination, these findings could point towards an involvement of p53 in the context of anterograde and retrograde receptor transport that harbors critical biological function in cellular homeostasis and tumorigenesis (Parachoniak and Park, 2012).

Interestingly, we also find SORBS2, a protein closely related to SORBS1, enriched in our SM dataset (SP: GM 0.48, SM 0.87). In high-throughput analyses SORBS1 and SORBS2 were previously reported to interact with PAK2 (Kärkkäinen *et al.*, 2006), which we identified with BioID, and SORBS2 was reported to interact with MDM2 (Wang *et al.*, 2011). In general, SORBS2 mainly acts as adaptor protein in signaling complexes that links kinase activities with structural cellular components (e.g., actin fibers, or focal adhesions). However, we should note that in the BioID study we observed a dissociation of p53/PAK2 under SM conditions, whereas with RIME we found an increased association with SORBS1/2 in cross-linked, isolated nuclei. The relationship between these seemingly orthogonal results and whether the interaction of p53/PAK2 and p53/SORBS1/2 is mutually exclusive would be interesting to explore in the future. In combination our complementary approaches with overlapping results render our findings relevant for follow-up studies. Together, in the context of nutrient deprivation the interaction of p53 with SORBS or SNX proteins could point towards an involvement of p53 in large-scale cellular rearrangements e.g., structural remodeling in the nucleus, receptor internalization, or nuclear receptor function (e.g., insulin receptor (Hancock *et al.*, 2019)).

With our crosslinking experiments we were also able to demonstrate nuclear p53 interaction with previously p53-associated proteins (BioGRID). DNA repair protein RAD50 (RAD50; SP GM 1 SM 1) Double-strand break repair protein MRE11 (MRE11; SP GM 0.65, SM 0.8), DNA topoisomerase 2-binding protein 1 (TOPBP1; SP: GM 0.96, SM 0.97) or Mediator of RNA polymerase II transcription subunit 12 (MED12; SP: GM 0.68, SM 0.97). Importantly, both RAD50 and MRE11 are central proteins of the MRN complex that not only has vital functions in sensing and repairing DNA damage, but also acts at stalled replication forks to mediate DNA replication stress response (Fournier, Kumar and Stirling, 2018; Bian *et al.*, 2019). In our context this interaction could imply, that nutrient deprivation directly leads to stalling in DNA replication that is sensed and mediated via p53/MRE11/RAD50 interaction. Research is currently ongoing to determine whether p53 is involved in replication stalling itself or in the resumption of replication. In any case it seem certain that p53 acts as component in the replisome machinery at replication forks (Ho, Tan and Lane, 2020) thereby influencing cellular and DNA integrity.

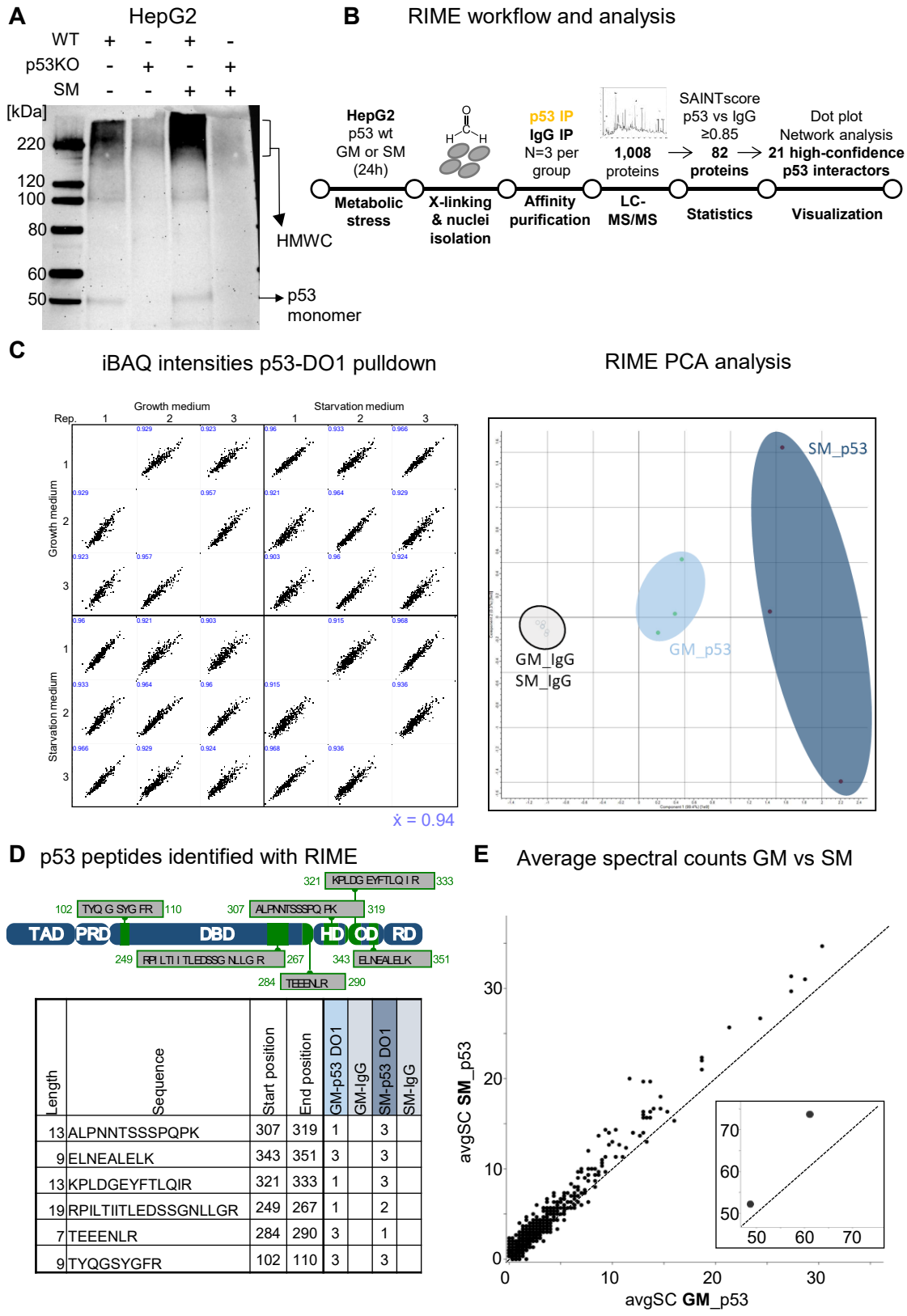

Length	Sequence	Start position	End position	GM-p53 DO1	GM-IgG	SM-p53 DO1	SM-IgG
13	ALPNNTSSSPQPK	307	319	1		3	
9	ELNEALELK	343	351	3		3	
13	KPLDGEYFTLQIR	321	333	1		3	
19	RPILTIITLEDSSGNLLGR	249	267	1		2	
7	TEEENLR	284	290	3		1	
9	TYQGSYGFR	102	110	3		3	

Figure 13 **Validation of the RIME approach. A** Western blot validating pulldown of p53 (DO1 antibody) high molecular weight complexes (HMWC) in crosslinked HepG2 wt cells vs HepG2 p53KO cells. **B** RIME workflow and statistical analysis. **C** (left) RIME multi-scatter plot showing average Pearson

correlation=0.94 between biological replicates. (right) PCA (principal component analysis) of RIME samples showing clustering of biological replicates. **D** p53 peptides found and annotated with RIME as well as number of peptides per sample group. **E** Average spectral counts in GM and SM reveals increased peptide abundance in SM samples. Reproduced from Galhuber et al. 2022 covered under the CC BY license.

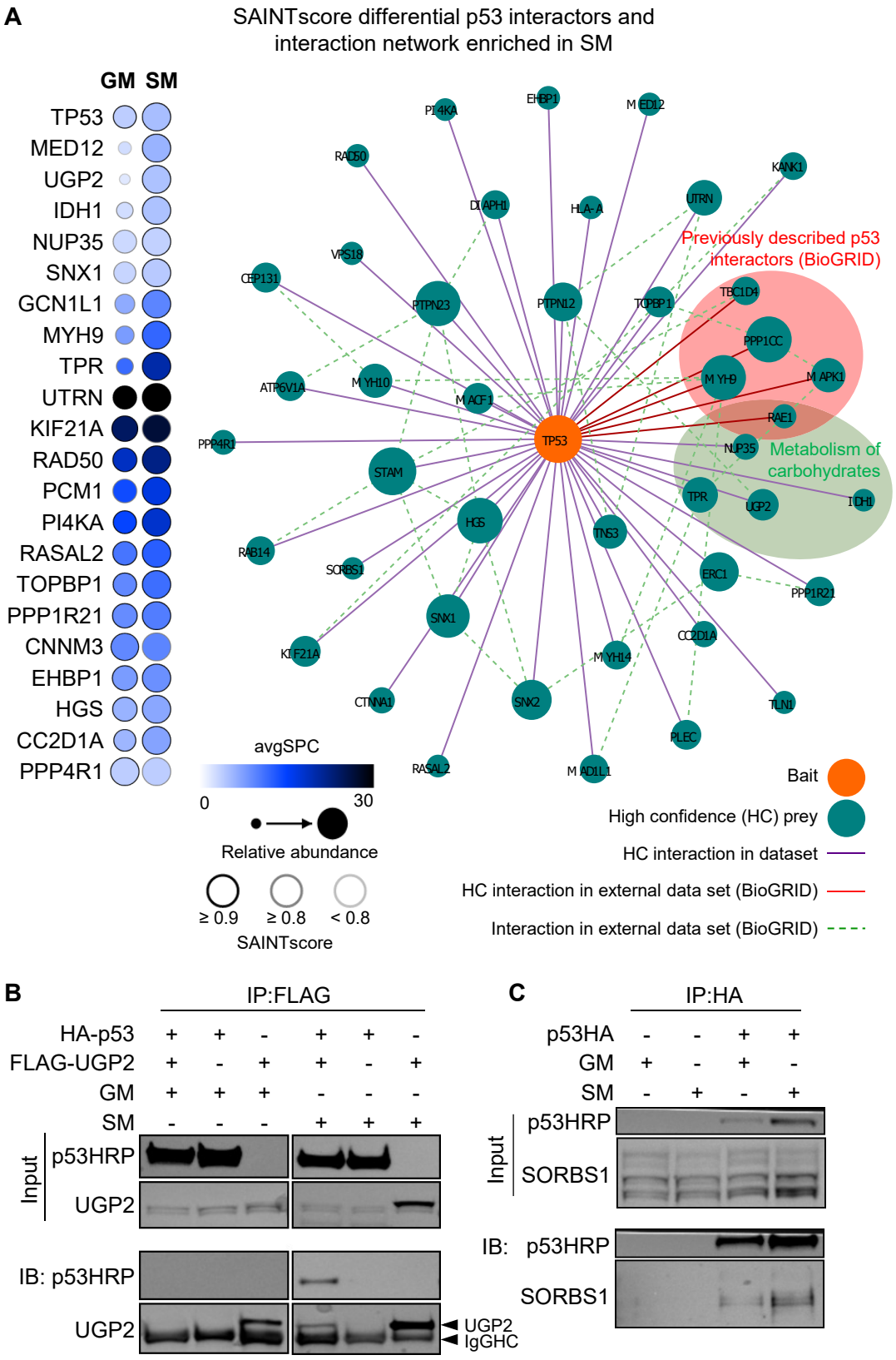

(Figure legend on next page)

Figure 14 **RIME results reveal vast p53 interaction network under SM conditions confirmed with co-immunoprecipitation (co-IP) experiments. A** (left) Dot blot showing SAINT score analysis of differential nuclear p53 interactors GM vs SM. Cut-offs SAINT probability (SP) ≥ 0.95; SP ≥ 0.8; SP < 0.8 indicated with grey scaled circles. Relative abundance represented by circle diameter. Blue tones indicate the respective average spectral counts (avgSPC). (right) p53 interaction network enriched under SM conditions. SAINT score analysis (cut off: SAINT probability SP≥0.9). Known p53 interactors (BioGRID, red) and/or map to the Reactome pathway "Metabolism of carbohydrates" (RSA-HAS-71387, green) indicated. **B** Western blot showing p53/UGP2 co-IP. **C** Western blot showing p53/SORBS1 co-IP. Reproduced from Galhuber et al. 2022 covered under the CC BY license.

p53 target gene activation upon starvation

Based on our initial hypothesis and supported by results from our nuclear p53 crosslinking experiments we intended to create a comprehensive transcriptome dataset of p53-mediated target gene expression upon nutrient deprivation. Therefore, we re-expressed FLAG-p53 in HepG2 p53KO cells and subjected the cells to either GM or SM. Subsequently we overlapped the four groups (FLAGp53_GM, FLAGp53_SM, p53KO_GM, p53KO_SM) in a Venn-diagram to identify p53- and starvation-specific differentially regulated transcripts (workflow Figure 15A). We confirmed successful FLAG-p53 re-expression as well as target protein expression for p21 by western blotting (Figure 15B). After validating our approach, we analyzed raw data with DEseq2 package in R and compared all 4 groups with each other. We filtered for minimally 2-fold differentially regulated transcripts in each group and overlapped these transcripts in a venn-diagram (Figure 15C). This enabled identification of transcripts that are highly abundant in the FLAGp53_SM group, enriched over both p53KO groups (GM and SM) as well as the FLAGp53_GM group. In total, we discovered 88 transcripts that meet the requirements of being starvation-induced exclusively in a p53-specific manner (Figure 15C white numbers in blue frames). Extending the knowledge on p53-dependent transcriptional targets under nutrient deprivation, we compared our putative p53 targets with commonly described targets summarized in a meta-analysis by Fischer et al. (2017). In this publication, the author computationally overlapped 13 high-throughput studies to derive high-confidence target genes. When comparing the 88 transcripts with this meta-dataset, we find 40 transcripts already described and 48 putative novel p53 target genes in the context of nutrient starvation (Figure 15D). Plotting their average abundances in a violin plot, shows increasing fold-changes in p53-overexpressing groups, which are more pronounced in FLAGp53_SM over FLAGp53_GM (Figure 15E). Examples of individual RNAseq expression of known p53 target genes (Protein BTG2 (BTG2), Pleckstrin homology-like domain family A member 3 (PHLDA3), Cytoplasmic FMR1-interacting protein 2 (CYFIP2), Zinc finger protein 385A (ZNF385A)) are shown in Figure 15F. Based on these expression patterns and their possible association with metabolism, we intended to validate some of our newly identified p53 targets. Therefore, we conducted RT-PCR for Meteorin-like protein (METRNL), Urokinase-type plasminogen

activator (PLAU), Pleckstrin homology domain-containing family G member 1 (PLEKHG1), VPS10 domain-containing receptor SorCS2 (SORCS2) and confirmed starvation-dependent induction patterns upon p53 re-expression similar to known p53 targets (Figure 15G). The complete list of 48 putative novel p53 targets is provided in Appendix Table 6.

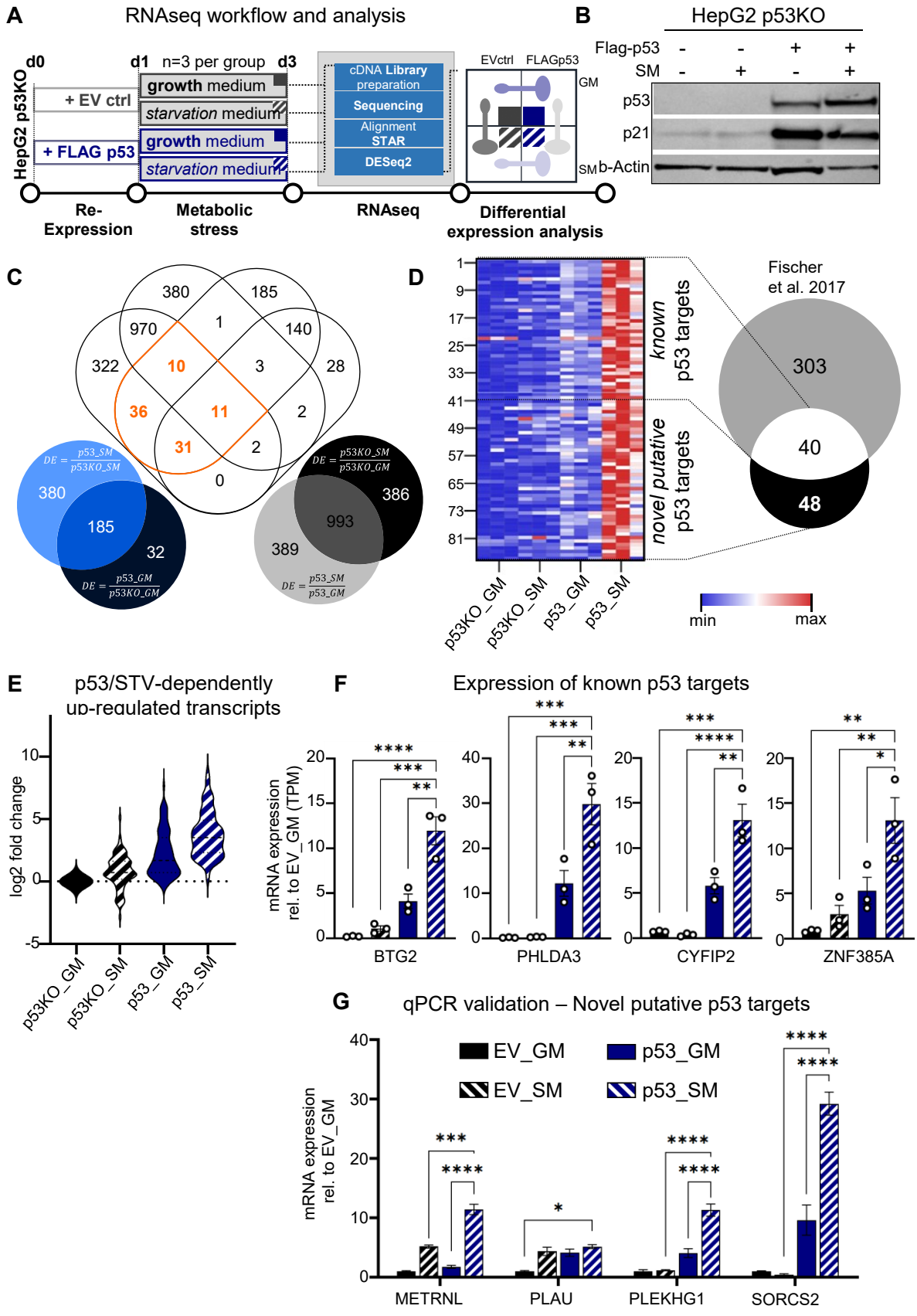

(Figure legend on next page)

Figure 15 **Transcriptome analysis reveals novel p53/starvation-specific differentially regulated transcripts in HepG2 cells. A** RNAseq workflow **B** Western blot showing successful FLAG-p53 re-expression under GM and SM conditions, as well as concomitant target protein induction (p21). Loading control beta-Actin. **C** Venn diagram showing overlaps of differential expression analysis (DEseq2, cutoff min 2-fol change, adjusted p-value<0.05, Benjamini-Hochberg) between each sample group. Orange numbers indicate groups of transcripts responsive to p53 re-expression and starvation stimulus. Group comparisons indicated within the colored circles. **D** Heat map showing 88 significantly differentially expressed gene transcripts (DESeq2, Wald-test with Benjamini-Hochberg correction, p<0.05) enriched in p53 overexpressing cells and sensitive to starvation. Venn diagram showing overlap with p53 target gene meta-analysis (Fischer et al., 2017) indicating 48 novel, starvation-specific p53 target genes. **E** Violin blot showing log2-fold change distribution of 88 gene transcripts between treatment groups. p53KO_GM set to 0. **F** mRNA expression of previously described p53 target gene in the RNAseq dataset. p53KO_GM set to 1. n=3; Mean values ± SEM are shown and two-way ANOVA, Tukey's multiple comparisons test was performed. **** p<0.001, *** p<0.005, * p<0.05. **G** RT-qPCR validation of novel p53 target genes found in the RNAseq data set. Data normalized to PPIA. n=3; statistical analyses as in F. Reproduced from Galhuber et al. 2022 covered under the CC BY license.

In a metabolism context, METRNL is an interesting molecule as it is related with white adipose tissue browning as well as insulin sensitization, and also seems to play a role in activating macrophages (Zheng *et al.*, 2016). Available expression data suggests that it is predominantly expressed in muscle, therefore acting as myokine, but as a secreted, circulating factor this does not exclude the possibility that METRNL exerts modulating functions in organ crosstalk e.g. liver-white adipose tissue-axis (Cheong and Xu, 2021). Nevertheless, to date METRNL has not been considered to originate from the liver and is therefore not referred to as a hepatokine, merely as myokine that positively influences energy expenditure (Meex and Watt, 2017; Dos Santos *et al.*, 2021). However, it would be highly interesting to test whether our observation that also hepatic tissues express and secrete METRNL stands up to scientific scrutiny in an organismic context.

Urokinase-type plasminogen activator PLAU (PLAU) represents another candidate p53 target in our expression data. However, the PLAU induction profile seems least pronounced in our qPCR validation, albeit with a significant mRNA level increase in FLAGp53_SM samples. PLAU itself does not exert a direct enzymatic function, but as protease cleaves plasminogen to form the active enzyme plasmin. In turn, plasmin fosters extracellular matrix (ECM) degradation and ultimately promotes cell migration or invasion (Mahmood, Mihalcioiu and Rabbani, 2018). From a tumor therapeutic point of view, it seems at first glance counterintuitive that starvation may lead to an increased migratory potential, which can be considered a detrimental metastasis-promoting outcome in the cancer context. On the other hand p53 was also reported to prevent ECM degradation by inducing PAI-1 that is a central PLAU inhibitor (Kunz *et al.*, 1995; Araki *et al.*, 2015) which renders this observation prone for further analysis. In line with PLAU, also PLEKHG1 as Rho family small GTPases (Rho) spatiotemporally regulates cell morphology and motility (Nakano *et al.*, 2022). This signaling pathway includes

Cell division control protein 42 homolog (CDC42) (Müller *et al.*, 2020) which in turn is an upstream activator of PAK2 (Renkema, Pulkkinen and Saksela, 2002) creating a possible line to our BioID-derived p53 interaction data. Connecting back to metabolism, such cell remodeling processes are suggested to play influential roles in the control of metabolic regulation and glucose homeostasis (Møller, Klip and Sylow, 2019; Møller *et al.*, 2020). In conclusion, the transactivation of PLAU and PLEKHG1 underpin p53's nuanced function in controlling ECM remodeling and its implications in cancer and point to nutrient deprivation as additional modulator of these processes.

Lastly, SORCS2 showed the most pronounced increase in mRNA levels upon p53 re-expression and starvation. However, establishing a direct link between SORCS2 and expression in liver-derived cells is somewhat difficult at the current state of knowledge. Currently it is clear that SORCS2 encodes a VPS10 receptor gene, which is predominantly expressed in brain and functions as transmembrane neuropeptide receptor and plays a central role in fetal mouse development (also showing high expressing in the developing liver) (Hampe *et al.*, 2001; Boggild *et al.*, 2016). Furthermore, SORCS2 was identified to protect neuronal cells from oxidative stress via its association with neuronal amino acid transporter EAAT3 (SLC1A1), facilitates cysteine import to fuel glutathione production (Malik *et al.*, 2019) and serves as major glutamate/aspartate transporter in renal tissue (Bailey *et al.*, 2011). Because SORCS2 and its involvement in amino acid transport in the liver or in liver cancer has not yet been systematically studied, the pronounced p53/starvation-dependent induction warrant further studies on amino acid balance and ROS protection under nutrient deprivation.

Proposed model

Overall, we propose a model for p53 under nutrient stress, where p53 protein stabilizes in nuclei in an Mdm2-dependent manner and invokes a starvation-specific p53 transcriptome response. While we found PAK2, 14-3-3 proteins, and numerous metabolic enzymes interacting with p53 under nutrient-proficient conditions in the cytoplasm, nuclear interaction was confirmed for UGP2 or SORBS1 under nutrient-poor conditions. Confirmational experiment for specific protein interactions (i.e. Co-IP, NMR) underpin the suitability of our MS methods (BioID, RIME) to interrogate p53 protein interactions and extends the landscape of tumor protein p53 in the context of nutrient availability.

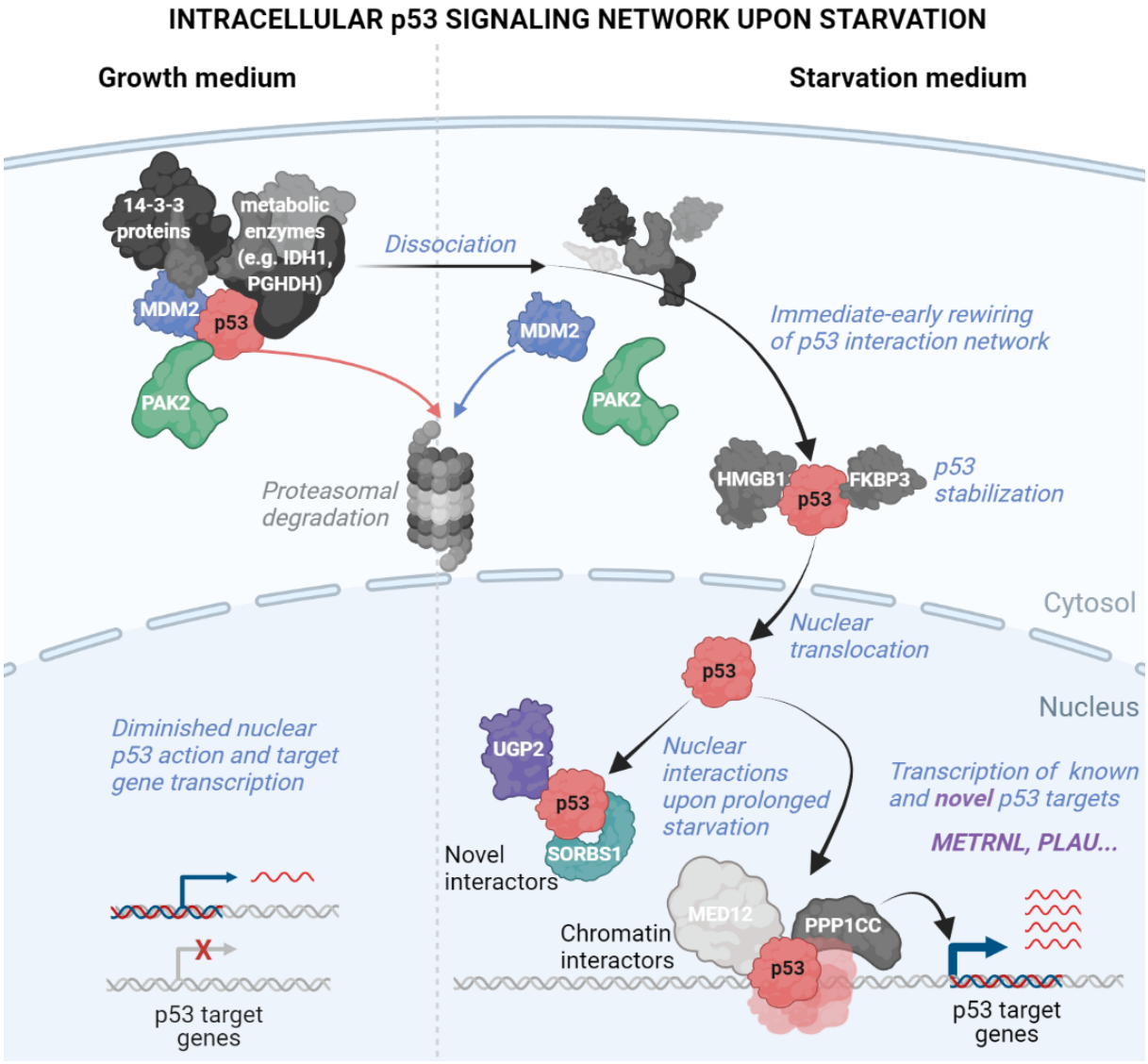

Figure 16 **Proposed model for p53 signaling and protein interactions upon nutrient-deprivation.** This Figure has been previously published in (Galhuber *et al.*, 2022) and is covered under the CC BY license.

Chapter 4: Discussion

In this work we aimed to find novel upstream p53 interactors that mediate nutrient deprivation signals towards p53. With our BioID approach we screened for potential p53 upstream regulators and found multiple potential upstream regulators of which a previously undescribed p53-interacting kinase PAK2 is a particular interesting candidate for further investigations. We confirmed this interaction of PAK2 N-terminal domain with the p53 DBD with NMR experiments. Furthermore, we confirmed that loss of p53/PAK2 interaction with either pharmacological inhibitors or via gene silencing leads to p53 nuclear translocation as well as target gene activation.

p21-activated kinases (PAK1-6) have a broad functional spectrum in various cellular processes that include motility, growth, apoptosis, or gene expression, many of them involved in pathogenesis (e.g. diabetes) and oncogenesis (Kumar *et al.*, 2017; Liu, Liu and Dong, 2021). Focusing on PAK2, it is known in murine models that PAK2 ablation led to embryonic death, most probably mediated via increased ROS burden, failures in spindle assembly, and accumulation of DNA damage underpinning its importance already in embryogenesis (Zeng *et al.*, 2021). Interestingly, the previously mentioned features are closely associated with functions reported for p53. Amongst all PAK family members, PAK2 shows the highest amplification frequency in cancer and has numerous substrates associated with cancer signaling and proliferation (Ye and Field, 2012; Zeng *et al.*, 2021). With respect to metabolism, the most striking overlap of p53 and PAK2 seems that both are reported as substrates of AMPK (Jones *et al.*, 2005; Banko *et al.*, 2011), that is highly induced by drops in the ATP/AMP ratio invoked by nutrient deprivation. AMPK mediates phosphorylation at p53 serine 15 (p53S15) which promotes its activation by blocking the p53/MDM2 interaction interface, leading to p21 induction. p53S15 phosphorylation is also facilitated by other kinases e.g. ataxia–telangiectasia mutated kinase (ATM) and checkpoint kinase 1/2 (CHK1/2) in the context of DNA damage and cell cycle progression (Shieh *et al.*, 1997, 2000). p53S15 is especially required for correct centrosome assembly and sensor for mitotic integrity preventing propagation of chromosomal defects (Contadini *et al.*, 2019). On the other hand, AMPK-dependent phosphorylation of PAK2 at serine 20 (PAK2S20) was confirmed in a study screening for AMPK substrates in the context of cell cycle progression (Banko *et al.*, 2011). PAK2-dependent phosphorylation of downstream targets includes Myosin regulatory light chain (MRLC) that together with AMPK is crucial for mitotic spindle orientation, thereby preventing aberrant cell cycle progression (Thaiparambil, Eggers and Marcus, 2012). In this

sense, our finding could imply a coordinated AMPK-dependent phosphorylation of PAK2 and p53 and represent a protective mechanism during mitotic cell cycle progression.

Another aspect of PAK2 is its involvement in receptor-dependent signaling and cytoskeletal architecture. Both of these biologic entities are involved in glucose homeostasis and metabolic integrity (Kumar *et al.*, 2017; Møller, Klip and Sylow, 2019). As previously mentioned, PAK2 is a downstream effector of Rho GTPases RAC1/CDC42 that receive numerous inputs from cell surface receptors. One important example of such a cellular receptor implicated in liver disease and cell proliferation is epidermal growth factor receptor (EGFR), also prominent target in cancer therapy (Komposch and Sibilia, 2016; Wee and Wang, 2017; Maldonado and Dharmawardhane, 2018). An interesting association of the EGFR-PAK2 receptor signaling axis has been established in a pancreatic cancer model (Lee *et al.*, 2019) where regional depletion of amino acids led to an increase of macropinocytosis that promoted tumor growth that was dependent on EGFR-PAK2 signaling. In this sense it would be interesting to explore the dependency of the p53/PAK-signaling axis in response to EGFR signaling. As previously mentioned, in times of nutrient scarcity or in tumor areas with limited access to nutrients, an opportunistic mode of nutrient acquisition is the inclusion of extracellular material either via macropinocytosis or phagocytosis (Pavlova and Thompson, 2016). If macropinocytosis is p53-mediated is currently not known. It has been shown in an earlier study from Lee et al. pharmacological inhibition of macropinocytosis abolished tumor growth (Commisso *et al.*, 2013), still they did not address the role of p53 in their experiments. Interestingly, in our BioID proteomics data we did not only observe an association of cytoplasmic p53 with PAK2 but also find RAC1;RAC3, enriched in GM samples, which is known as PAK2 activator. In this context, further experiments are necessary.

In our BioID dataset, the presence of metabolic enzymes was quite unexpected. In terms of energy sensing we were surprised to find GTP-binding protein Rheb (RHEB) in our GM_up interaction dataset, that is known to positively regulate mTOR signaling (Cui *et al.*, 2021). That would imply that beyond known p53 transcriptional targets (e.g., AMPKβ, TSC2, PTEN, SESN1/2), the p53 protein may be physically located in the vicinity of a central modulator of growth regulation and might directly influence mTOR signaling via protein-protein interaction (Budanov and Karin, 2008b; Cui *et al.*, 2021). Twenty-five proteins in GM_up dataset are part of Panther protein class metabolite interconversion enzyme (PC00262) and 20 of those part of KEGG annotation Metabolic pathways (hsa01100). Biochemical data for physical protein-protein interaction so far has only been found for G6PD (Jiang *et al.*, 2011). Whether the association of p53 with numerous metabolic enzymes is biologically plausible, is an open

question. Considering the importance of protein-protein interactions that is necessary to maintain biological function, suggests that the metabolic enzymes themselves are assembled in large protein complexes. Evidence for compartmentalization and spatially highly organized multienzyme complexes for glycolysis has been presented recently (Kohnhorst *et al.*, 2017; Fuller and Kim, 2021). Different terms for these assemblies of glycolytic enzymes have been suggested e.g., glycolytic granules ("G-bodies") or "glucosomes", and refer to cellular structures that condensate in a process called phase separation in reaction to metabolic clues and are highly volatile. Interestingly, in the study of Kohnhorst et al. (2017) the size of glucosomes changed with metabolic perturbations that activate the pentose phosphate pathway, showing that the composition of the multienzyme complex change with metabolic challenges. On top of that, they show that EGF treatment resulted in the largest protein assemblies they observed, resulting in increased glucose flux into serine biosynthesis. These observations are in perfect alignment to our results, where serum proficient medium promotes p53 association with glycolytic proteins (G6PD, TPI1, ALDOA, LDHA) as well as with serine biosynthesis proteins (PHGDH, PSAT1) interaction. Of note, G-bodies were mainly interrogated in yeast and hypoxic conditions foster their formation but also in HepG2 cells (Jin *et al.*, 2017). In hypoxic conditions further components of G-bodies, such as glycolytic enzymes, chaperones (e.g. Hsp70), DEAD box helicases, fatty acid biosynthesis enzymes, stress response proteins, and 26S proteasome components were identified (Jin *et al.*, 2017). Whether our described co-localization of p53 in the vicinity of glucosomes is functional, remains currently elusive. However, hypothetically, if proteasomes are indeed associated with G-bodies as shown in the mentioned study, our finding might be a by-product of ubiquitinated p53 degraded in proteasomes in the vicinity of those structures. Evidence for co-localization of p53 at proteasomal subunits in our GM_up dataset is given with 26S proteasome subunits 3, 7, and 11 (PMSD3, PMSC2, PMSD11). Future studies will need to clarify if p53 is a metabolic regulator in an enzyme super-complex or if metabolic enzymes and p53 are merely proximal in the proteasomal pathway.

Highlighting another potential p53 interactor in the BioID GM_up dataset, Cullin-5 (CUL5) is a core component of the Elongin-Cullin2/5-SOCS-box protein complex, that acts as E3 ubiquitin-protein ligase complex (Kamura *et al.*, 2001, 2004; Zhao, Xiong and Sun, 2020). CUL5 was shown to targets p53/MDM2 for dissociation and subsequent p53 poly-ubiquitination and proteasomal degradation in viral contexts (Sato, Kamura, *et al.*, 2009; Sato, Shirata, *et al.*, 2009). Considering the permanent protein turnover in the MDM2-p53 hub, this mode of action could also apply in our experiments. CUL5 was not only shown to interfere at the MDM2/p53-hub but mediates and regulates total protein ubiquitination as well as neddylation (NEDD8

ubiquitin like modifier (NEDD8)- conjugation). NEDD8 is structurally different from ubiquitin (60% similarity) but has distinct functions and targets including processes like cell cycle progression, metabolism, immunity, and tumorigenesis (Kumar, Yoshida and Noda, 1993; Lobato-Gil *et al.*, 2021; Zou and Zhang, 2021). Both PTMs, ubiquitination and neddylation, are associated with p53 stabilization, degradation, or subcellular localization (Liu, Tavana and Gu, 2019; Mayo and Nus, 2022). Importantly, CUL5 activity relies on partnering with a second E3 ubiquitin ligase called E3s ubiquitin ligase ARIH2 (also called TRIAD1) and its activity as a complex is only given when NEDD8 is linked to CUL5 (Kostrhon *et al.*, 2021) and even amplifies TRIAD1 ubiquitin ligase activity (Kelsall *et al.*, 2013). This is an important observation as TRIAD1 was reported to directly bind to p53 C-terminal domain and facilitate dissociation and ubiquitination of MDM2, thereby promoting p53 stability, a mode of action to be expected under SM conditions (Bae *et al.*, 2012). On the other hand, both proteins p53 as well as MDM2 are subjected to neddylation under certain circumstances and MDM2 itself can switch its E3 ligase activity from ubiquitination to neddylation (Batuello *et al.*, 2015). For example, MDM2 mediated p53 neddylation at lysine residues (K370, K372, K373), which was reported to inhibit p53 transcriptional activation as well as cytoplasmic sequestration (Xirodimas *et al.*, 2004; Liu and Xirodimas, 2010). In conclusion, further investigation of p53/MDM2 and ubiquitination and neddylation in the context of tumor growth control could reveal new modes of p53 regulation.

In our nuclear interaction dataset, we confirmed UGP2 as p53 interactor with co-IP. As mentioned, consistent UGP2 co-overexpression was difficult to achieve in our experiments as stable UGP2 levels were observed only in nutrient deprived HepG2 cells. Further tests with different ratios of p53 and UGP2 unveiled that co-overexpression efficiency of both proteins was mutually exclusive (data not shown). UGP2 in its symmetric, octameric form (Führing *et al.*, 2015) is catalyzing the conversion of glucose-1-phosphate into UDP-glucose that is substrate for glycogen production via glycogenin (GYG1/2) (Zois and Harris, 2016), glycosylation (Reily *et al.*, 2019), and glucuronidation (Yang *et al.*, 2017) and therefore a key metabolite for pathways involved in metabolism, cellular detoxification, protein folding control, cancer, or receptor signaling. UGP2 was found to localize in cytoplasm as well as nuclei, where it contributes to nuclear glycogen metabolism that has been reported in multiple tumors, also it harbors several ubiquitination sites (Sun *et al.*, 2019; Lobato-Gil *et al.*, 2021). Interestingly, UDP-glucose was attributed with tumor-suppressive roles in lung cancer metastasis via interaction of UDP-glucose 6-dehydrogenase (UGDH) with Hu antigen R (HuR) (a neddylation target of MDM2), that was attenuated by UGP2 depletion (Embade *et al.*, 2012; Wang *et al.*, 2019). Opposing results were reported in a multi-omics study in hepatocellular carcinomas that revealed persistent upregulation of UGP2 coincided with metastatic potential mediated through

increased glycogen synthesis rates (Li *et al.*, 2018). UGP2 was also necessary for maintaining cellular growth in pancreatic ductal adenocarcinoma and UGP2 depletion led to decreased glycogen levels, protein glycosylation (including EGFR) and impaired tumor growth (Wolfe *et al.*, 2021). In the latter study, the authors describe the YAP-TEAD complex as transcriptional regulator of UGP2 expression, which is overlapping with one of our findings in the BioID dataset (Appendix Table 2). YAP1 play centrals roles in metabolic reprogramming in cancer by modulating glucose metabolism (e.g. GLUT3 or HK2 expression) and fully active YAP1 leads to increased glucose uptake and glycolysis rate (Zhang *et al.*, 2018). Also intensive crosstalk between YAP1 and p53 family members is a known phenomenon in nutrient homeostasis and cancer development (Raj and Bam, 2019). Again, more experiments are needed to shed light on the mechanistic details and biological consequences of the p53/UGP2 interaction.

Technical considerations

With proximity-based biotin labelling we used a proteomics method to unravel the p53 interactome at the onset of nutrient starvation. p53 is known for its vast variety of binding partners and its regulation through numerous PPIs. As mentioned, BioID harbors some benefits in MS analysis e.g., the use of a tagged protein that is located in intact complexes within living cells and allows for labeling in its natural environment under physiological conditions (*in situ*). There it not only captures its direct binding partners but also vicinal proteins in larger complexes. When we tried co-IP experiments for five (14-3-3, FKBP25, IDH1, TFAM, TPI1) potential interaction partners derived from BioID, we were not successful. We consider that those candidate interactors might rely on linker or adaptor proteins in the in vivo situation assembled in larger complexes, which difficult to maintain throughout a co-IP experiment. Therefore, for some targets it is difficult to find the optimal settings for validation experiments. Also, we know that complex formation and decay are highly dynamic and biotin labelling allows to capture transient, early, intermediate or late interactors in biological processes. In validation experiments the exact time point during dynamic experimental situation is also unknown. Furthermore, tagged proteins in biological experiments (BioID) alter their shape and interaction surfaces that could also lead to inaccurate or skewed results, that are later not replicable with endogenous proteins. To target subcellular compartments, we chose to fuse cytoplasmic localization tags as well as the biotin ligase to the N-terminus of p53. To omit steric hindrance in a BioID experiment and produce a complete picture of a tagged protein interaction it would be most meaningful to use different baits e.g., N-terminally and C-terminally tagged protein. However, for MS experiments we chose the construct of biotin ligase C-terminal to p53, to

minimize potential steric hindrance at the N-terminal p53 transactivation domains, which seemed more important to remain accessible based on our hypothesis. The p53 C-terminus harbors important residues for acetylation, ubiquitination, methylation, or neddylation, that mediate between stability/degradation or transactivation potential. We cannot exclude the possibility that C-terminal fusion altered the p53 function when compared to endogenous protein by obstructing interaction surfaces at the C-terminal domain.

A notable advantage of BioID is that covalently bound biotin allows for harsh cell lysis methods to efficiently lyse even hard to access organelles of the cell. However, to date four carboxylases are known to harbor biotinylation as a natural occurring PTM. In BioID experiments we cannot distinguish if the captured peptides are biotinylated by endogenous biotin ligases or due to bait protein interaction, which in part can be circumvented by using multiple controls (e.g., untransfected background). However, if the naturally occurring biotinylation is very low abundant or active, it might be masked by artificial biotinylation. Also, biotinylation needs accessible lysine residues at target proteins within range of the biotin ligase. As those lysine residues are limited and also targeted for other PTMs this is most probably a competitive situation and therefore can evade biotinylation.

We used transient protein overexpression that is susceptible to unequal expression levels of the bait protein across replicates or experiments and could not be consistent with endogenous protein expression levels. We controlled our experiments by choosing the optimal vector amounts to resemble endogenous protein levels. However, the optimal BioID experiment makes use of expression of a fusion protein from the endogenous locus. This can be either achieved by generating stably expressing cells lines through viral transfection or through CRISPR/Cas9 gene editing targeting the gene locus.

Another observation in both our BioID and RIME data sets is that we found candidate interactors that were previously not associated with the targeted subcellular compartment. For instance, we found several nuclear proteins in our cytoplasm-targeted BioID analysis and vice versa in our RIME experiments, where we found many cytoplasmic or membrane bound proteins, while actually analyzing isolated nuclei. In subcellular fractionation experiments we observed some spillover of our fusion protein into the nuclear fraction, which is most probably the reason for finding those nuclear proteins in the MS analysis. On the other hand, RIME makes use of formaldehyde crosslinking of intact cells with subsequent nuclei isolation. We observed considerable visual and behavioral differences in cell structure and lysis efficiency between crosslinked versus non-crosslinked HepG2 cells, and even between non-starved or starved cells. Although we optimized cell lysis with several douncing and sonification steps,

whole cell crosslinking experiments come along with impurities due to “bleed over” from other compartments. These limitations render validation experiments even more important.

With regards to different nutrient availability in the context of p53, cellular proliferation states need to be addressed. While cells kept in GM conditions likely proliferate and constantly change between different stages of the cell cycle, cells kept in SM conditions maintain pronounced levels of p21 protein (Figure 1B) and most likely are more uniformly distributed in regards of cell cycle progression. Therefore, we would also expect a less volatile, more synchronized metabolic state that may lead to a lower number of potential interaction partners, especially for p53 that is localized in different compartments and associated with numerous pathways. This is especially important in our BioID experiments, where we find interaction partners that are associated with mitotic spindles or centrosomes or midbody, that form during cell division but at the same time are associated with ribosome hibernation (i.e., CCDC124). The finale stages of cytokinesis are also associated with many membrane/actin skeleton adaptations in the dividing cells where not only p53 is implicated but also PAK2 (Banko *et al.*, 2011). This makes it hard to distinguish whether our experimental settings are related to cytokinesis or receptor-related cytoskeletal and membrane adaptations or neither of both. To refine the interpretations of our data, cell cycle analyses in GM and SM conditions need to be performed and/or cell cycle synchronizing agents need to be applied to GM conditions.

Lastly, our experiments were obtained in a tumoral cell line (HepG2) and were not comprehensively interrogated in alternative, non-tumorigenic systems. Therefore, some of the identified proteins and genes might have a limited physiological relevance and validation experiments in other cell systems would be much needed in follow-up studies.

Overall, we successfully validated the interaction for p53/PAK2, p53/UGP2 and p53/SORBS1 that renders our complementary proteomics approaches as suitable for interrogating PPIs in the cytoplasm and in nuclei. Still, with our acquired knowledge and experience, we consider further methodological improvements are feasible and think that even better results are obtainable for any bait protein in future studies.

Appendix

Table 2 **List of 272 proteins enriched with BioID in p53-miniTurbo samples over EGFP-miniTurbo samples.** Known physical p53 interactors retrieved from BioGRID and candidate interactors from BioID are indicated on left or right side of gene names with (+). Reproduced from Galhuber et al. 2022 covered under the CC BY license

known interactor	Gene names	candidate	known interactor	Gene names	candidate	known interactor	Gene names	candidate
+	ABR			PSMD3	+		CCDC9	+
+	ACTB			PSME2	+		CD3EAP	+
	ACTC1;ACTA1	+		PTPN1	+		CHMP2A	+
+	ACTG1		+	PYGL			CHMP2B	+
	ACTR2	+	+	QARS			CHMP3	+
+	ACTR3			RAB6A	+		CLMN	+
+	AKR1A1			RAC1;RAC3	+		CWC27	+
	AKR1B1	+		RFC5	+		DEK	+
	ALDOA	+		RHEB	+		DENR	+
+	ANXA2;ANXA2P2		+	RPLP0;RPLP0P6			DIDO1	+
	ARHGDIA	+		RPSA	+		DNAJC17	+
	ATAD3B	+	+	S100A4			DNAJC21	+
+	ATP5A1		+	SEC23A			DNAJC8	+
	ATP5B	+		SEPT2	+		DTD1	+
	ATP5L	+		SMIM15	+		EDF1	+
	BLVRA	+		SRP54	+		EIF1AX	+
	BZW1	+		SRP68	+	+	EIF5B	
	C14orf166	+		SSR3	+		ESF1	+
	CAP1	+		ST13;ST13P5;ST13P4	+		FABP7	+
	CAPN2	+		STIP1	+		FAM50A	+
+	CCT2			STPG2	+	+	FKBP3	
+	CCT4			SULT2A1	+		GGH	+
	CFL1	+		TAGLN2	+		GTF2E2	+
	CS	+		TNPO1	+		HDGFRP2	+
	CSRP1	+		TNS3	+	+	HMGA1	
	CUL5	+		TPI1	+	+	HMGA2	
	DDX39A	+	+	TPM3		+	HMGB1;HMGB1P1	
+	DDX3X		+	TPM3			HMGB2	+
	DPP3	+		TRAP1	+		HMGB3	+
	DSTN	+	+	TTK			HMGN1	+
	DYNC1LI1	+		TUBA1B	+		HNRNPAB	+
	EEF1D	+	+	TUBA1C		+	HNRNPD	
+	EEF2		+	TUBB			INTS12	+
+	EFTUD2		+	TUBB4B			KIAA1522	+
	EIF2A	+	+	UBA1			KIN	+
	EIF4H	+	+	UPF1			LAD1	+
	EIF5A;EIF5AL1	+	+	USP7			LYPLA2	+
	ENO1	+		VCL	+		MAP1B	+
	FARP1	+	+	WDR1		+	MAP4	
+	FBL			YARS	+		MAP7D2	+
+	FLNA		+	YWHAB			MARCKS	+
	FSCN1	+	+	YWHAE		+	MECP2	
+	FUBP1			YWHAG	+		MESDC2	+

known interactor	Gene names	candidate
	G6PD	+
	GGA3;GGA1;GGA2	+
+	GNB2L1	
	GTF3C5	+
+	HNRNPK	
+	HSP90AA1	
+	HSP90AB1	
+	HSP90AB2P	
+	HSP90B1	
+	HSPA5	
+	HSPA8	
+	HSPA9	
	HSPD1	+
+	HSPE1;HSPE1-MOB4	
	IDH1	+
	INPP5D	+
+	KPNB1	
+	LDHA	
+	LYZ	
+	MAP2K3	
	MDH2	+
	METTL1	+
	MOB1A;MOB1B	+
	NMD3	+
	NME1-NME2;NME2	+
+	NPEPPS	
+	NQO1	
	NUDC	+
	P4HB	+
+	PCBP1	
	PCBP2	+
	PDIA3	+
	PDLIM5	+
	PFN1	+
	PGK1	+
	PGM1	+
+	PHB	
	PHGDH	+
+	PKM	
	POR	+
	PPIA	+
	PPME1	+
+	PPP2R1A	
+	PRDX1	
+	PRDX2	
+	PRDX6	
	PRPS1	+
	PSMC2	+
+	PSMD11	

known interactor	Gene names	candidate
	YWHAQ	+
+	YWHAZ	
	AGFG1	+
+	ARGLU1	
	CCNL2	+
	CD2AP	+
	CLIC1	+
	CNN2	+
	CPLX2	+
	CTTN	+
+	DNAH10	
+	EIF4B	
+	GSPT1	
	HDGF	+
	HN1L	+
+	HNRNPA1;HNRNPA1L2	
+	HNRNPA2B1	
+	HNRNPF	
	IGBP1	+
	KIAA1598	+
	KPNA3	+
	MED15	+
+	MRE11A	
	NACA	+
	PAK2	+
	PPP1R2;PPP1R2P3	+
	RBM17	+
+	SEC24A	
+	SMAP;C11orf58	
+	STAT3	
	TAF15	+
	TAGLN	+
	TCEA1	+
+	TP53	
	TTC1	+
+	TXN	
	UBAP2	+
+	VCP	
+	YAP1	
+	ALYREF	
	ATP5E;ATP5EP2	+
	C19orf52	+
	C1orf131	+
+	CALD1	
+	CALD1	
	CAST	+
	CBX8	+
	CCDC124	+

known interactor	Gene names	candidate
	MKI67	+
	MRPL1	+
	MRPL40	+
	MRRF	+
+	NCL	
	NDUFS4	+
	NELFE	+
	NOLC1	+
+	NPM1	
	PDAP1	+
	PIN4	+
+	PRRC2A	
	PSIP1	+
+	RBBP6	
	RBM27	+
	RBM33	+
	RPAP3	+
+	RPL10	
	RPL22	+
+	RPS19	
	RRBP1	+
+	S100A1	
	SARNP	+
	SCAF11	+
	SEC61B	+
+	SERBP1	
	SLC16A3	+
	SMNDC1	+
	SRRM1	+
	SRRM2	+
	SSR1	+
	STAU1	+
+	SUB1	
+	SUMO3	
	TCERG1	+
	TCOF1	+
	TFAM	+
	TPX2	+
	UBTF	+
	UPF3B	+
	WBP11	+
	WDR13	+
	WIBG	+
	ZC3H11A	+
+	ZMAT2	

up_p53
up_p53_GM&SM
up_p53_SM

Table 3 **List of proteins not occurring in at least 2/3 replicates in untransfected HepG2 background controls.**

Protein names	Gene names	GM repl 1	GM repl 2	GM repl 3	SM repl 1	SM repl 2	SM repl 3
Arf-GAP domain and FG repeat-containing protein 1	AGFG1	0	0	0	0	159350	0
Coiled-coil domain-containing protein 9	CCDC9	0	0	0	0	0	184140
Cyclin-L2	CCNL2	0	0	96604	0	114430	100380
Complexin-2	CPLX2	0	0	0	0	0	0
Dynein heavy chain 10, axonemal	DNAH10	0	0	0	0	0	0
Cytoplasmic dynein 1 light intermediate chain 1	DYNC1LI1	0	0	0	0	0	0
Eukaryotic translation initiation factor 4H	EIF4H	0	0	0	0	0	0
Far upstream element-binding protein 1	FUBP1	0	0	0	0	36650	0
Hematological and neurological expressed 1-like protein	HN1L	0	0	0	0	237140	0
Heterogeneous nuclear ribonucleoprotein F	HNRNPF	126310	0	0	0	0	141800
Immunoglobulin-binding protein 1	IGBP1	0	0	0	0	0	0
Uncharacterized protein KIAA1522	KIAA1522	0	0	0	0	86819	652510
Shootin-1	KIAA1598	0	0	0	0	114150	225280
Acyl-protein thioesterase 2	LYPLA2	0	0	0	0	425010	0
Mediator of RNA polymerase II transcription subunit 15	MED15	0	0	0	0	0	0
Double-strand break repair protein MRE11A	MRE11A	0	31299	20989	0	0	0
Nuclear migration protein nudC	NUDC	262840	0	0	0	0	152280
Serine/threonine-protein kinase PAK 2;PAK-2p27;PAK-2p34	PAK2	0	0	30849	0	62704	191450
Poly(rC)-binding protein 1	PCBP1	0	0	165810	96633	295110	307310
PDZ and LIM domain protein 5	PDLIM5	0	0	0	0	132770	83491
26S protease regulatory subunit 7	PSMC2	0	0	77990	0	104520	154680
Splicing factor 45	RBM17	0	0	0	0	0	0
RNA polymerase II-associated protein 3	RPAP3	0	0	14748	0	0	122570
Protein SCAF11	SCAF11	0	0	0	0	0	168300
Protein transport protein Sec23A	SEC23A	177340	233950	93055	0	56932	0
Small acidic protein	SMAP; C11orf58	289540	0	0	0	0	0
Hsc70-interacting protein;Putative protein FAM10A5;Putative protein FAM10A4	ST13; ST13P5; ST13P4	0	0	0	0	194670	492600
TATA-binding protein-associated factor 2N	TAF15	0	0	0	0	0	0
Tensin-3	TNS3	0	0	53898	0	0	0
Cellular tumor antigen p53	TP53	0	0	0	0	417830	0
Tropomyosin alpha-3 chain	TPM3	4131600	1400400	283090	0	0	173450
Tetratricopeptide repeat protein 1	TTC1	0	0	0	0	0	149480
Ubiquitin-associated protein 2	UBAP2	68086	0	0	0	0	44359
Ubiquitin carboxyl-terminal hydrolase 7;Ubiquitin carboxyl-terminal hydrolase	USP7	0	0	0	0	27588	0
WD repeat-containing protein 13	WDR13	0	0	0	0	0	0
Transcriptional coactivator YAP1	YAP1	0	0	0	0	0	0

Table 4 **List of biotinylated peptide counts in background controls VS p53-miniturbo overexpressing samples.** Peptides specific for p53-miniTurbo samples and missing in all background controls indicated in green.

Protein names	Gene names	noTF_GM	noTF_SM	EGFP_GM	EGFP_SM	sum_bkgd_ctrls	p53_GM	p53_SM
Acyl-coenzyme A thioesterase 2, mitochondrial;Acyl-coenzyme A thioesterase 1	ACOT2;ACOT1	0	0	1	2	3	3	3
ADP-ribosylation factor GTPase-activating protein 1	ARFGAP1	0	0	2	1	3	3	3
Brain-enriched guanylate kinase-associated protein	BEGAIN	1	2	2	2	7	3	3
Butyrophilin subfamily 2 member A1	BTN2A1	3	3	3	3	12	2	1
Butyrophilin subfamily 2 member A1	BTN2A1	3	3	3	3	12	2	1
Butyrophilin subfamily 2 member A1	BTN2A1	3	3	3	3	12	2	1
Uncharacterized protein C11orf84	C11orf84	3	3	3	3	12	3	3
Nuclear nucleic acid-binding protein C1D	C1D	0	0	1	2	3	0	0
Nuclear nucleic acid-binding protein C1D	C1D	0	0	1	2	3	0	0
Uncharacterized protein C4orf45	C4orf45	0	0	1	1	2	1	0
T-complex protein 1 subunit theta	CCT8	0	0	2	2	4	3	3
Charged multivesicular body protein 4b	CHMP4B	0	0	0	0	**0**	1	2
Chymase	CMA1	3	3	3	3	12	3	3
Calponin-3	CNN3	0	0	0	0	**0**	1	0
Complexin-2	CPLX2	0	0	3	3	6	3	3
Src substrate cortactin	CTTN	0	0	0	0	**0**	1	0
Eukaryotic translation initiation factor 3 subunit D	EIF3D	0	0	1	0	1	2	2
ELAV-like protein 2;ELAV-like protein 4;ELAV-like protein	ELAVL2;ELAVL4	3	3	3	3	12	3	3
Protein FAM81B	FAM81B	0	1	1	1	3	1	2
Golgin subfamily A member 1	GOLGA1	3	3	2	1	9	3	3
Glutathione S-transferase A5	GSTA5	0	2	3	2	7	1	0
Probable ATP-dependent DNA helicase HFM1	HFM1	1	1	2	3	7	2	0
Probable ATP-dependent DNA helicase HFM1	HFM1	1	1	2	3	7	2	0
Keratin, type I cytoskeletal 18	KRT18	0	0	3	3	6	0	1
Keratin, type I cytoskeletal 18	KRT18	0	0	3	3	6	3	3
Microtubule-associated protein 9	MAP9	0	0	2	2	4	3	2
Non-POU domain-containing octamer-binding protein	NONO	0	0	2	2	4	3	3
Serine/threonine-protein kinase PAK 2; PAK-2p27;PAK-2p34	PAK2	0	0	0	0	**0**	**3**	**1**
Pyruvate carboxylase, mitochondrial	PC	2	2	3	3	10	2	2
Phosphodiesterase	PDE4D	1	2	2	3	8	3	2
Centrosomal protein POC5	POC5	3	1	2	2	8	3	2
Peroxisome proliferator-activated receptor gamma coactivator 1-beta	PPARGC1B	3	2	3	3	11	3	2
26S proteasome non-ATPase regulatory subunit 13	PSMD13	3	3	3	3	12	3	1
GTP-binding protein Rheb	RHEB	0	1	0	0	1	0	1

Protein names	Gene names	noTF_GM	noTF_SM	EGFP_GM	EGFP_SM	sum_bkgd_ctrls	p53_GM	p53_SM
GTP-binding protein Rheb	RHEB	0	1	0	0	1	0	1
Receptor-interacting serine/threonine-protein kinase 2	RIPK2	0	1	3	2	6	2	3
Receptor-interacting serine/threonine-protein kinase 2	RIPK2	0	1	3	2	6	2	3
RRP12-like protein	RRP12	3	3	3	3	12	3	3
RRP12-like protein	RRP12	3	3	3	3	12	3	3
RRP12-like protein	RRP12	3	3	3	3	12	3	3
Protein RUFY3	RUFY3	0	1	1	1	3	1	0
Protein RUFY3	RUFY3	0	1	1	1	3	1	0
RWD domain-containing protein 2B	RWDD2B	2	1	0	0	3	1	2
Lactosylceramide alpha-2,3-sialyltransferase	ST3GAL5	3	3	0	0	6	1	2
Serine/threonine-protein kinase 3;Serine/threonine-protein kinase 3 36kDa subunit;Serine/threonine-protein kinase 3 20kDa subunit	STK3	1	1	0	0	2	0	0
Stomatin-like protein 2, mitochondrial	STOML2	0	0	0	0	**0**	1	0
Stomatin-like protein 2, mitochondrial	STOML2	0	0	0	0	**0**	1	0
Transcription initiation factor TFIID subunit 4B	TAF4B	3	2	3	3	11	3	2
Transcription initiation factor TFIID subunit 4B	TAF4B	3	2	3	3	11	3	2
Transgelin	TAGLN	0	0	0	0	**0**	2	3
Transgelin	TAGLN	1	2	1	1	5	3	0
Transcription elongation factor, mitochondrial	TEFM	1	2	2	2	7	0	1
Transmembrane channel-like protein 2	TMC2	0	1	2	1	4	3	0
Transmembrane emp24 domain-containing protein 9	TMED9	1	1	0	0	2	0	1
Cellular tumor antigen p53	TP53	0	0	0	0	**0**	**3**	**3**
Cellular tumor antigen p53	TP53	0	0	0	0	**0**	**3**	**2**
Cellular tumor antigen p53	TP53	0	0	0	0	**0**	**3**	**2**
Thyroid receptor-interacting protein 11	TRIP11	3	2	3	3	11	3	3
Tetratricopeptide repeat protein 39A	TTC39A	3	3	3	2	11	3	3
Tubulin delta chain	TUBD1	2	2	3	3	10	2	3
NEDD8-conjugating enzyme Ubc12	UBE2M	0	1	0	0	1	0	1
NEDD8-conjugating enzyme Ubc12	UBE2M	0	1	0	0	1	0	1
Probable ubiquitin carboxyl-terminal hydrolase FAF-X;Probable ubiquitin carboxyl-terminal hydrolase FAF-Y	USP9X;USP9Y	0	1	0	1	2	0	0
Probable ubiquitin carboxyl-terminal hydrolase FAF-X;Probable ubiquitin carboxyl-terminal hydrolase FAF-Y	USP9X;USP9Y	0	1	0	0	1	0	0
Vacuolar protein sorting-associated protein 35	VPS35	1	2	2	2	7	2	0

Table 5 **Unique peptides in p53-miniTurbo sample undetected in EGFP-miniTurbo samples or untransfected background controls.**

Protein names	Gene names	sum_noTF	EGFP_GM	EGFP_SM	sum_bkgd_ctrls	p53_GM	p53_SM
ATP-binding cassette sub-family B member 7, mitochondrial	ABCB7	0	0	0	0	3	1
Apoptotic chromatin condensation inducer in the nucleus	ACIN1	0	0	0	0	3	3
Long-chain-fatty-acid--CoA ligase 3	ACSL3	0	0	0	0	1	3
Arf-GAP domain and FG repeat-containing protein 1	AGFG1	0	0	0	0	1	3
Arf-GAP domain and FG repeat-containing protein 1	AGFG1	0	0	0	0	2	3
Bromodomain-containing protein 9	BRD9	0	0	0	0	1	3
UPF0461 protein C5orf24	C5orf24	0	0	0	0	3	3
Caldesmon	CALD1	0	0	0	0	3	1
Caldesmon	CALD1	0	0	0	0	1	3
Craniofacial development protein 1	CFDP1	0	0	0	0	1	3
Cytoskeleton-associated protein 4	CKAP4	0	0	0	0	2	2
Creatine kinase U-type, mitochondrial	CKMT1A; CKMT1B	0	0	0	0	3	1
Calmin	CLMN	0	0	0	0	1	3
Coronin;Coronin-7	CORO7-PAM16; CORO7	0	0	0	0	3	1
Src substrate cortactin	CTTN	0	0	0	0	1	3
Dystonin	DST	0	0	0	0	2	2
Elongation factor 1-beta	EEF1B2	0	0	0	0	2	2
Elongation factor 1-beta	EEF1B2	0	0	0	0	2	2
Eukaryotic translation initiation factor 4B	EIF4B	0	0	0	0	2	3
Eukaryotic translation initiation factor 4H	EIF4H	0	0	0	0	3	1
WASH complex subunit FAM21A;WASH complex subunit FAM21C	FAM21A; FAM21C	0	0	0	0	1	3
Protein FAM91A1	FAM91A1	0	0	0	0	3	1
Pre-mRNA 3-end-processing factor FIP1	FIP1L1	0	0	0	0	1	3
GA-binding protein alpha chain	GABPA	0	0	0	0	2	2
Polypeptide N-acetylgalactosaminyltransferase 6	GALNT6	0	0	0	0	2	2
Glutathione S-transferase kappa 1	GSTK1	0	0	0	0	3	1

Protein names	Gene names	sum_noTF	EGFP_GM	EGFP_SM	sum_bkgd_ctrls	p53_GM	p53_SM
Glutathione S-transferase P	GSTP1	0	0	0	0	3	1
Hematological and neurological expressed 1-like protein	HN1L	0	0	0	0	3	1
Hematological and neurological expressed 1-like protein	HN1L	0	0	0	0	3	3
Heterogeneous nuclear ribonucleoprotein A1;Heterogeneous nuclear ribonucleoprotein A1, N-terminally processed;Heterogeneous nuclear ribonucleoprotein A1-like 2;Heterogeneous nuclear ribonucleoprotein A3	HNRNPA1; HNRNPA1L2; HNRNPA3	0	0	0	0	2	2
Heterogeneous nuclear ribonucleoprotein F;Heterogeneous nuclear ribonucleoprotein F, N-terminally processed	HNRNPF	0	0	0	0	2	2
KH domain-containing, RNA-binding, signal transduction-associated protein 1	KHDRBS1	0	0	0	0	2	3
Shootin-1	KIAA1598	0	0	0	0	2	2
Shootin-1	KIAA1598	0	0	0	0	2	3
Lipoma-preferred partner	LPP	0	0	0	0	1	3
Lipoma-preferred partner	LPP	0	0	0	0	1	3
Double-strand break repair protein MRE11A	MRE11A	0	0	0	0	2	2
Protein LYRIC	MTDH	0	0	0	0	1	3
Nuclear cap-binding protein subunit 2	NCBP2	0	0	0	0	3	2
Nucleolin	NCL	0	0	0	0	3	2
Serine/threonine-protein kinase Nek9	NEK9	0	0	0	0	2	2
Nuclear factor of activated T-cells 5	NFAT5	0	0	0	0	3	1
Non-POU domain-containing octamer-binding protein	NONO	0	0	0	0	3	1
Nuclear pore complex protein Nup214	NUP214	0	0	0	0	2	2
Serine/threonine-protein kinase PAK 2;PAK-2p27;PAK-2p34	PAK2	0	0	0	0	2	2
Serine/threonine-protein kinase PAK 2;PAK-2p27;PAK-2p34	PAK2	0	0	0	0	3	3
PEST proteolytic signal-containing nuclear protein	PCNP	0	0	0	0	2	2
PEST proteolytic signal-containing nuclear protein	PCNP	0	0	0	0	3	3
PEST proteolytic signal-containing nuclear protein	PCNP	0	0	0	0	2	3

Protein names	Gene names	sum_noTF	EGFP_GM	EGFP_SM	sum_bkgd_ctrls	p53_GM	p53_SM
28 kDa heat- and acid-stable phosphoprotein	PDAP1	0	0	0	0	1	3
Programmed cell death protein 5	PDCD5	0	0	0	0	3	3
Prohibitin-2	PHB2	0	0	0	0	3	2
DNA-directed RNA polymerase III subunit RPC2	POLR3B	0	0	0	0	2	2
Protein phosphatase inhibitor 2;Protein phosphatase inhibitor 2-like protein 3	PPP1R2; PPP1R2P3	0	0	0	0	3	1
Protein phosphatase inhibitor 2;Protein phosphatase inhibitor 2-like protein 3	PPP1R2; PPP1R2P3	0	0	0	0	2	2
Ran-specific GTPase-activating protein	RANBP1	0	0	0	0	3	2
Splicing factor 45	RBM17	0	0	0	0	2	3
RNA-binding protein 26	RBM26	0	0	0	0	1	3
SEC23-interacting protein	SEC23IP	0	0	0	0	3	3
Pre-mRNA-splicing factor SLU7	SLU7	0	0	0	0	1	3
Signal recognition particle subunit SRP68	SRP68	0	0	0	0	2	2
SRSF protein kinase 1;SRSF protein kinase 3;SRSF protein kinase 2;SRSF protein kinase 2 N-terminal;SRSF protein kinase 2 C-terminal	SRPK1;SRPK3; SRPK2	0	0	0	0	2	2
Transforming acidic coiled-coil-containing protein 1	TACC1	0	0	0	0	2	3
Transcription initiation factor TFIID subunit 7	TAF7	0	0	0	0	2	3
Transgelin	TAGLN	0	0	0	0	2	3
Testin	TES	0	0	0	0	2	2
Testin	TES	0	0	0	0	2	3
Tight junction protein ZO-2	TJP2	0	0	0	0	2	2
Talin-1	TLN1	0	0	0	0	2	2
Cellular tumor antigen p53	TP53	0	0	0	0	3	3
Cellular tumor antigen p53	TP53	0	0	0	0	3	3
Cellular tumor antigen p53	TP53	0	0	0	0	2	3
Cellular tumor antigen p53	TP53	0	0	0	0	3	3
Cellular tumor antigen p53	TP53	0	0	0	0	3	3
Cellular tumor antigen p53	TP53	0	0	0	0	3	3
Cellular tumor antigen p53	TP53	0	0	0	0	3	1
Cellular tumor antigen p53	TP53	0	0	0	0	3	2
Cellular tumor antigen p53	TP53	0	0	0	0	3	3
Cellular tumor antigen p53	TP53	0	0	0	0	2	2

Protein names	Gene names	sum_noTF	EGFP_GM	EGFP_SM	sum_bkgd_ctrls	p53_GM	p53_SM
Cellular tumor antigen p53	TP53	0	0	0	0	2	3
Cellular tumor antigen p53	TP53	0	0	0	0	2	3
Cellular tumor antigen p53	TP53	0	0	0	0	3	3
Cellular tumor antigen p53	TP53	0	0	0	0	3	3
Cellular tumor antigen p53	TP53	0	0	0	0	3	2
Cellular tumor antigen p53	TP53	0	0	0	0	3	3
Cellular tumor antigen p53	TP53	0	0	0	0	3	3
Cellular tumor antigen p53	TP53	0	0	0	0	3	2
Cellular tumor antigen p53	TP53	0	0	0	0	3	3
Cellular tumor antigen p53	TP53	0	0	0	0	3	3
Cellular tumor antigen p53	TP53	0	0	0	0	2	3
Tumor protein D52	TPD52	0	0	0	0	3	1
Transcription intermediary factor 1-alpha	TRIM24	0	0	0	0	2	2
Thioredoxin	TXN	0	0	0	0	3	3
Ubiquitin-associated protein 2-like	UBAP2L	0	0	0	0	2	3
UHRF1-binding protein 1	UHRF1BP1	0	0	0	0	2	3
Regulator of nonsense transcripts 1	UPF1	0	0	0	0	2	2
Regulator of nonsense transcripts 1	UPF1	0	0	0	0	3	3
Regulator of nonsense transcripts 1	UPF1	0	0	0	0	2	3
Vinculin	VCL	0	0	0	0	3	1
WD repeat-containing protein 70	WDR70	0	0	0	0	2	2
14-3-3 protein eta	YWHAH	0	0	0	0	1	3
Zinc finger protein 638	ZNF638	0	0	0	0	2	2
Zyxin	ZYX	0	0	0	0	3	1

Table 6 **48 p53/starvation-dependently differentially regulated transcripts.**

gene_id	gene_symbol	avg_p53KO GM	avg_p53KO SM	avg_FLAGp53 GM	avg_FLAGp53 SM
ENSG00000180672	AC007362.1	0.152	0.211	0.224	0.777
ENSG00000087085	ACHE	0.249	0.877	1.108	3.098
ENSG00000136378	ADAMTS7	0.014	0.058	0.200	0.799
ENSG00000184060	ADAP2	0.411	0.867	0.496	2.010
ENSG00000164742	ADCY1	0.206	0.300	0.335	0.607
ENSG00000029534	ANK1	0.046	0.018	0.375	0.933
ENSG00000225485	ARHGAP23	0.061	0.508	1.369	2.256
ENSG00000165895	ARHGAP42	0.282	0.809	0.357	1.077
ENSG00000154040	CABYR	0.118	0.378	0.569	1.570
ENSG00000130940	CASZ1	0.302	1.000	0.491	2.862
ENSG00000111860	CEP85L	0.299	0.488	0.783	2.514
ENSG00000172346	CSDC2	0.899	4.471	1.831	9.998
ENSG00000134762	DSC3	0.017	0.113	1.073	1.988
ENSG00000122877	EGR2	0.222	0.468	0.534	1.637
ENSG00000113578	FGF1	1.047	1.348	1.644	3.088
ENSG00000144596	GRIP2	0.059	0.059	0.691	1.861
ENSG00000198857	HSD3BP5	0.016	0.549	0.999	3.845
ENSG00000163395	IGFN1	0.076	0.086	0.151	0.383
ENSG00000143195	ILDR2	0.062	0.056	0.056	0.362
ENSG00000161896	IP6K3	0.047	0.015	0.300	0.902
ENSG00000165757	KIAA1462	0.020	0.007	0.131	0.573
ENSG00000162849	KIF26B	0.057	0.118	0.093	0.777
ENSG00000078081	LAMP3	0.076	0.385	1.376	3.195
ENSG00000250337	LINC01021	5.335	2.810	9.152	26.042
ENSG00000182759	MAFA	0.090	0.371	0.768	1.704
ENSG00000176845	METRNL	3.058	20.326	7.323	44.791
ENSG00000258590	NBEAP1	0.013	0.073	0.572	1.577
ENSG00000064300	NGFR	0.435	1.233	1.299	4.278
ENSG00000118257	NRP2	0.341	1.061	0.828	3.824
ENSG00000065320	NTN1	0.102	0.213	0.553	1.257
ENSG00000178602	OTOS	0.051	0.000	1.092	5.916
ENSG00000145431	PDGFC	1.207	1.089	0.926	3.189
ENSG00000122861	PLAU	0.256	0.743	0.814	1.314
ENSG00000120278	PLEKHG1	0.028	0.017	0.202	0.467
ENSG00000244694	PTCHD4	0.066	0.169	1.125	3.297
ENSG00000163564	PYHIN1	0.011	0.031	0.186	0.452
ENSG00000213694	S1PR3	0.012	0.065	0.738	3.439
ENSG00000185669	SNAI3	0.345	0.398	1.080	2.760
ENSG00000184985	SORCS2	0.057	0.015	0.982	2.655
ENSG00000128487	SPECC1	0.589	1.421	0.627	2.162
ENSG00000162009	SSTR5	6.300	5.387	7.896	9.797
ENSG00000198075	SULT1C4	0.589	0.483	0.537	1.535
ENSG00000104055	TGM5	0.319	0.883	1.317	3.273
ENSG00000122574	WIPF3	0.020	0.060	0.054	0.515
ENSG00000143816	WNT9A	0.018	0.198	0.254	0.960
ENSG00000151789	ZNF385D	0.055	0.086	0.191	1.065

Table 7 **qPCR primer list.**

qPCR primer		
B2M(housekeeper)	CCACTGAAAAAGATGAGTATGCCT	CCAATCCAAATGCGGCATCTTCA
CDKN1A	GGCAGACCAGCATGACAGATT	GCGGATTAGGGCTTCCTCTT
GADD45A	GAGAGCAGAAGACCGAAAGGA	CACAACACCACGTTATCGGG
MDM2	GAATCATCGGACTCAGGTACATC	TCTGTCTCACTAATTGCTCTCCT
METRNL	AGTGGATGTACCCAACAGGTG	TACCAGCAGTCTCAGTTCTCC
PAK2	ACCCTTTGTCAGCCAATCAC	AACATGGATGGTGTGCTCAA
PHLDA3	CTGGATGGTCCCAGACTCTCAG	CTAAGAGCAGTCTGCAGGACAG
PLAU	GCTTGTCCAAGAGTGCATGGT	CAGGGCTGGTTCTCGATGG
PLEKHG1	GCAGCAGAATGACCTTAGTTTCA	GCTCCAGTTTTATGGCCCCTA
PPIA(housekeeper)	GGCAAATGCTGGACCCAACACA	TGCTGGTCTTGCCATTCCTGGA
SESN1	CTACATTGGAATAATGGCTGCGG	AGGTCTATGGGCTAACACTTTGT
SORCS2	TGTACGCCCAAATGCACAAC	CTCTCGGGAGTTGATGCTCA
TIGAR	ACTCAAGACTTCGGGAAAGGA	CACGCATTTTCACCTGGTCC
TP53 Pb1	CAGCACATGACGGAGGTTGT	TCATCCAAATACTCCACACGC
TP53 Pb2	GAGGTTGGCTCTGACTGTACC	TCCGTCCCAGTAGATTACCAC

Bibliography

Adeva-Andany, M. M. *et al.* (2016) 'Glycogen metabolism in humans', *BBA Clinical*, 5, pp. 85–100. doi: 10.1016/j.bbacli.2016.02.001.

Agledal, L., Niere, M. and Ziegler, M. (2010) 'The phosphate makes a difference: Cellular functions of NADP', *Redox Report*, 15(1), pp. 2–10. doi: 10.1179/174329210X12650506623122.

Akella, N. M., Ciraku, L. and Reginato, M. J. (2019) 'Fueling the fire: Emerging role of the hexosamine biosynthetic pathway in cancer', *BMC Biology*, 17(1), pp. 1–14. doi: 10.1186/s12915-019-0671-3.

Anand, S. *et al.* (2017) 'Label-based and label-free strategies for protein quantitation', *Methods in Molecular Biology*, 1549, pp. 31–43. doi: 10.1007/978-1-4939-6740-7_4.

Aquilano, K., Baldelli, S. and Ciriolo, M. R. (2014) 'Glutathione: New roles in redox signalling for an old antioxidant', *Frontiers in Pharmacology*, 5 AUG(August), pp. 1–12. doi: 10.3389/fphar.2014.00196.

Araki, K. *et al.* (2015) 'P53 regulates cytoskeleton remodeling to suppress tumor progression', *Cellular and Molecular Life Sciences*, 72(21), pp. 4077–4094. doi: 10.1007/s00018-015-1989-9.

Aubrey, B. J. *et al.* (2018) 'How does p53 induce apoptosis and how does this relate to p53-mediated tumour suppression?', *Cell Death and Differentiation*, 25(1), pp. 104–113. doi: 10.1038/cdd.2017.169.

Bae, S. *et al.* (2012) 'TRIAD1 inhibits MDM2-mediated p53 ubiquitination and degradation', *FEBS Letters*, 586(19), pp. 3057–3063. doi: 10.1016/j.febslet.2012.07.022.

Bailey, C. G. *et al.* (2011) 'Loss-of-function mutations in the glutamate transporter SLC1A1 cause human dicarboxylic aminoaciduria', *Journal of Clinical Investigation*, 121(1), pp. 446–453. doi: 10.1172/JCI44474.

Balsa, E. *et al.* (2020) 'Defective NADPH production in mitochondrial disease complex I causes inflammation and cell death', *Nature Communications*, 11(1), pp. 1–12. doi: 10.1038/s41467-020-16423-1.

Banko, M. R. *et al.* (2011) 'Chemical Genetic Screen for AMPKα2 Substrates Uncovers a Network of Proteins Involved in Mitosis', *Molecular Cell*, 44(6), pp. 878–892. doi:

10.1016/j.molcel.2011.11.005.

Barker, D. F. and Campbell, A. M. (1981) 'Genetic and biochemical characterization of the birA gene and its product: Evidence for a direct role of biotin holoenzyme synthetase in repression of the biotin operon in Escherichia coli', *Journal of Molecular Biology*, 146(4), pp. 469–492. doi: 10.1016/0022-2836(81)90043-7.

Bartman, C. R. *et al.* (2021) 'Slow TCA flux implies low ATP production in tumors'.

Bartrons, R. *et al.* (2018) 'Fructose 2,6-bisphosphate in cancer cell metabolism', *Frontiers in Oncology*, 8(SEP). doi: 10.3389/fonc.2018.00331.

Batuello, C. N. *et al.* (2015) 'Src phosphorylation converts Mdm2 from a ubiquitinating to a neddylating E3 ligase', *Proceedings of the National Academy of Sciences*, 112(6), pp. 1749–1754. doi: 10.1073/pnas.1416656112.

Baumann, C. A. *et al.* (2000) 'CAP defines a second signalling pathway required for insulin-stimulated glucose transport', *Nature*, 407(6801), pp. 202–207. doi: 10.1038/35025089.

Bensaad, K. *et al.* (2006) 'TIGAR, a p53-Inducible Regulator of Glycolysis and Apoptosis', *Cell*, 126(1), pp. 107–120. doi: 10.1016/j.cell.2006.05.036.

Bian, L. *et al.* (2019) 'MRE11-RAD50-NBS1 complex alterations and DNA damage response: Implications for cancer treatment', *Molecular Cancer*, 18(1), pp. 1–14. doi: 10.1186/s12943-019-1100-5.

Boggild, S. *et al.* (2016) 'Spatiotemporal patterns of sortilin and SorCS2 localization during organ development', *BMC Cell Biology*, 17(1), pp. 1–18. doi: 10.1186/s12860-016-0085-9.

Boidot, R. *et al.* (2012) 'Regulation of monocarboxylate transporter MCT1 expression by p53 mediates inward and outward lactate fluxes in tumors', *Cancer Research*, 72(4), pp. 939–948. doi: 10.1158/0008-5472.CAN-11-2474.

Branon, T. C. *et al.* (2018) 'Efficient proximity labeling in living cells and organisms with TurboID', *Nature Biotechnology*, 36(9), pp. 880–898. doi: 10.1038/nbt.4201.

Breitkreutz, A. *et al.* (2010) 'A Global Protein Kinase and Phosphatase Interaction Network in Yeast', *Science*, 328(5981), pp. 1043–1046. doi: 10.1126/science.1176495.

Breuhahn, K., Longerich, T. and Schirmacher, P. (2006) 'Dysregulation of growth factor signaling in human hepatocellular carcinoma', *Oncogene*, 25(27), pp. 3787–3800. doi: 10.1038/sj.onc.1209556.

Budanov, A. V. and Karin, M. (2008a) ‘p53 Target Genes Sestrin1 and Sestrin2 Connect Genotoxic Stress and mTOR Signaling’, *Cell*, 134(3), pp. 451–460. doi: 10.1016/j.cell.2008.06.028.

Budanov, A. V. and Karin, M. (2008b) ‘p53 Target Genes Sestrin1 and Sestrin2 Connect Genotoxic Stress and mTOR Signaling’, *Cell*, 134(3), pp. 451–460. doi: 10.1016/j.cell.2008.06.028.

de Cabo, R. and Mattson, M. P. (2019) ‘Effects of Intermittent Fasting on Health, Aging, and Disease’, *New England Journal of Medicine*, 381(26), pp. 2541–2551. doi: 10.1056/nejmra1905136.

Celestini, V. *et al.* (2018) ‘Uncoupling FoxO3A mitochondrial and nuclear functions in cancer cells undergoing metabolic stress and chemotherapy article’, *Cell Death and Disease*, 9(2). doi: 10.1038/s41419-018-0336-0.

Chapman-Smith, A. and Cronan, J. E. (1999) ‘The enzymatic biotinylation of proteins: A post-translational modification of exceptional specificity’, *Trends in Biochemical Sciences*, 24(9), pp. 359–363. doi: 10.1016/S0968-0004(99)01438-3.

Cheong, L. Y. and Xu, A. (2021) ‘Intercellular and inter-organ crosstalk in browning of white adipose tissue: Molecular mechanism and therapeutic complications’, *Journal of Molecular Cell Biology*, 13(7), pp. 466–479. doi: 10.1093/jmcb/mjab038.

Choi, H. *et al.* (2011) ‘SAINT: Probabilistic scoring of affinity purificationg-mass spectrometry data’, *Nature Methods*, 8(1), pp. 70–73. doi: 10.1038/nmeth.1541.

Choi, H. *et al.* (2012) ‘SAINT-MS1: Protein-protein interaction scoring using label-free intensity data in affinity purification-mass spectrometry experiments’, *Journal of Proteome Research*, 11(4), pp. 2619–2624. doi: 10.1021/pr201185r.

Choi, Y.-K. and Park, K.-G. (2017) ‘Targeting Glutamine Metabolism for Cancer Treatment’, *Biomolecules & Therapeutics*, 26(1), pp. 19–28. doi: 10.4062/biomolther.2017.178.

Comel, A. *et al.* (2014) ‘The cytoplasmic side of p53’s oncosuppressive activities’, *FEBS Letters*, 588(16), pp. 2600–2609. doi: 10.1016/j.febslet.2014.04.015.

Commisso, C. *et al.* (2013) ‘Macropinocytosis of protein is an amino acid supply route in Ras-transformed cells’, *Nature*, 497(7451), pp. 633–637. doi: 10.1038/nature12138.

Contadini, C. *et al.* (2019) ‘p53 mitotic centrosome localization preserves centrosome integrity and works as sensor for the mitotic surveillance pathway’, *Cell Death & Disease*, 10(11), p.

850. doi: 10.1038/s41419-019-2076-1.

Cox, J. *et al.* (2014) 'Accurate proteome-wide label-free quantification by delayed normalization and maximal peptide ratio extraction, termed MaxLFQ', *Molecular and Cellular Proteomics*, 13(9), pp. 2513–2526. doi: 10.1074/mcp.M113.031591.

Cui, D. *et al.* (2021) 'The Cross Talk Between p53 and mTOR Pathways in Response to Physiological and Genotoxic Stresses', *Frontiers in Cell and Developmental Biology*, 9. doi: 10.3389/fcell.2021.775507.

DeBerardinis, R. J. *et al.* (2007) 'Beyond aerobic glycolysis: Transformed cells can engage in glutamine metabolism that exceeds the requirement for protein and nucleotide synthesis', *Proceedings of the National Academy of Sciences of the United States of America*, 104(49), pp. 19345–19350. doi: 10.1073/pnas.0709747104.

DeBerardinis, R. J. and Chandel, N. S. (2016) 'Fundamentals of cancer metabolism', *Science Advances*, 2(5), p. e1600200. doi: 10.1126/sciadv.1600200.

Deligiorgi, M. V., Liapi, C. and Trafalis, D. T. (2020) 'How Far Are We from Prescribing Fasting as Anticancer Medicine?', *International journal of molecular sciences*, 21(23), pp. 1–30. doi: 10.3390/ijms21239175.

Deng, L. *et al.* (2020) 'p53-mediated control of aspartate-asparagine homeostasis dictates LKB1 activity and modulates cell survival', *Nature Communications*, 11(1). doi: 10.1038/s41467-020-15573-6.

Donner, A. J. *et al.* (2007) 'Stimulus-specific transcriptional regulation within the p53 network', *Cell Cycle*, 6(21), pp. 2594–2598. doi: 10.4161/cc.6.21.4893.

Ducker, G. S. and Rabinowitz, J. D. (2017) 'One-Carbon Metabolism in Health and Disease', *Cell Metabolism*, 25(1), pp. 27–42. doi: 10.1016/j.cmet.2016.08.009.

Dunham, W. H., Mullin, M. and Gingras, A. C. (2012) 'Affinity-purification coupled to mass spectrometry: Basic principles and strategies', *Proteomics*, 12(10), pp. 1576–1590. doi: 10.1002/pmic.201100523.

Elia, N. *et al.* (2011) 'Dynamics of endosomal sorting complex required for transport (ESCRT) machinery during cytokinesis and its role in abscission', *Proceedings of the National Academy of Sciences of the United States of America*, 108(12), pp. 4846–4851. doi: 10.1073/pnas.1102714108.

Embade, N. *et al.* (2012) 'Murine double minute 2 regulates Hu antigen R stability in human

liver and colon cancer through NEDDylation', *Hepatology*, 55(4), pp. 1237–1248. doi: 10.1002/hep.24795.

Eriksson, M. *et al.* (2017) 'Effect of Mutant p53 Proteins on Glycolysis and Mitochondrial Metabolism', *Molecular and Cellular Biology*, 37(24), pp. 1–17. doi: 10.1128/MCB.00328-17.

Eriksson, S. E. *et al.* (2019) 'P53 as a hub in cellular redox regulation and therapeutic target in cancer', *Journal of Molecular Cell Biology*, 11(4), pp. 330–341. doi: 10.1093/jmcb/mjz005.

Falcicchio, M. *et al.* (2020) 'Regulation of p53 by the 14-3-3 protein interaction network: new opportunities for drug discovery in cancer.', *Cell death discovery*, 6(1), p. 126. doi: 10.1038/s41420-020-00362-3.

Fan, J. *et al.* (2015) 'Human phosphoglycerate dehydrogenase produces the oncometabolite D-2-hydroxyglutarate', *ACS Chemical Biology*, 10(2), pp. 510–516. doi: 10.1021/cb500683c.

Faubert, B., Solmonson, A. and DeBerardinis, R. J. (2020) 'Metabolic reprogramming and cancer progression', *Science*, 368(6487). doi: 10.1126/science.aaw5473.

Feng, Z. (2010) 'p53 regulation of the IGF-1/AKT/mTOR pathways and the endosomal compartment.', *Cold Spring Harbor perspectives in biology*, 2(2), pp. 1–10. doi: 10.1101/cshperspect.a001057.

Fischer, M. (2017) 'Census and evaluation of p53 target genes.', *Oncogene*, 36(28), pp. 3943–3956. doi: 10.1038/onc.2016.502.

Flöter, J., Kaymak, I. and Schulze, A. (2017) 'Regulation of Metabolic Activity by p53.', *Metabolites*, 7(2), p. 21. doi: 10.3390/metabo7020021.

Fournier, L. A., Kumar, A. and Stirling, P. C. (2018) 'Chromatin as a platform for modulating the replication stress response', *Genes*, 9(12), pp. 1–17. doi: 10.3390/genes9120622.

Franklin, D. A. *et al.* (2016) 'P53 coordinates DNA repair with nucleotide synthesis by suppressing PFKFB3 expression and promoting the pentose phosphate pathway', *Scientific Reports*, 6(March), pp. 1–13. doi: 10.1038/srep38067.

Führing, J. I. *et al.* (2015) 'A Quaternary Mechanism Enables the Complex Biological Functions of Octameric Human UDP-glucose Pyrophosphorylase, a Key Enzyme in Cell Metabolism', *Scientific Reports*, 5, pp. 1–11. doi: 10.1038/srep09618.

Fuller, G. G. and Kim, J. K. (2021) 'Compartmentalization and metabolic regulation of glycolysis', *Journal of Cell Science*, 134(20). doi: 10.1242/jcs.258469.

Galhuber, M. *et al.* (2022) ‘Complementary omics strategies to dissect p53 signaling networks under nutrient stress’, *Cellular and Molecular Life Sciences*, 79(6). doi: 10.1007/s00018-022-04345-8.

Geeraerts, S. L. *et al.* (2021) ‘The ins and outs of serine and glycine metabolism in cancer’, *Nature Metabolism*, 3(2), pp. 131–141. doi: 10.1038/s42255-020-00329-9.

Gingras, A.-C. *et al.* (2013) ‘SAINTexpress: Improvements and additional features in Significance Analysis of INTeractome software’, *Journal of Proteomics*, 100, pp. 37–43. doi: 10.1016/j.jprot.2013.10.023.

Gonzalez-Rellan, M. J. *et al.* (2021) ‘O-GlcNAcylated p53 in the liver modulates hepatic glucose production.’, *Nature communications*, 12(1), p. 5068. doi: 10.1038/s41467-021-25390-0.

Green, N. M. (1975) ‘Avidin’, in *Bioactive Egg Compounds*, pp. 85–133. doi: 10.1016/S0065-3233(08)60411-8.

Hafner, A. *et al.* (2019) ‘The multiple mechanisms that regulate p53 activity and cell fate’, *Nature Reviews Molecular Cell Biology*, 20(4), pp. 199–210. doi: 10.1038/s41580-019-0110-x.

Hafner, A. *et al.* (2020) ‘Identification of universal and cell-Type specific p53 DNA binding’, *BMC Molecular and Cell Biology*, 21(1), pp. 1–12. doi: 10.1186/s12860-020-00251-8.

Hampe, W. *et al.* (2001) ‘The genes for the human VPS10 domain-containing receptors are large and contain many small exons’, *Human Genetics*, 108(6), pp. 529–536. doi: 10.1007/s004390100504.

Hancock, M. L. *et al.* (2019) ‘Insulin Receptor Associates with Promoters Genome-wide and Regulates Gene Expression’, *Cell*, 177(3), pp. 722-736.e22. doi: 10.1016/j.cell.2019.02.030.

Hardie, D. G. (2015) ‘AMPK: positive and negative regulation, and its role in whole-body energy homeostasis.’, *Current opinion in cell biology*, 33, pp. 1–7. doi: 10.1016/j.ceb.2014.09.004.

Harton, M. D. *et al.* (2019) ‘P53 Pulse Modulation Differentially Regulates Target Gene Promoters To Regulate Cell Fate Decisions’, *Molecular Systems Biology*, 15(9), pp. 1–15. doi: 10.15252/msb.20188685.

Heiden, M. G. V., Cantley, L. C. and Thompson, C. B. (2009) ‘Understanding the warburg effect: The metabolic requirements of cell proliferation’, *Science*, 324(5930), pp. 1029–1033. doi: 10.1126/science.1160809.

Hensley, C. T., Wasti, A. T. and DeBerardinis, R. J. (2013) 'Glutamine and cancer: cell biology, physiology, and clinical opportunities', *Journal of Clinical Investigation*, 123(9), pp. 3678–3684. doi: 10.1172/JCI69600.

Ho, T., Tan, B. X. and Lane, D. (2020) 'How the other half lives: What p53 does when it is not being a transcription factor', *International Journal of Molecular Sciences*, 21(1). doi: 10.3390/ijms21010013.

Hock, A. K. and Vousden, K. H. (2014) 'The role of ubiquitin modification in the regulation of p53', *Biochimica et Biophysica Acta - Molecular Cell Research*, 1843(1), pp. 137–149. doi: 10.1016/j.bbamcr.2013.05.022.

Hoffman, E. A. *et al.* (2015) 'Formaldehyde crosslinking: A tool for the study of chromatin complexes', *Journal of Biological Chemistry*, 290(44), pp. 26404–26411. doi: 10.1074/jbc.R115.651679.

Hosios, A. M. *et al.* (2016) 'Amino Acids Rather than Glucose Account for the Majority of Cell Mass in Proliferating Mammalian Cells', *Developmental Cell*, 36(5), pp. 540–549. doi: 10.1016/j.devcel.2016.02.012.

Hu, W. *et al.* (2010) 'Glutaminase 2, a novel p53 target gene regulating energy metabolism and antioxidant function', *Proceedings of the National Academy of Sciences*, 107(16), pp. 7455–7460. doi: 10.1073/pnas.1001006107.

Ji, X. *et al.* (2015) 'Chromatin proteomic profiling reveals novel proteins associated with histone-marked genomic regions', *Proceedings of the National Academy of Sciences of the United States of America*, 112(12), pp. 3841–3846. doi: 10.1073/pnas.1502971112.

Jiang, P. *et al.* (2011) 'p53 regulates biosynthesis through direct inactivation of glucose-6-phosphate dehydrogenase', *Nature Cell Biology*, 13(3), pp. 310–316. doi: 10.1038/ncb2172.

Jin, M. *et al.* (2017) 'Glycolytic Enzymes Coalesce in G Bodies under Hypoxic Stress', *Cell Reports*, 20(4), pp. 895–908. doi: 10.1016/j.celrep.2017.06.082.

Jones, R. G. *et al.* (2005) 'AMP-activated protein kinase induces a p53-dependent metabolic checkpoint', *Molecular Cell*, 18(3), pp. 283–293. doi: 10.1016/j.molcel.2005.03.027.

Kamura, T. *et al.* (2001) 'MUF1, A Novel Elongin BC-interacting Leucine-rich Repeat Protein That Can Assemble with Cul5 and Rbx1 to Reconstitute a Ubiquitin Ligase', *Journal of Biological Chemistry*, 276(32), pp. 29748–29753. doi: 10.1074/jbc.M103093200.

Kamura, T. *et al.* (2004) 'VHL-box and SOCS-box domains determine binding specificity for

Cul2-Rbx1 and Cul5-Rbx2 modules of ubiquitin ligases', *Genes & Development*, 18(24), pp. 3055–3065. doi: 10.1101/gad.1252404.

Kärkkäinen, S. *et al.* (2006) 'Identification of preferred protein interactions by phage-display of the human Src homology-3 proteome', *EMBO Reports*, 7(2), pp. 186–191. doi: 10.1038/sj.embor.7400596.

Kastenhuber, E. R. and Lowe, S. W. (2017) 'Putting p53 in Context', *Cell*, 170(6), pp. 1062–1078. doi: 10.1016/j.cell.2017.08.028.

Kawauchi, K. *et al.* (2008) 'p53 regulates glucose metabolism through an IKK-NF-κB pathway and inhibits cell transformation', *Nature Cell Biology*, 10(5), pp. 611–618. doi: 10.1038/ncb1724.

Kelsall, I. R. *et al.* (2013) 'TRIAD1 and HHARI bind to and are activated by distinct neddylated Cullin-RING ligase complexes', *The EMBO Journal*, 32(21), pp. 2848–2860. doi: 10.1038/emboj.2013.209.

Kim, D. I. *et al.* (2014) 'Probing nuclear pore complex architecture with proximity-dependent biotinylation', *Proceedings of the National Academy of Sciences of the United States of America*, 111(24), pp. 2453–2461. doi: 10.1073/pnas.1406459111.

Kim, D. I. *et al.* (2016) 'An improved smaller biotin ligase for BioID proximity labeling', *Molecular Biology of the Cell*, 27(8), pp. 1188–1196. doi: 10.1091/mbc.E15-12-0844.

Kim, D. I. and Roux, K. J. (2016) 'Filling the Void : Proximity- Based Labeling of Proteins in Living Cells', *Trends in Cell Biology*, 26(11), pp. 804–817. doi: 10.1016/j.tcb.2016.09.004.

Kitamura, N. *et al.* (2011) 'Mieap, a p53-inducible protein, controls mitochondrial quality by repairing or eliminating unhealthy mitochondria', *PLoS ONE*, 6(1). doi: 10.1371/journal.pone.0016060.

Knight, J. D. R. *et al.* (2015) 'A web-tool for visualizing quantitative protein-protein interaction data', *Proteomics*, 15(8), pp. 1432–1436. doi: 10.1002/pmic.201400429.

Kohnhorst, C. L. *et al.* (2017) 'Identification of a multienzyme complex for glucose metabolism in living cells', *Journal of Biological Chemistry*, 292(22), pp. 9191–9203. doi: 10.1074/jbc.M117.783050.

Komposch, K. and Sibilia, M. (2016) 'EGFR signaling in liver diseases', *International Journal of Molecular Sciences*, 17(1). doi: 10.3390/ijms17010030.

Kondoh, H. *et al.* (2005) 'Glycolytic enzymes can modulate cellular life span', *Cancer Research*, 65(1), pp. 177–185.

Kostrhon, S. *et al.* (2021) 'CUL5-ARIH2 E3-E3 ubiquitin ligase structure reveals cullin-specific NEDD8 activation', *Nature Chemical Biology*, 17(10), pp. 1075–1083. doi: 10.1038/s41589-021-00858-8.

Krstic, J. *et al.* (2018) 'p53 as a Dichotomous Regulator of Liver Disease: The Dose Makes the Medicine', *International Journal of Molecular Sciences*, 19(3), p. 921. doi: 10.3390/ijms19030921.

Krstic, J. *et al.* (2022) 'Fasting improves therapeutic response in hepatocellular carcinoma through p53-dependent metabolic synergism', *Science Advances*, 8(3). doi: 10.1126/sciadv.abh2635.

Kruiswijk, F., Labuschagne, C. F. and Vousden, K. H. (2015) 'P53 in Survival, Death and Metabolic Health: a Lifeguard With a Licence To Kill', *Nature Reviews Molecular Cell Biology*, 16(7), pp. 393–405. doi: 10.1038/nrm4007.

Kumar, R. *et al.* (2017) 'Structure, biochemistry, and biology of PAK kinases', *Gene*, 605(77), pp. 20–31. doi: 10.1016/j.gene.2016.12.014.

Kumar, S., Yoshida, Y. and Noda, M. (1993) 'Cloning of a cDNA Which Encodes a Novel Ubiquitin-like Protein', *Biochemical and Biophysical Research Communications*, 195(1), pp. 393–399. doi: 10.1006/bbrc.1993.2056.

Kunz, C. *et al.* (1995) 'Differential regulation of plasminogen activator and inhibitor gene transcription by the tumor suppressor p53', *Nucleic Acids Research*, 23(18), pp. 3710–3717. doi: 10.1093/nar/23.18.3710.

Kussie, P. H. *et al.* (1996) 'Structure of the MDM2 Oncoprotein Bound to the p53 Tumor Suppressor Transactivation Domain', *Science*, 274(5289), pp. 948–953. doi: 10.1126/science.274.5289.948.

Kwon, K. and Beckett, D. (2000) 'Function of a conserved sequence motif in biotin holoenzyme synthetases', *Protein Science*, 9(8), pp. 1530–1539. doi: 10.1110/ps.9.8.1530.

Lacroix, M. *et al.* (2020) 'Metabolic functions of the tumor suppressor p53: Implications in normal physiology, metabolic disorders, and cancer', *Molecular Metabolism*, 33(October 2019), pp. 2–22. doi: 10.1016/j.molmet.2019.10.002.

Lahalle, A. *et al.* (2021) 'The p53 pathway and metabolism: The tree that hides the forest',

Cancers, 13(1), pp. 1–17. doi: 10.3390/cancers13010133.

Lambrus, B. G. and Holland, A. J. (2017) 'A New Mode of Mitotic Surveillance', *Trends in Cell Biology*, 27(5), pp. 314–321. doi: 10.1016/j.tcb.2017.01.004.

Lange, M. *et al.* (2011) 'Combinatorial assembly and function of chromatin regulatory complexes', *Epigenomics*, 3(5), pp. 567–580. doi: 10.2217/epi.11.83.

Laubach, K., Zhang, J. and Chen, X. (2021) 'The p53 Family: A Role in Lipid and Iron Metabolism', *Frontiers in Cell and Developmental Biology*, 9(July), pp. 1–11. doi: 10.3389/fcell.2021.715974.

Lee, S. M. *et al.* (2009) 'A nucleocytoplasmic malate dehydrogenase regulates p53 transcriptional activity in response to metabolic stress', *Cell Death and Differentiation*, 16(5), pp. 738–748. doi: 10.1038/cdd.2009.5.

Lee, S. W. *et al.* (2019) 'EGFR-Pak Signaling Selectively Regulates Glutamine Deprivation-Induced Macropinocytosis', *Developmental Cell*, 50(3), pp. 381-392.e5. doi: 10.1016/j.devcel.2019.05.043.

Leung, R. W. T. *et al.* (2019) 'ENPD-A Database of Eukaryotic Nucleic Acid Binding Proteins: Linking Gene Regulations to Proteins', *Nucleic Acids Research*, 47(D1), pp. D322–D329. doi: 10.1093/nar/gky1112.

Levine, A. J. (2020) 'P53: 800 Million Years of Evolution and 40 Years of Discovery', *Nature Reviews Cancer*, 20(8), pp. 471–480. doi: 10.1038/s41568-020-0262-1.

Li, X. *et al.* (2016) 'The MDM2-p53-pyruvate carboxylase signalling axis couples mitochondrial metabolism to glucose-stimulated insulin secretion in pancreatic β-cells', *Nature Communications*, 7. doi: 10.1038/ncomms11740.

Li, Yongmei *et al.* (2018) 'Multiomics integration reveals the landscape of prometastasis metabolism in hepatocellular carcinoma', *Molecular and Cellular Proteomics*, 17(4), pp. 607–618. doi: 10.1074/mcp.RA118.000586.

Liao, Y. *et al.* (2019) 'WebGestalt 2019: gene set analysis toolkit with revamped UIs and APIs', *Nucleic Acids Research*, 47(W1), pp. W199–W205. doi: 10.1093/nar/gkz401.

Licciulli, S. *et al.* (2013) 'FRAX597, a small molecule inhibitor of the p21-activated kinases, inhibits tumorigenesis of neurofibromatosis type 2 (NF2)-associated schwannomas', *Journal of Biological Chemistry*, 288(40), pp. 29105–29114. doi: 10.1074/jbc.M113.510933.

Liebl, M. C. and Hofmann, T. G. (2019) 'Cell Fate Regulation upon DNA Damage: p53 Serine 46 Kinases Pave the Cell Death Road', *BioEssays*, 41(12), pp. 1–11. doi: 10.1002/bies.201900127.

Liu, B., Chen, Y. and St. Clair, D. K. (2008) 'ROS and p53: A versatile partnership', *Free Radical Biology and Medicine*, 44(8), pp. 1529–1535. doi: 10.1016/j.freeradbiomed.2008.01.011.

Liu, G. and Xirodimas, D. P. (2010) 'NUB1 promotes cytoplasmic localization of p53 through cooperation of the NEDD8 and ubiquitin pathways', *Oncogene*, 29(15), pp. 2252–2261. doi: 10.1038/onc.2009.494.

Liu, H., Liu, K. and Dong, Z. (2021) 'The Role of p21-Activated Kinases in Cancer and Beyond: Where Are We Heading?', *Frontiers in Cell and Developmental Biology*, 9(March), pp. 1–12. doi: 10.3389/fcell.2021.641381.

Liu, Y., Tavana, O. and Gu, W. (2019) 'P53 Modifications: Exquisite Decorations of the Powerful Guardian', *Journal of molecular cell biology*, 11(7), pp. 564–577. doi: 10.1093/jmcb/mjz060.

Lobato-Gil, S. *et al.* (2021) 'Proteome-wide identification of NEDD8 modification sites reveals distinct proteomes for canonical and atypical NEDDylation', *Cell Reports*, 34(3), p. 108635. doi: 10.1016/j.celrep.2020.108635.

Longo, V. D. and Mattson, M. P. (2014) 'Fasting: Molecular mechanisms and clinical applications', *Cell Metabolism*, 19(2), pp. 181–192. doi: 10.1016/j.cmet.2013.12.008.

Luck, K. *et al.* (2020) 'A reference map of the human binary protein interactome', *Nature*, 580(7803), pp. 402–408. doi: 10.1038/s41586-020-2188-x.

Lundberg, E. and Borner, G. H. H. (2019) 'Spatial proteomics: a powerful discovery tool for cell biology', *Nature Reviews Molecular Cell Biology*, 20(5), pp. 285–302. doi: 10.1038/s41580-018-0094-y.

Maddocks, O. D. K. *et al.* (2013) 'Serine starvation induces stress and p53-dependent metabolic remodelling in cancer cells', *Nature*, 493(7433), pp. 542–546. doi: 10.1038/nature11743.

Maddocks, O. D. K. and Vousden, K. H. (2011) 'Metabolic regulation by p53', *Journal of Molecular Medicine*, 89(3), pp. 237–245. doi: 10.1007/s00109-011-0735-5.

Mahmood, N., Mihalcioiu, C. and Rabbani, S. A. (2018) 'Multifaceted role of the urokinase-type

plasminogen activator (uPA) and its receptor (uPAR): Diagnostic, prognostic, and therapeutic applications', *Frontiers in Oncology*, 8(FEB). doi: 10.3389/fonc.2018.00024.

Maiuri, M. C. *et al.* (2010) 'Autophagy regulation by p53', *Current Opinion in Cell Biology*, 22(2), pp. 181–185. doi: 10.1016/j.ceb.2009.12.001.

Maki, C. G. and Howley, P. M. (1997) 'Ubiquitination of p53 and p21 is differentially affected by ionizing and UV radiation', *Molecular and Cellular Biology*, 17(1), pp. 355–363. doi: 10.1128/mcb.17.1.355.

Maldonado, M. del M. and Dharmawardhane, S. (2018) 'Targeting Rac and Cdc42 GTPases in Cancer', *Cancer Research*, 78(12), pp. 3101–3111. doi: 10.1158/0008-5472.CAN-18-0619.

Malik, A. R. *et al.* (2019) 'SorCS2 Controls Functional Expression of Amino Acid Transporter EAAT3 and Protects Neurons from Oxidative Stress and Epilepsy-Induced Pathology', *Cell Reports*, 26(10), pp. 2792-2804.e6. doi: 10.1016/j.celrep.2019.02.027.

Mallik, R., Kundu, A. and Chaudhuri, S. (2018) 'High mobility group proteins: the multifaceted regulators of chromatin dynamics', *Nucleus*, 61(3), pp. 213–226. doi: 10.1007/s13237-018-0257-4.

Maltzman, W. and Czyzyk, L. (1984) 'UV irradiation stimulates levels of p53 cellular tumor antigen in nontransformed mouse cells', *Molecular and Cellular Biology*, 4(9), pp. 1689–1694. doi: 10.1128/mcb.4.9.1689-1694.1984.

Mantovani, F. *et al.* (2015) 'Interaction of p53 with prolyl isomerases: Healthy and unhealthy relationships', *Biochimica et Biophysica Acta - General Subjects*, 1850(10), pp. 2048–2060. doi: 10.1016/j.bbagen.2015.01.013.

Mantovani, F., Collavin, L. and Del Sal, G. (2019) 'Mutant p53 as a guardian of the cancer cell', *Cell Death and Differentiation*, 26(2), pp. 199–212. doi: 10.1038/s41418-018-0246-9.

Martínez-Reyes, I. and Chandel, N. S. (2021) 'Cancer metabolism: looking forward', *Nature Reviews Cancer*. doi: 10.1038/s41568-021-00378-6.

Mathiassen, S. G., De Zio, D. and Cecconi, F. (2017) 'Autophagy and the Cell Cycle: A Complex Landscape', *Frontiers in Oncology*, 7(March), pp. 1–16. doi: 10.3389/fonc.2017.00051.

Mathupala, S. P., Heese, C. and Pedersen, P. L. (1997) 'Glucose catabolism in cancer cells. The type II hexokinase promoter contains functionally active response elements for the tumor suppressor p53', *Journal of Biological Chemistry*, 272(36), pp. 22776–22780. doi:

10.1074/jbc.272.36.22776.

Matoba, S. (2006) ‘p53 Regulates Mitochondrial Respiration’, *Science*, 312(5780), pp. 1650–1653. doi: 10.1126/science.1126863.

Mayo, L. and Nus, J. (2022) ‘Phosphorylation regulates E3 ligase activity of Mdm2’, *The FASEB Journal*, 36(S1). doi: 10.1096/fasebj.2022.36.S1.L7965.

Meex, R. C. R. and Watt, M. J. (2017) ‘Hepatokines: Linking nonalcoholic fatty liver disease and insulin resistance’, *Nature Reviews Endocrinology*, 13(9), pp. 509–520. doi: 10.1038/nrendo.2017.56.

Mellacheruvu, D. *et al.* (2013) ‘The CRAPome: A contaminant repository for affinity purification-mass spectrometry data’, *Nature Methods*, 10(8), pp. 730–736. doi: 10.1038/nmeth.2557.

Mereiter, S. *et al.* (2019) ‘Glycosylation in the Era of Cancer-Targeted Therapy: Where Are We Heading?’, *Cancer Cell*, 36(1), pp. 6–16. doi: 10.1016/j.ccell.2019.06.006.

Mohammed, H. *et al.* (2016) ‘Rapid immunoprecipitation mass spectrometry of endogenous proteins (RIME) for analysis of chromatin complexes’, *Nature Protocols*, 11(2), pp. 316–326. doi: 10.1038/nprot.2016.020.

Møller, L. L. V. *et al.* (2020) ‘Insulin-stimulated glucose uptake partly relies on p21-activated kinase (PAK)2, but not PAK1, in mouse skeletal muscle’, *Journal of Physiology*, 598(23), pp. 5351–5377. doi: 10.1113/JP280294.

Møller, L. L. V., Klip, A. and Sylow, L. (2019) ‘Rho GTPases—Emerging Regulators of Glucose Homeostasis and Metabolic Health’, *Cells*, 8(5), p. 434. doi: 10.3390/cells8050434.

Morachis, J. M., Murawsky, C. M. and Emerson, B. M. (2010) ‘Regulation of the p53 transcriptional response by structurally diverse core promoters’, *Genes & Development*, 24(2), pp. 135–147. doi: 10.1101/gad.1856710.

Mrakovcic, M. and Fröhlich, L. F. (2018) ‘P53-mediated molecular control of autophagy in tumor cells’, *Biomolecules*, 8(2). doi: 10.3390/biom8020014.

Müller, P. M. *et al.* (2020) ‘Systems analysis of RhoGEF and RhoGAP regulatory proteins reveals spatially organized RAC1 signalling from integrin adhesions’, *Nature Cell Biology*, 22(4), pp. 498–511. doi: 10.1038/s41556-020-0488-x.

Nakano, S. *et al.* (2022) ‘The Rho guanine nucleotide exchange factor PLEKHG1 is activated by interaction with and phosphorylation by Src family kinase member FYN’, *Journal of*

Biological Chemistry, 298(2), p. 101579. doi: 10.1016/j.jbc.2022.101579.

Nencioni, A. *et al.* (2018) 'Fasting and cancer: molecular mechanisms and clinical application', *Nature Reviews Cancer*, 18(11), pp. 707–719. doi: 10.1038/s41568-018-0061-0.

Nesvizhskii, A. I., Vitek, O. and Aebersold, R. (2007) 'Analysis and validation of proteomic data generated by tandem mass spectrometry', *Nature Methods*, 4(10), pp. 787–797. doi: 10.1038/nmeth1088.

Nössing, C. (2017) 'Mechanisms of starvation-induced p53 stabilization in hepatocytes', *Diploma thesis*, (March).

O. Warburg (1956) 'On the Origin of Cancer Cells', *Science*, 123(3191), pp. 309–314.

Ochocka, A. M. *et al.* (2009) 'FKBP25, a novel regulator of the p53 pathway, induces the degradation of MDM2 and activation of p53', *FEBS Letters*, 583(4), pp. 621–626. doi: 10.1016/j.febslet.2009.01.009.

Oliner, J. D. *et al.* (1993) 'Oncoprotein MDM2 conceals the activation domain of tumour suppressor p53', *Nature*, 362(6423), pp. 857–860. doi: 10.1038/362857a0.

Ou, Y. *et al.* (2015) 'p53 Protein-mediated regulation of phosphoglycerate dehydrogenase (PHGDH) is crucial for the apoptotic response upon serine starvation', *Journal of Biological Chemistry*, 290(1), pp. 457–466. doi: 10.1074/jbc.M114.616359.

Ozturk, N. *et al.* (2014) 'HMGA proteins as modulators of chromatin structure during transcriptional activation', *Frontiers in Cell and Developmental Biology*, 2(MAR), pp. 1–9. doi: 10.3389/fcell.2014.00005.

Pant, V. and Lozano, G. (2014) 'Limiting the power of p53 through the ubiquitin proteasome pathway', *Genes and Development*, 28(16), pp. 1739–1751. doi: 10.1101/gad.247452.114.

Parachoniak, C. A. and Park, M. (2012) 'Dynamics of receptor trafficking in tumorigenicity', *Trends in Cell Biology*, 22(5), pp. 231–240. doi: 10.1016/j.tcb.2012.02.002.

Parrales, A. and Iwakuma, T. (2016) 'P53 As a Regulator of Lipid Metabolism in Cancer', *International Journal of Molecular Sciences*, 17(12). doi: 10.3390/ijms17122074.

Pavlova, N. N. and Thompson, C. B. (2016) 'The Emerging Hallmarks of Cancer Metabolism', *Cell Metabolism*. doi: 10.1016/j.cmet.2015.12.006.

Pfeiffer, T., Schuster, S. and Bonhoeffer, S. (2001) 'Cooperation and Competition in the Evolution of ATP-Producing Pathways', *Science*, 292(5516), pp. 504–507. doi:

10.1126/science.1058079.

Pietrocola, F. *et al.* (2015) 'Acetyl coenzyme A: A central metabolite and second messenger', *Cell Metabolism*, 21(6), pp. 805–821. doi: 10.1016/j.cmet.2015.05.014.

Porter, J. R., Fisher, B. E. and Batchelor, E. (2016) 'P53 Pulses Diversify Target Gene Expression Dynamics in an mRNA Half-Life-Dependent Manner and Delineate Co-regulated Target Gene Subnetworks', *Cell Systems*, 2(4), pp. 272–282. doi: 10.1016/j.cels.2016.03.006.

Prokesch, A. *et al.* (2017) 'Liver p53 is stabilized upon starvation and required for amino acid catabolism and gluconeogenesis', *The FASEB Journal*, 31(2), pp. 732–742. doi: 10.1096/fj.201600845R.

Raj, N. and Attardi, L. D. (2017) 'The transactivation domains of the p53 protein', *Cold Spring Harbor Perspectives in Medicine*, 7(1), pp. 1–18. doi: 10.1101/cshperspect.a026047.

Raj, N. and Bam, R. (2019) 'Reciprocal Crosstalk Between YAP1/Hippo Pathway and the p53 Family Proteins: Mechanisms and Outcomes in Cancer', *Frontiers in Cell and Developmental Biology*, 7. doi: 10.3389/fcell.2019.00159.

Reddy, B. A. *et al.* (2014) 'Nucleotide Biosynthetic Enzyme GMP Synthase Is a TRIM21-Controlled Relay of p53 Stabilization', *Molecular Cell*, 53(3), pp. 458–470. doi: 10.1016/j.molcel.2013.12.017.

Reily, C. *et al.* (2019) 'Glycosylation in health and disease', *Nature Reviews Nephrology*, 15(6), pp. 346–366. doi: 10.1038/s41581-019-0129-4.

Renkema, G. H., Pulkkinen, K. and Saksela, K. (2002) 'Cdc42/Rac1-Mediated Activation Primes PAK2 for Superactivation by Tyrosine Phosphorylation', *Molecular and Cellular Biology*, 22(19), pp. 6719–6725. doi: 10.1128/mcb.22.19.6719-6725.2002.

Richards, A. L., Eckhardt, M. and Krogan, N. J. (2021) 'Mass spectrometry-based protein–protein interaction networks for the study of human diseases', *Molecular Systems Biology*, 17(1), pp. 1–18. doi: 10.15252/msb.20188792.

Riley, T. *et al.* (2008) 'Transcriptional control of human p53-regulated genes', *Nature Reviews Molecular Cell Biology*, 9(5), pp. 402–412. doi: 10.1038/nrm2395.

Rinn, J. L. and Huarte, M. (2011) 'To repress or not to repress: This is the guardian's question', *Trends in Cell Biology*, 21(6), pp. 344–353. doi: 10.1016/j.tcb.2011.04.002.

Riscal, R. *et al.* (2016) 'Chromatin-Bound MDM2 Regulates Serine Metabolism and Redox

Homeostasis Independently of p53', *Molecular Cell*, 62(6), pp. 890–902. doi: 10.1016/j.molcel.2016.04.033.

Ros, S. *et al.* (2017) '6-Phosphofructo-2-kinase/fructose-2,6-biphosphatase 4 is essential for p53-null cancer cells', *Oncogene*, 36(23), pp. 3287–3299. doi: 10.1038/onc.2016.477.

Roux, K. J. *et al.* (2012) 'A promiscuous biotin ligase fusion protein identifies proximal and interacting proteins in mammalian cells', *Journal of Cell Biology*, 196(6), pp. 801–810. doi: 10.1083/jcb.201112098.

Roux, K. J. *et al.* (2018) 'BioID: A Screen for Protein-Protein Interactions', *Current Protocols in Protein Science*, 91(1), pp. 19.23.1-19.23.15. doi: 10.1002/cpps.51.

Sammons, M. A. *et al.* (2015) 'TP53 engagement with the genome occurs in distinct local chromatin environments via pioneer factor activity', *Genome Research*, 25(2), pp. 179–188. doi: 10.1101/gr.181883.114.

Sane, S. and Rezvani, K. (2017) 'Essential roles of E3 ubiquitin ligases in p53 regulation', *International Journal of Molecular Sciences*, 18(2). doi: 10.3390/ijms18020442.

Dos Santos, A. R. de O. *et al.* (2021) 'Adipokines, myokines, and hepatokines: Crosstalk and metabolic repercussions', *International Journal of Molecular Sciences*, 22(5), pp. 1–23. doi: 10.3390/ijms22052639.

Sato, Y., Kamura, T., *et al.* (2009) 'Degradation of Phosphorylated p53 by Viral Protein-ECS E3 Ligase Complex', *PLoS Pathogens*. Edited by B. Sugden, 5(7), p. e1000530. doi: 10.1371/journal.ppat.1000530.

Sato, Y., Shirata, N., *et al.* (2009) 'Expression of Epstein–Barr virus BZLF1 immediate-early protein induces p53 degradation independent of MDM2, leading to repression of p53-mediated transcription', *Virology*, 388(1), pp. 204–211. doi: 10.1016/j.virol.2009.03.017.

Schvartzman, J. M., Thompson, C. B. and Finley, L. W. S. (2018) 'Metabolic regulation of chromatin modifications and gene expression', 217(7), pp. 2247–2259.

Schwanhäusser, B. *et al.* (2011) 'Global quantification of mammalian gene expression control', *Nature*, 473(7347), pp. 337–342. doi: 10.1038/nature10098.

Senitzki, A. *et al.* (2021) 'The complex architecture of p53 binding sites', *Nucleic Acids Research*, 49(3), pp. 1364–1382. doi: 10.1093/nar/gkaa1283.

Shackelford, D. B. and Shaw, R. J. (2009) 'The LKB1-AMPK pathway: Metabolism and growth

control in tumour suppression', *Nature Reviews Cancer*, 9(8), pp. 563–575. doi: 10.1038/nrc2676.

Shieh, S.-Y. *et al.* (1997) 'DNA Damage-Induced Phosphorylation of p53 Alleviates Inhibition by MDM2 phosphorylated at sites within its N-terminal and C-termi-nal regions, and several protein kinases have been shown to phosphorylate p53 in vitro. One such kinase', *Cell*, 91, pp. 325–334.

Shieh, S. Y. *et al.* (2000) 'The human homologs of checkpoint kinases Chk1 and Cds1 (Chk2) phosphorylate, p53 at multiple DNA damage-inducible sites', *Genes and Development*, 14(3), pp. 289–300. doi: 10.1101/gad.14.3.289.

Simabuco, F. M. *et al.* (2018) 'P53 and Metabolism: From Mechanism To Therapeutics', *Oncotarget*, 9(34), pp. 23780–23823. doi: 10.18632/oncotarget.25267.

Stelzl, U. *et al.* (2005) 'A human protein-protein interaction network: A resource for annotating the proteome', *Cell*, 122(6), pp. 957–968. doi: 10.1016/j.cell.2005.08.029.

Sullivan, K. D. *et al.* (2018) 'Mechanisms of transcriptional regulation by p53', *Cell Death and Differentiation*, 25(1), pp. 133–143. doi: 10.1038/cdd.2017.174.

Sun, R. C. *et al.* (2019) 'Nuclear Glycogenolysis Modulates Histone Acetylation in Human Non-Small Cell Lung Cancers.', *Cell metabolism*, 30(5), pp. 903-916.e7. doi: 10.1016/j.cmet.2019.08.014.

Suzuki, S. *et al.* (2010) 'Phosphate-activated glutaminase (GLS2), a p53-inducible regulator of glutamine metabolism and reactive oxygen species', *Proceedings of the National Academy of Sciences*, 107(16), pp. 7461–7466. doi: 10.1073/pnas.1002459107.

Tajan, M. *et al.* (2018) 'A Role for p53 in the Adaptation to Glutamine Starvation through the Expression of SLC1A3', *Cell Metabolism*, pp. 1–16. doi: 10.1016/j.cmet.2018.07.005.

Tajan, M. *et al.* (2021) 'Serine synthesis pathway inhibition cooperates with dietary serine and glycine limitation for cancer therapy', *Nature Communications*, 12(1), pp. 1–16. doi: 10.1038/s41467-020-20223-y.

Tavana, O. and Gu, W. (2017) 'Modulation of the p53/MDM2 interplay by HAUSP inhibitors', *Journal of molecular cell biology*, 9(1), pp. 45–52. doi: 10.1093/jmcb/mjw049.

Telkoparan, P. *et al.* (2013) 'Coiled-Coil Domain Containing Protein 124 Is a Novel Centrosome and Midbody Protein That Interacts with the Ras-Guanine Nucleotide Exchange Factor 1B and Is Involved in Cytokinesis', *PLoS ONE*, 8(7). doi:

10.1371/journal.pone.0069289.

Thaiparambil, J. T., Eggers, C. M. and Marcus, A. I. (2012) 'AMPK Regulates Mitotic Spindle Orientation through Phosphorylation of Myosin Regulatory Light Chain', *Molecular and Cellular Biology*, 32(16), pp. 3203–3217. doi: 10.1128/mcb.00418-12.

Titeca, K. *et al.* (2019) 'Discovering cellular protein-protein interactions: Technological strategies and opportunities', *Mass Spectrometry Reviews*, 38(1), pp. 79–111. doi: 10.1002/mas.21574.

Tyanova, S., Temu, T. and Cox, J. (2016) 'The MaxQuant computational platform for mass spectrometry-based shotgun proteomics', *Nature Protocols*, 11(12), pp. 2301–2319. doi: 10.1038/nprot.2016.136.

Ursini, M. V. *et al.* (1997) 'Enhanced expression of glucose-6-phosphate dehydrogenase in human cells sustaining oxidative stress', *Biochemical Journal*, 323(3), pp. 801–806. doi: 10.1042/bj3230801.

Varki, A. (2017) 'Biological roles of glycans', *Glycobiology*, 27(1), pp. 3–49. doi: 10.1093/glycob/cww086.

Vousden, K. H. and Prives, C. (2009) 'Blinded by the Light: The Growing Complexity of p53', *Cell*, 137(3), pp. 413–431. doi: 10.1016/j.cell.2009.04.037.

Wade, M., Wang, Y. V. and Wahl, G. M. (2010) 'The p53 orchestra: Mdm2 and Mdmx set the tone', *Trends in Cell Biology*, 20(5), pp. 299–309. doi: 10.1016/j.tcb.2010.01.009.

Wang, J. *et al.* (2011) 'Toward an understanding of the protein interaction network of the human liver', *Molecular Systems Biology*, 7(536), pp. 1–10. doi: 10.1038/msb.2011.67.

Wang, W. *et al.* (2021) 'PRDX2 promotes the proliferation of colorectal cancer cells by increasing the ubiquitinated degradation of p53', *Cell Death & Disease*, 12(6), p. 605. doi: 10.1038/s41419-021-03888-1.

Wang, X. *et al.* (2019) 'UDP-glucose accelerates SNAI1 mRNA decay and impairs lung cancer metastasis', *Nature*, 571(7763), pp. 127–131. doi: 10.1038/s41586-019-1340-y.

Wee, P. and Wang, Z. (2017) 'Epidermal growth factor receptor cell proliferation signaling pathways', *Cancers*, 9(5), pp. 1–45. doi: 10.3390/cancers9050052.

Van Weering, J. R. T. *et al.* (2012) 'Molecular basis for SNX-BAR-mediated assembly of distinct endosomal sorting tubules', *EMBO Journal*, 31(23), pp. 4466–4480. doi:

10.1038/emboj.2012.283.

Wells, J. N. *et al.* (2020) 'Structure and function of yeast Lso2 and human CCDC124 bound to hibernating ribosomes', *PLoS Biology*, 18(7), pp. 1–24. doi: 10.1371/journal.pbio.3000780.

White, E. (2016) 'Autophagy and p53', *Cold Spring Harbor Perspectives in Medicine*, 6(4), p. a026120. doi: 10.1101/cshperspect.a026120.

Wierer, M. and Mann, M. (2016) 'Proteomics to study DNA-bound and chromatin-associated gene regulatory complexes', *Human Molecular Genetics*, 25(R2), pp. R106–R114. doi: 10.1093/hmg/ddw208.

Wise, D. R. and Thompson, C. B. (2010) 'Glutamine addiction: a new therapeutic target in cancer', *Trends in Biochemical Sciences*, 35(8), pp. 427–433. doi: 10.1016/j.tibs.2010.05.003.

Wolfe, A. L. *et al.* (2021) 'UDP-glucose pyrophosphorylase 2, a regulator of glycogen synthesis and glycosylation, is critical for pancreatic cancer growth', *Proceedings of the National Academy of Sciences of the United States of America*, 118(31). doi: 10.1073/pnas.2103592118.

Xirodimas, D. P. *et al.* (2004) 'Mdm2-Mediated NEDD8 Conjugation of p53 Inhibits Its Transcriptional Activity', *Cell*, 118(1), pp. 83–97. doi: 10.1016/j.cell.2004.06.016.

Xue, L. *et al.* (2003) 'Wild-type p53 regulates human ribonucleotide reductase by protein-protein interaction with p53R2 as well as hRRM2 subunits', *Cancer Research*, 63(5), pp. 980–986.

Yang, G. *et al.* (2017) 'Glucuronidation: driving factors and their impact on glucuronide disposition', *Drug Metabolism Reviews*, 49(2), pp. 105–138. doi: 10.1080/03602532.2017.1293682.

Ye, D. Z. and Field, J. (2012) 'PAK signaling in cancer', *Cellular Logistics*, 2(2), pp. 105–116. doi: 10.4161/cl.21882.

Yoshida, Y. *et al.* (2003) 'p53 physically interacts with mitochondrial transcription factor A and differentially regulates binding to damaged DNA', *Cancer Research*, 63(13), pp. 3729–3734.

Zempleni, J. (2005) 'Uptake, localization, and noncarboxylase roles of biotin', *Annual Review of Nutrition*, 25, pp. 175–196. doi: 10.1146/annurev.nutr.25.121304.131724.

Zeng, J. *et al.* (2021) 'Pak2 reduction induces a failure of early embryonic development in mice', *Reproductive Biology and Endocrinology*, 19(1), pp. 1–10. doi: 10.1186/s12958-021-

00865-3.

Zhang, C. *et al.* (2014) ‘Tumor suppressor p53 negatively regulates glycolysis stimulated by hypoxia through its target RRAD’, *Oncotarget*, 5(14), pp. 5535–5546. doi: 10.18632/oncotarget.2137.

Zhang, J., Pavlova, N. N. and Thompson, C. B. (2017) ‘Cancer cell metabolism: the essential role of the nonessential amino acid, glutamine’, *The EMBO Journal*, 36(10), pp. 1302–1315. doi: 10.15252/embj.201696151.

Zhang, X. *et al.* (2018) ‘The role of YAP/TAZ activity in cancer metabolic reprogramming’, *Molecular Cancer*, 17(1), pp. 1–10. doi: 10.1186/s12943-018-0882-1.

Zhao, Y., Xiong, X. and Sun, Y. (2020) ‘Cullin-RING Ligase 5: Functional characterization and its role in human cancers’, *Seminars in Cancer Biology*, 67, pp. 61–79. doi: 10.1016/j.semcancer.2020.04.003.

Zheng, S. L. *et al.* (2016) ‘Metrnl: A secreted protein with new emerging functions’, *Acta Pharmacologica Sinica*, 37(5), pp. 571–579. doi: 10.1038/aps.2016.9.

Zois, C. E. and Harris, A. L. (2016) ‘Glycogen metabolism has a key role in the cancer microenvironment and provides new targets for cancer therapy’, *Journal of Molecular Medicine*, 94(2), pp. 137–154. doi: 10.1007/s00109-015-1377-9.

Zou, T. and Zhang, J. (2021) ‘Diverse and pivotal roles of neddylation in metabolism and immunity’, *FEBS Journal*, 288(13), pp. 3884–3912. doi: 10.1111/febs.15584.